NUREG/CR-4027
SAND84-2161
R4
Printed February 1986

TRAC-PF1/MOD1 Independent Assessment: Condensation in Stratified Cocurrent Flow

Rupert K. Byers

Prepared by
Sandia National Laboratories
Albuquerque, New Mexico 87185 and Livermore, California 94550
for the United States Department of Energy
under Contract DE-AC04-76DP00789

Prepared for
U. S. NUCLEAR REGULATORY COMMISSION

Available from

Superintendent of Documents
U.S. Government Printing Office
Post Office Box 37082
Washington, D.C. 20013-7982

and

National Technical Information Service
Springfield, VA 22161

NUREG/CR-4027
SAND84-2161
R4

TRAC-PF1/MOD1 Independent Assessment: Condensation in Stratified Cocurrent Flow

Rupert K. Byers

Date Published: February 1986

Sandia National Laboratories
Albuquerque, NM 87185
Operated by
Sandia Corporation
for the
U. S. Department of Energy

Prepared for
Reactor Systems Research Branch
Division of Accident Evaluation
Office of Nuclear Regulatory Research
U. S. Nuclear Regulatory Commission
Washington, DC 20555
Under Memorandum of Understanding DOE 40-550-75
NRC FIN No. A-1374

Abstract

The USNRC is funding efforts at several laboratories to assess the adequacy of various advanced, best-estimate systems codes for predicting the behavior of LWRs in accident and abnormal conditions. Sandia's participation in this project includes the use of TRAC-PF1/MOD1 to model stratified, horizontal cocurrent flow, for comparison with experimental data produced at Northwestern University. The experiments are very simple, and the results should display the effects of mass, momentum, and energy transfer at the interface, as well as those of wall friction.

Analyses were performed for four of the Northwestern experiments, which involved condensing steam/water flow in a rectangular channel. The study showed that the code's timestep control algorithm and criteria for steady-state convergence need attention, and that the interfacial heat transfer model generally overpredicts the rate of phase change for conditions of the experiments. In TRAC, horizontal stratified flow is assumed to occur in a channel of circular cross section; this precludes a simple and detailed quantitative comparison between calculated results and the reported experimental data. However, the qualitative effects of various changes in experimental conditions are well predicted in most cases. A very simple ad hoc modification to the interface treatment, based on boundary layer theory, was able to remove some of the larger discrepancies between the experimental and calculated results. Further improvements could probably result from analysis of the data in a different way from that presented in the experiment report, but this possibility was only briefly examined.

TABLE OF CONTENTS

LIST OF ILLUSTRATIONS

ACKNOWLEDGMENTS

Millie Elrick's work in code maintenance and modifications, both for TRAC and its auxiliary programs, was very helpful during the course of this study.

Luba Kmetyk offered many suggestions and comments on the form and content of this report.

Jan Frey, as always, was cheerful and efficient during the final preparation of this document.

Executive Summary

The modelling of condensation and the resulting heating of liquid (for example, during ECC injection) can play an important role in the analysis of hypothetical LOCAs. In order to further understand this phenomenon, the steady, stratified flow of water vapor and liquid in a horizontal, rectangular channel was studied in a number of experiments performed at Northwestern University. The data from these experiments were selected for comparison with results of TRAC-PF1/MOD1 calculations, as part of the independent code assessment project at Sandia.

The results of preliminary calculations indicate that TRAC's timestep selection algorithm and initialization procedure may not be adequate for conditions in which two-phase flow is the dominant feature at the beginning of an analysis. This situation is, of course, not surprising in codes originally designed to analyze large-break LOCAs in PWRs. It was necessary to impose an upper limit on the calculational timestep in order to achieve convergence to a steady state in a reasonable amount of computer time, and this need was obvious from the results. However, the value of the maximum timestep also affected the ultimate conditions attained when the steady-state criterion was satisfied, and further timestep reductions were required to eliminate this effect. Unless a more stringent criterion for convergence to a steady state is implemented in the code, our experience suggests that a number of such states should be generated and compared.

TRAC does not model horizontal stratified flow in a rectangular channel, so that detailed, direct, and quantitative comparison of calculated and experimental results was not possible. (The manual states that a VESSEL component may be described in two-dimensional rectangular geometry, but that component is also basically assumed to be vertically oriented.) We therefore performed calculations for only a few of the tests. For the four experiments considered, the general character of the results was acceptable; in particular, the qualitative effects of changes in inlet flows and liquid temperature were consistent with experimental observations. Major discrepancies (e.g., two cases with regions of countercurrent flow) were eliminated by very simple modifications to interfacial heat transfer coefficients, showing that a more general correction, if desired, could probably be implemented fairly easily.

From the point of view of model (as opposed to code) assessment, there were several difficulties with the experimental data as presented. First, analysis of the data in order to infer heat transfer coefficients requires values for the axial gradient of the mass flows; flow values were given at only six points on the flow path, so the details of fitting these profiles can have a significant influence on the results obtained. In the fitting process, one might wish to employ different functional forms, depending on the character of the interface. The experiment report contained no quantitative information that would allow a choice of fitting functions based on the geometry of the interface. A less important failing was the fact that liquid temperature profiles did not appear in the report, and this required some assumptions to be made in analyzing the data. Finally, the experimenters analyzed the data in order to obtain correlations defining heat transfer coefficients as functions of various thermodynamic and dimensionless quantities. Unfortunately, those correlations considered axially averaged values, and these are of no use in TRAC.

Because of their simplicity, separate effects tests of the kind considered in this study have great potential value as guides for developing code models for phenomena of interest, and, in cases where the experiments can be simulated directly, as standards for measuring the accuracy of those models when used in calculations. That this potential was not realized here was partially due to the geometric dichotomy between TRAC's available components and the test configuration. However, we believe that, given more experimental information and/or a different manner of presenting the data, the results of the experiments could be used to improve the interfacial energy transfer models used in the code. We briefly explored one possible method of analyzing the data in order to obtain interfacial heat transfer coefficients, but an extensive effort of that nature was not within the scope of this work.

1.0 Introduction

The TRAC-PF1/MOD1 independent assessment project at Sandia National Laboratories (SNLA) is part of an effort funded by the U. S. Nuclear Regulatory Commission to determine the ability of various systems codes to predict the behavior of light-water reactors (LWRs) during accidents and abnormal operating conditions. TRAC-PF1/MOD1 [1] was developed at Los Alamos National Laboratory, and its capabilities are such that thermal/hydraulic experiments of many kinds may be analyzed, as well as various transients in full-scale LWRs. The code contains a two-fluid nonequilibrium hydrodynamics treatment, with provisions for including the flow of a noncondensable gas, and various flow-regime-dependent models.

TRAC-PF1/MOD1 is being assessed at SNLA against experimental data from both integral and separate effects test facilities. The separate effects portion of the assessment data list includes the results of a set of 40 experiments performed at Northwestern University [2]; inclusion of these tests in the assessment matrix is intended to investigate TRAC's ability to model stratified, horizontal cocurrent flow. The code's treatment of interfacial energy and mass transfer, under various combinations of inlet flow rates and liquid subcooling and levels, is of particular interest.

This report recapitulates the results of analyses carried out for a subset of the tests described in the experiment report. The code used was essentially Version 11.1 of TRAC-PF1/MOD1, with some additions and modifications specific to the purposes of this study. Section 2 contains a description of the equipment and procedure used in the tests, and of the reported data. In Sections 3 and 4, we describe the input model and the results of some preliminary calculations investigating steady-state convergence of the analyses, boundary conditions, and interfacial heat transfer. The results of variations in inlet flow rates, liquid temperature, and vapor composition are treated in Section 5. Conclusions drawn from this study, and their possible implications for further assessment and development of TRAC, are presented in Section 6. Appendix A is a brief investigation of possible means of analyzing the data in a way that could permit a reasonable quantitative comparison with the results yielded by TRAC's models, and form a basis for any changes deemed necessary in those models. The UPDATES used to modify TRAC are contained in Appendix B, and Appendix C provides input data for the analyses.

2.0 Experimental Apparatus, Procedure, and Reported Data

The experiments [2] consisted of cocurrent flow of liquid water and steam (at roughly atmospheric pressure) in a horizontal, rectangular channel about 1.6 m long, 0.3 m wide, and 0.06 m high. The channel was constructed of 6.4 mm thick stainless steel, and was insulated on the upper and lower surfaces with 50 mm layers of fiberglass. Instruments for measuring steam velocity, static pressure, liquid layer thickness, and temperature were located at 5 positions along the channel to a distance of ~ 1.23 m. Vapor velocities were measured at vertical increments of about 4 mm from the liquid surface, and integrated to provide mass flow rates at each axial station. The vapor was superheated, and variations were performed on inlet flow rates, liquid level, and the amount of subcooling of the liquid (Figure 2.1). Steam flowed from a building source through the channel and exhausted to the atmosphere, while liquid collected in the exit plenum was returned through a heat exchanger to the tank used for the liquid source. The steam flow was established at a constant value for at least 10 minutes before beginning the liquid flow, and all data were taken in steady-state conditions.

For 14 of the test conditions indicated in Figure 2.1, data for liquid layer thickness, vapor flow rate, and differential pressure (referred to the inlet of the test section) were tabulated at the 5 locations along the flow path, together with flow rates and liquid temperatures at the inlet and outlet and inlet vapor temperatures. Tabulated data for the remainder of the tests did not include the pressure differences. Since no absolute pressures or downstream vapor temperatures were mentioned, we inferred that these quantities were substantially constant for a given test. The data for the lowest values of inlet flow rates showed a liquid inlet temperature of ~ 274 K, in conflict with that shown in the figure. (Reference 2 contains a figure, from which Figure 2.1 was derived, which also shows 5 tests as being "with air," but no further mention of these experiments occurs in the report.) The report also contained graphs showing local and average heat transfer coefficients, which resulted from analyses using the measured flows.

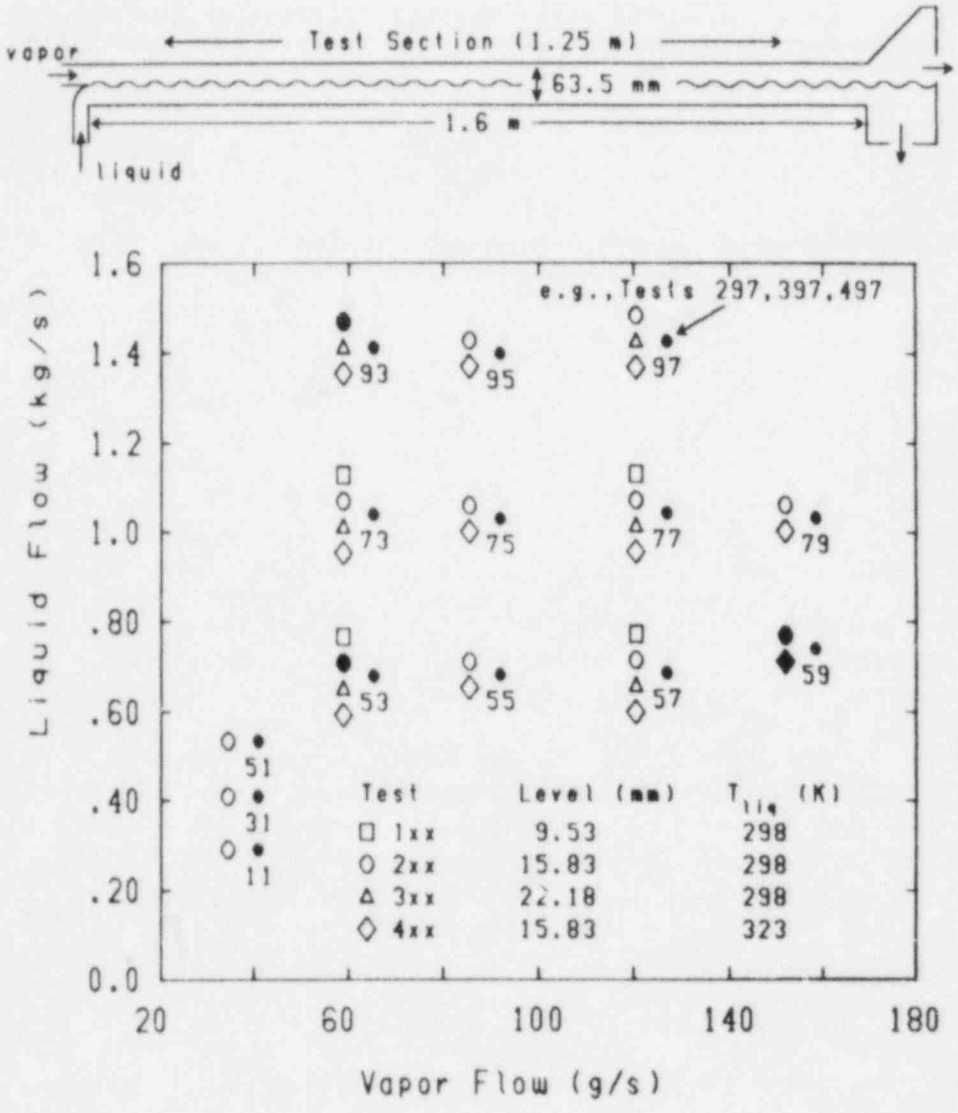

Figure 2.1 Test Configuration and Nominal Inlet Conditions for Stratified Flow Experiments (after NUREG/CR-2289)

3.0 TRAC Model and Calculational Timestep Control

3.1 Nodalization for TRAC Calculations

In TRAC-PF1/MOD1, the only apparent means of modelling a rectangular channel is by specifying a VESSEL component which has one azimuthal segment. (One must read the input requirements section of the manual carefully to discover this fact.) The VESSEL component is essentially vertically oriented; in fact, the manual's description of horizontal stratified flow implies that this regime is available only in one-dimensional components. Thus, it appears that TRAC-PF1/MOD1 can model condensing flow parallel to a horizontal vapor-liquid interface only in a PIPE component.

The TRAC nodalization for the calculations, shown schematically in Figure 3.1.1, consists of a source for vapor and liquid at the inlet, a 1.25 m flow channel consisting of 50 equal cells, and an outlet sink. Flow areas were made equal to that of the experiment channel, and, where relevant, hydraulic diameters computed from the perimeter of the channel. In order to facilitate later analysis of the results, 20 types of "signal variables" were recorded at every other cell or cell edge. Half of these variables were created by modifying the code, either because they were not available on the standard form of the graphics output file or because of errors (since corrected) in the code. Our plotting program and several special purpose programs were used to produce other quantities not normally available in the code output. For preliminary calculations, input conditions corresponding to Test 253 were specified, and the analyses carried out using TRAC's steady-state solution option.

In the case of the source boundary, a constant-state FILL component was used; the pressure was assumed (since it was not given in the experiment report) to be atmospheric (i.e., 0.101 MPa). TRAC permits independent specification of velocities for the two phases, but not of mass flows. For this reason, the FILL's volume fractions were specified to be equal to the experimental values; the velocities required to achieve the mass flows were obtained from these volume fractions and the phase densities for the pressure and the given temperatures, and those velocities then specified as boundary conditions.

Initial conditions at the ends of the PIPE component modelling the flow path were derived in a similar fashion as those for the source, using the given increases in pressure and liquid temperature for the downstream end. In hopes of accelerating the convergence to a steady state as determined by the code, linear interpolation was used to obtain initial conditions for pressures, volume fractions, velocities, and liquid temperatures along the flow path. We inferred from the data report that the outlet liquid temperatures were recorded in the exit plenum; therefore, the initial increases in liquid temperature were reduced because the calculation describes a shorter flow path than the total channel length (as shown earlier in Figure 2.1).

The sink adjacent to the outlet end of the flow path was specified as a constant-state BREAK with conditions identical to those in the last cell of the channel, except that the liquid was defined to be saturated. (The first attempt to use this input option disclosed that, contrary to the specification in the code manual, the liquid temperature was set equal to the vapor temperature. This discrepancy was easily rectifiable, and was reported to TRAC's developers.)

3.2 Timestep Control and Convergence to a Steady State

In the initial calculations, TRAC was allowed to choose a timestep as large as 1 s, and recommended values for control of the steady-state convergence option were used. The results suggested that the timestep selection algorithm is inadequate for initialization in situations with two-phase flow dominating. This was evidenced by repeated sequences in which the timestep grew at the maximum rate, and was then sharply reduced; other calculated results also showed no prospect of reaching a steady state, at least in a reasonable amount of computer time. Figure 3.2.1 presents typical histories for the timestep and the liquid velocity halfway down the flow channel. Results were improved by reducing the maximum allowable timestep to 0.5 s, but the coding determined that a steady state had not been reached by 500 s of problem time.

Continued factor-of-two reductions in the maximum timestep showed that the criteria for a steady state would be met in ~ 60 s of problem time (and ~ 110 CPU s on a CYBER76) at a maximum timestep of 0.25 s. A further timestep reduction resulted in convergence in 35 - 40 s of computed time; however, the final state was not the same as that attained with the larger timestep. As may be seen in Figure 3.2.2, calculations with maximum timesteps of 0.125 s and 0.0625 s did yield virtually identical results, so the larger of these two timesteps was chosen as the maximum for most of the subsequent analyses.

For convergence to a steady state, TRAC requires that normalized rates of change of pressures, velocities, volume fractions, and temperatures be less than an input quantity (the suggested value is 0.0001), and a test for this situation is performed every 100 cycles. We first modified TRAC so that the convergence check would be performed on each computational cycle, in order to obtain more information on how rapidly a calculation actually meets the criterion. Next, for a closer approximation to the global conservation equations, the convergence test was modified to check normalized rates-of-change of the fluxes of mass, momentum, and total energy for each phase. As we expected, convergence to a steady state using this alteration required slightly more computed (and computer) time; otherwise, there was no discernible effect on the results. In particular, the influence of maximum timestep size on the converged solution was still observed.

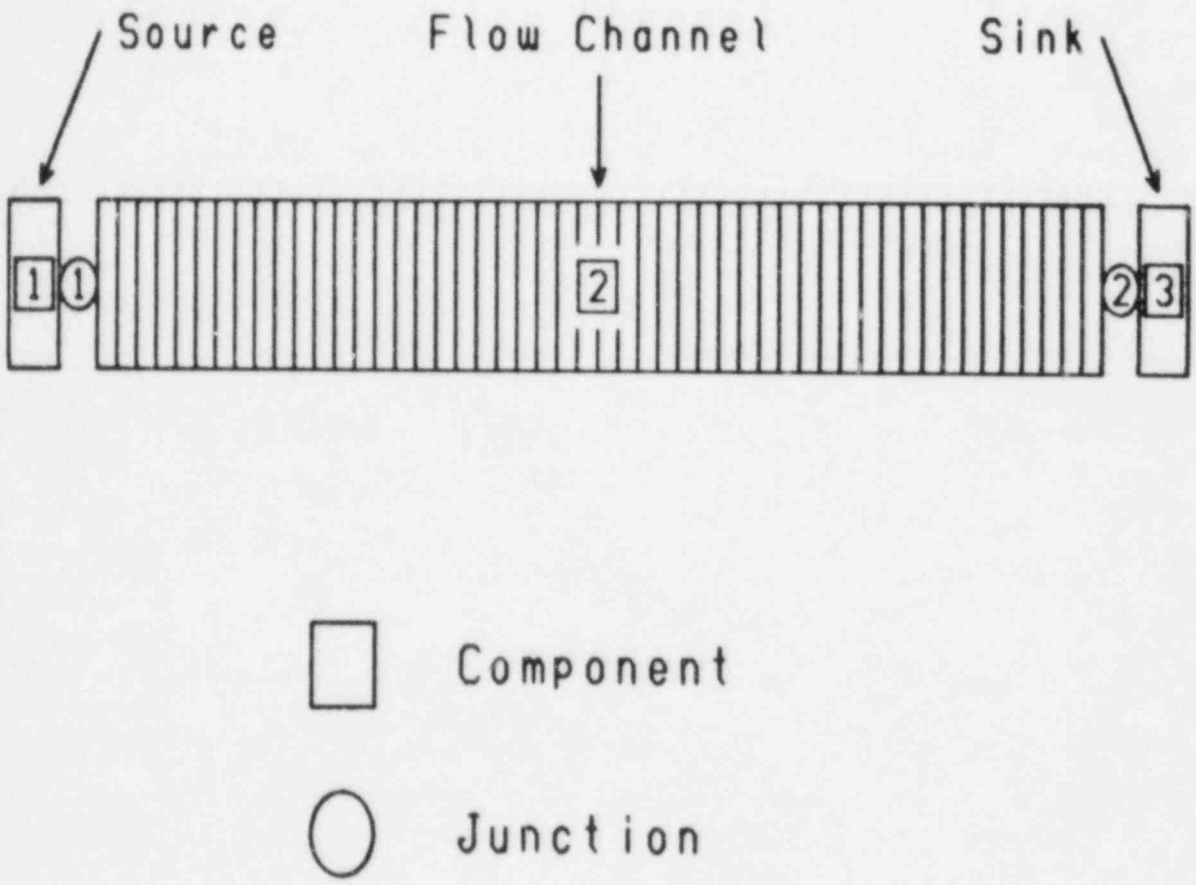

Figure 3.1.1 Nodalization for TRAC Calculations

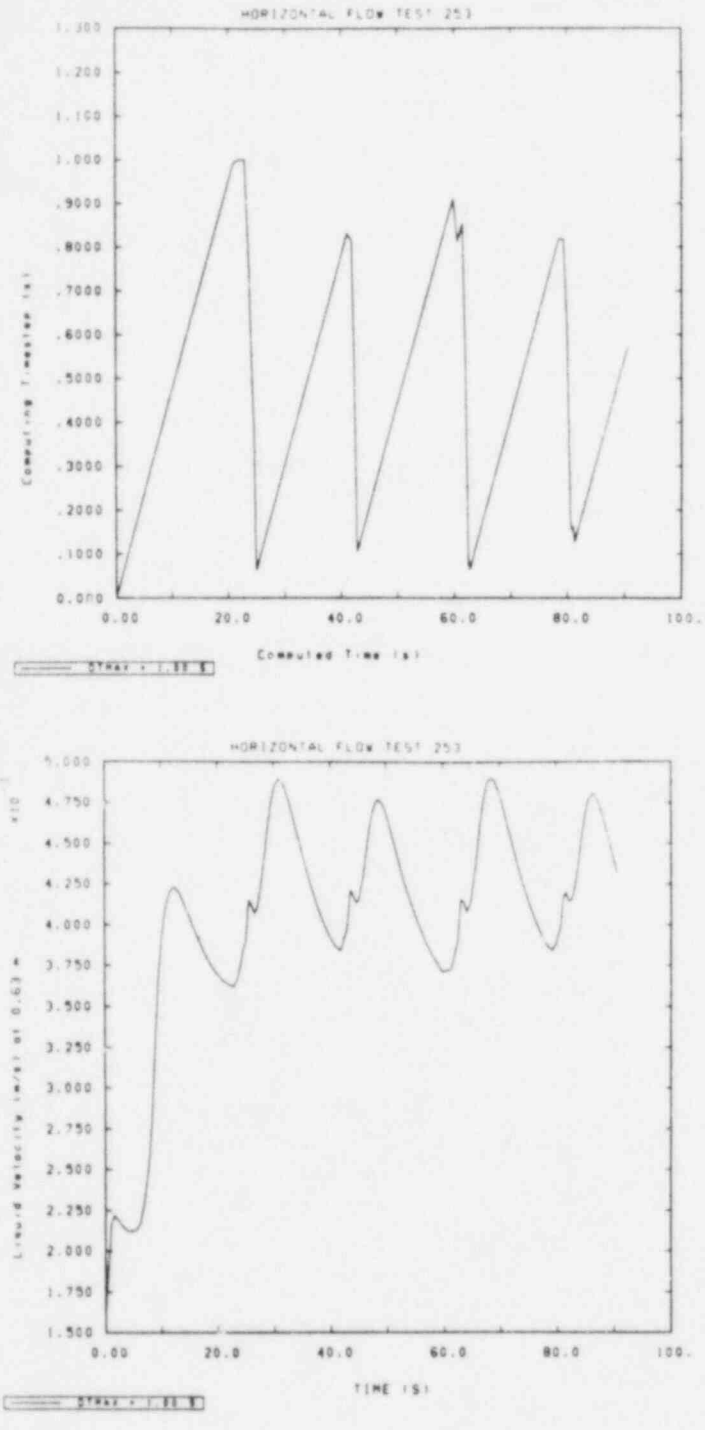

Figure 3.2.1 Results from Steady State Attempt using a Maximum Timestep of 1 s: Timestep (above) and Liquid Velocity (below)

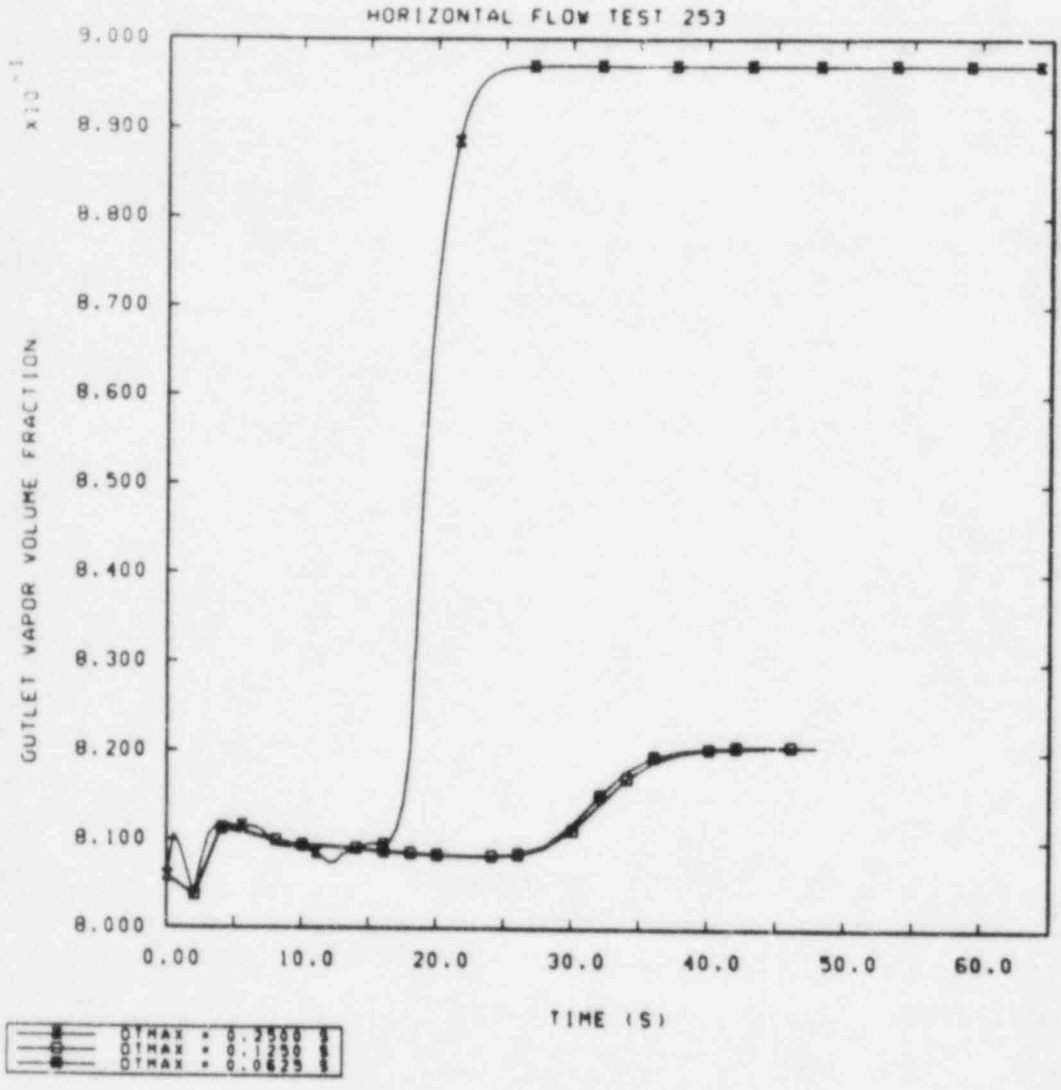

Figure 3.2.2 Outlet Vapor Volume Fraction from Converged Steady-State Results: Maximum Timesteps of 0.250, 0.125, and 0.0625 s

4.0 Calculations for Test 253

4.1 Results of Initial Calculations

We did not expect that TRAC would give highly accurate quantitative results compared to the experimental data, principally because a PIPE has a circular cross section. This geometrical restriction has the obvious consequence that liquid level and interfacial area are coupled in the calculations. Calculated interphase transfer of mass, momentum, and energy at a point in the flow path are thus more strongly affected by upstream condensation than would be the case with a constant interface area. The calculated pressure profile, compared with data in Figure 4.1.1, showed a somewhat larger increase than was measured, but was not altogether unreasonable. However, another feature of the calculated results showed a serious qualitative flaw: the calculated vapor flow (Figure 4.1.2) was negative for flow distances greater than about 0.9 m. (The higher calculated vapor mass flow at the inlet was due to an increase in vapor volume fraction from its value in the source. One may speculate that the rate of phase change is improperly "donored" at a FILL in TRAC's difference scheme.)

Because of the flow results noted in the previous paragraph, it seemed advisable to see whether a velocity boundary condition at the outlet (a "negative" FILL) would eliminate the region of countercurrent flow. The velocities, volume fractions, temperatures and pressure were specified to be the same as for the last cell in the PIPE. As shown in Figure 4.1.3, the velocity boundary condition did indeed remove the negative calculated vapor flow in the downstream portion of the channel. The calculated profiles are plotted only for points in the PIPE component, and Figure 4.1.3 also demonstrates that mass flows for each phase are not continuous at either boundary, whether or not a velocity boundary condition is used at the outlet; this is most clearly seen by the unequal vapor mass flows appearing at X=0 for identical FILL conditions upstream of X=0. The code did, however, calculate the total mass flow to be the value defined at the inlet, regardless of outlet boundary condition.

Figure 4.1.4 compares experimental and calculated inlet-to-station pressure differences for the two outlet boundary conditions. As seen earlier, the calculated result with the pressure boundary condition is only numerically wrong, but the velocity outlet boundary condition yields a qualitatively incorrect pressure profile - a significant expansion appears near the inlet. This expansion was sufficient to override the effect of the increase in vapor volume fraction alluded to earlier, and resulted in the low vapor flow at the inlet for this case. Thus, contrary to our expectations, neither of the outlet boundary conditions would produce qualitatively correct results for both pressure and the distribution of mass flow between the phases.

The results using a pressure outlet boundary condition immediately suggest the hypothesis that interfacial energy transfer model in TRAC predicts too much condensation for the conditions under study. In this calculation, the condensation rate integrated to some point on the flow path exceeded the inlet vapor mass flux, without supplying enough liquid to make the flow single phase. From this point downstream, vapor was supplied from the BREAK at the outlet, in order to satisfy the mass balance equation. With a FILL at the outlet, the calculated pressure and vapor temperature and density in the flow channel were much lower than their values at the inlet FILL, suggesting that too much energy was removed from the

vapor, which again indicates an excessive condensation rate. The resulting outlet vapor mass flow was lower than the value specified by the boundary condition, even though the velocity boundary condition was satisfied. For both the outlet boundary conditions, then, TRAC computes a steady state that is qualitatively inconsistent with experimental data, either in the flow regime or in the vapor's thermodynamic state.

4.2 Modifications to the Interfacial Energy Transfer Model

Since both calculations described in the previous Section exhibited evidence that the computed interfacial energy transfer was too high, it seemed appropriate to examine the details of the model for that process. The code manual gives no indication that an input quantity can affect mass or energy transfer, so any changes in that model would apparently require modifications to the code.

TRAC computes terms which represent the product of heat transfer coefficient and area, for interactions between each phase and the interface. With the interface assumed to be at saturation temperature, these terms are multiplied by the appropriate temperature differences and summed to arrive at a total power to the interface. Since the interface cannot store energy, the phase change rate for a cell is the ratio of that power to the jump in specific enthalpy required for phase change at saturation. Thus, the interfacial heat transfer coefficients and the effective areas are the quantities which control the process. For the interface-to-liquid contribution, the term of interest is proportional to the product of liquid velocity, density, specific heat, and the interface area (i.e., the liquid Stanton number is constant). The vapor-to-interface contribution is more complicated, and appears to be a sum of terms related to dispersed and annular flow regimes. The effective area in this part of the model does not depend directly on the stratified interface area.

In order to test the "over-condensation" hypothesis, we made a very simple alteration in the models for interfacial heat transfer in completely stratified flow. For either phase, our modification prescribes the Stanton number to be proportional to a product of powers of the Reynolds and Prandtl numbers, as in the analysis for a boundary layer along a flat plate. (See, for example, Reference 3.) For the liquid-to-interface term, the effect is one of multiplying TRAC's standard heat transfer coefficient by a constant, a power of the Prandtl number, and a power of the Reynolds number. The vapor-to-interface and liquid-to-interface terms in our modification are identical in form, differing only in the quantities used to evaluate them. The area of the stratified interface thus affects energy transfer for both phases. The mean relative velocity is used in the Reynolds number for each phase; because of the boundary layer approach, the characteristic length is the distance from the inlet. The multiplicative constant and the exponent on the Reynolds number depend on whether the flow is laminar or turbulent, and transition between those regimes is accomplished by a cubic in the velocity. The liquid-to-interface heat transfer may be expected to dominate in the situations of interest here, and Figure 4.2.1 shows the large reduction in the coefficient resulting from our modification. Although we expected frictional effects to be of minor importance in these calculations, we used Reynolds' analogy to produce a similar treatment for wall friction, for the sake of consistency. In this case, of course, the mean velocity of each phase is used. No alterations to the interfacial friction description were made.

Figure 4.2.2 compares the differential pressure profiles from calculations using both outlet boundary conditions and both standard and modified models for wall friction and interfacial heat transfer. With our modification, the boundary condition selected had a much smaller apparent effect on the results, and pressures increased monotonically with distance along the flow path. However, the reader should be aware that the calculated differences are referred to the pressure in the first cell of the flow path; as we have seen, this is not necessarily the same as the pressure in the source volume. In contrast to the results using the standard version of the code, the modified treatment and the velocity boundary at the outlet produced a compression at the inlet. As Figures 4.2.3 and 4.2.4 show, the vapor thermodynamic state at the inlet closely approximated that of the source (i.e., 411 K and 101 kPa) only when the pressure boundary was used at the outlet.

Comparisons of vapor mass flux, defined here as the density-velocity product, are similar to those for pressure, as shown in Figure 4.2.5, with the modified treatment producing positive flux for either boundary condition. Again, specifying a BREAK at the outlet was necessary to avoid a flux discontinuity at the inlet. Note also that the results using the modified models show outlet mass fluxes that are very nearly equal to the experimental values, even when the outlet flows are not explicitly prescribed by a boundary condition.

As a result of performing these preliminary calculations, we decided to use a maximum timestep of 0.125 s in all subsequent analyses, prescribing inlet mass flows and outlet pressures as described above. One of our goals was to attempt to perform calculations in roughly the same range of thermodynamic variables that occurred in the experiments, and a FILL at the downstream end of the PIPE apparently made that difficult, if not impossible. Furthermore, the use of a velocity boundary condition at the outlet seemed a somewhat unfair attempt to force the code to calculate given mass flows (hence total condensation), and one would not normally specify what would be a break velocity in other contexts.

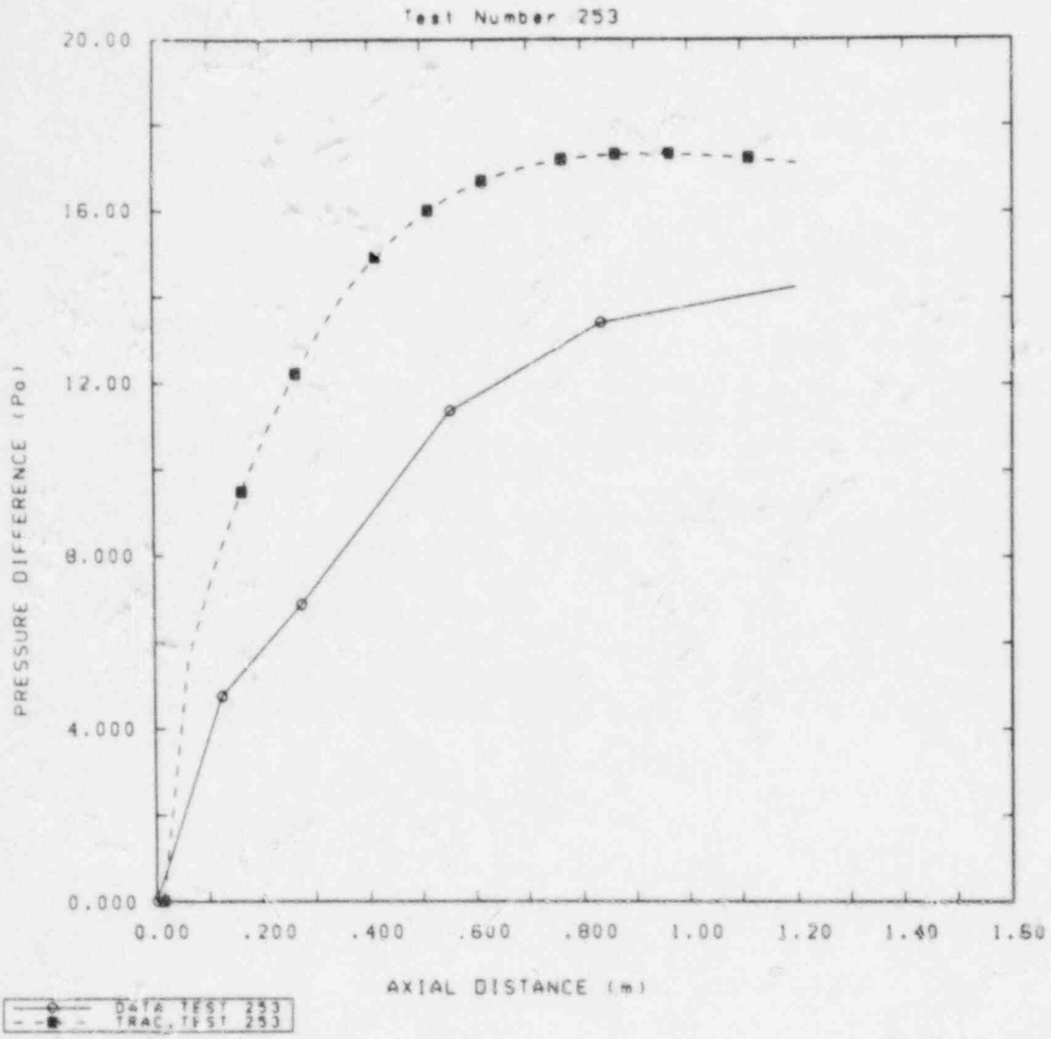

Figure 4.1.1 Differential Pressure Profiles for Test 253

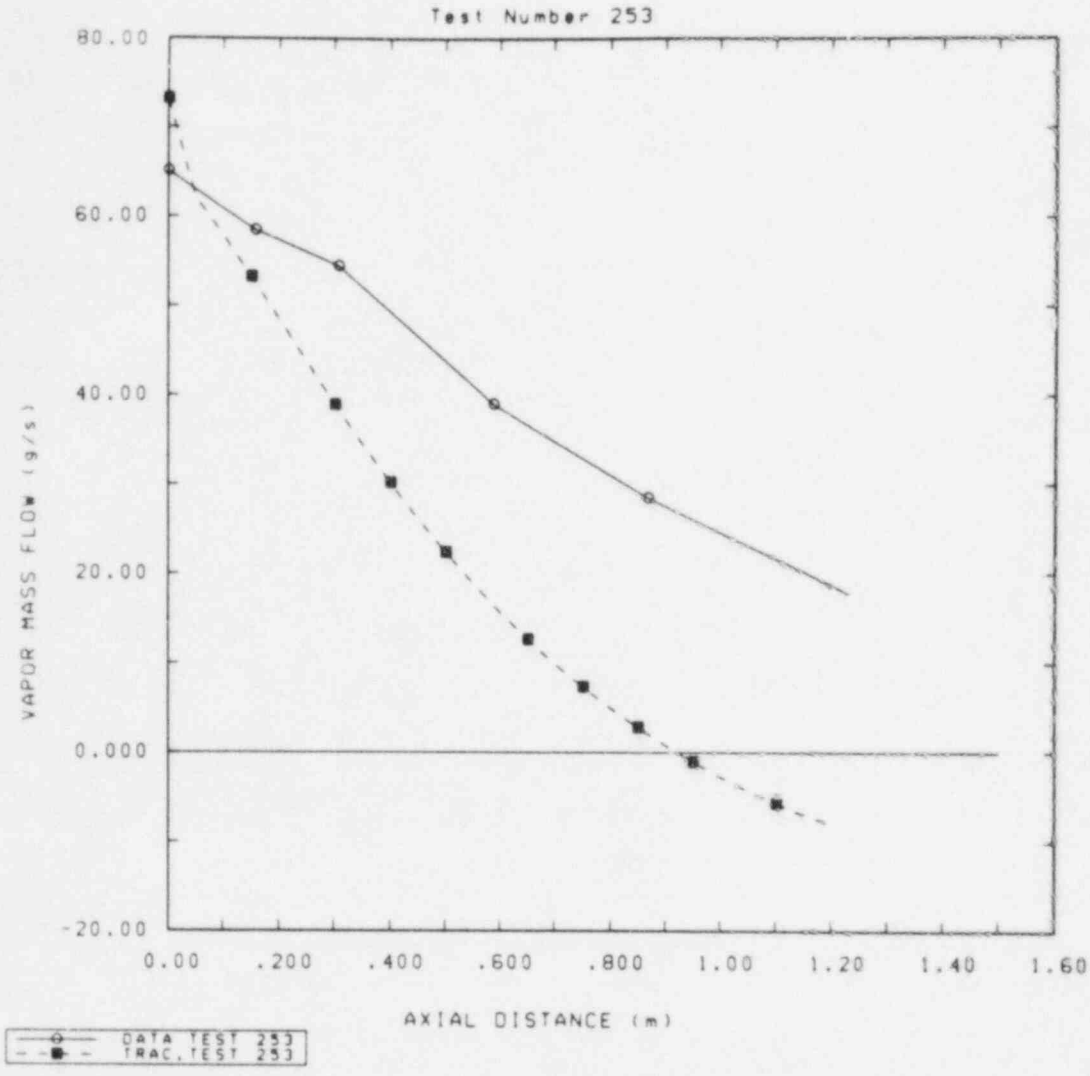

Figure 4.1.2 Vapor Flow Profiles for Test 253

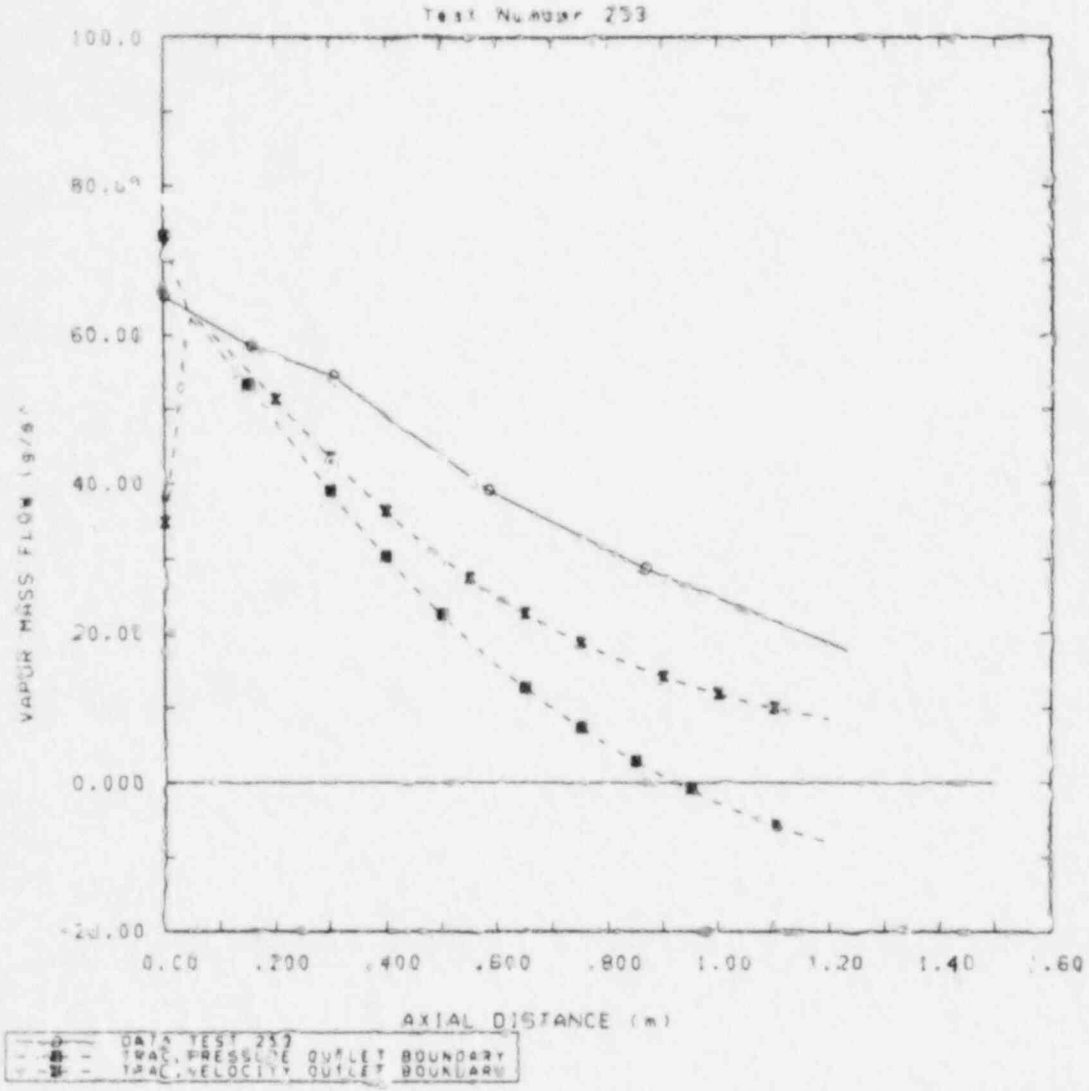

Figure 4.1.3 Vapor Flow Profiles for Test 253 with Two Outlet Boundary Conditions

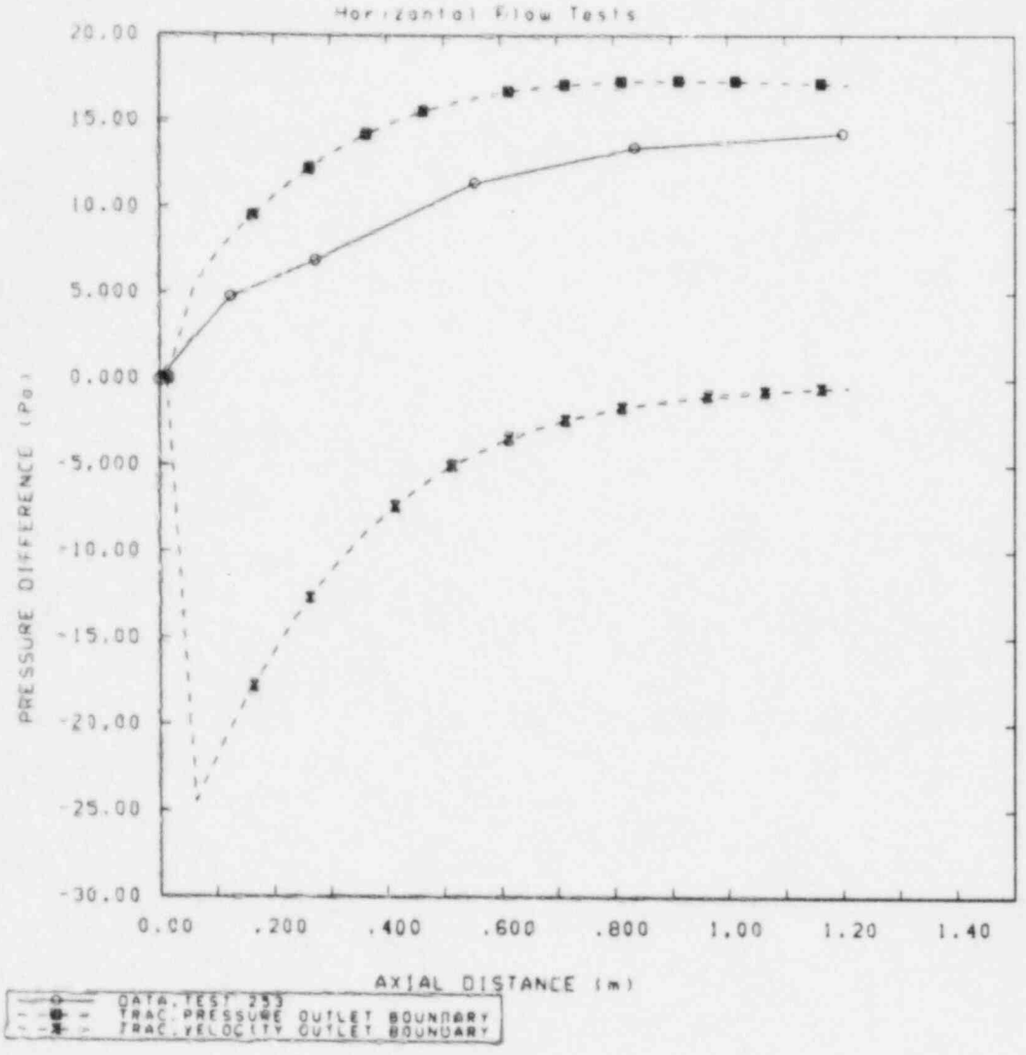

Figure 4.1.4 Differential Pressure Profiles for Test 253 with Two Outlet Boundary Conditions

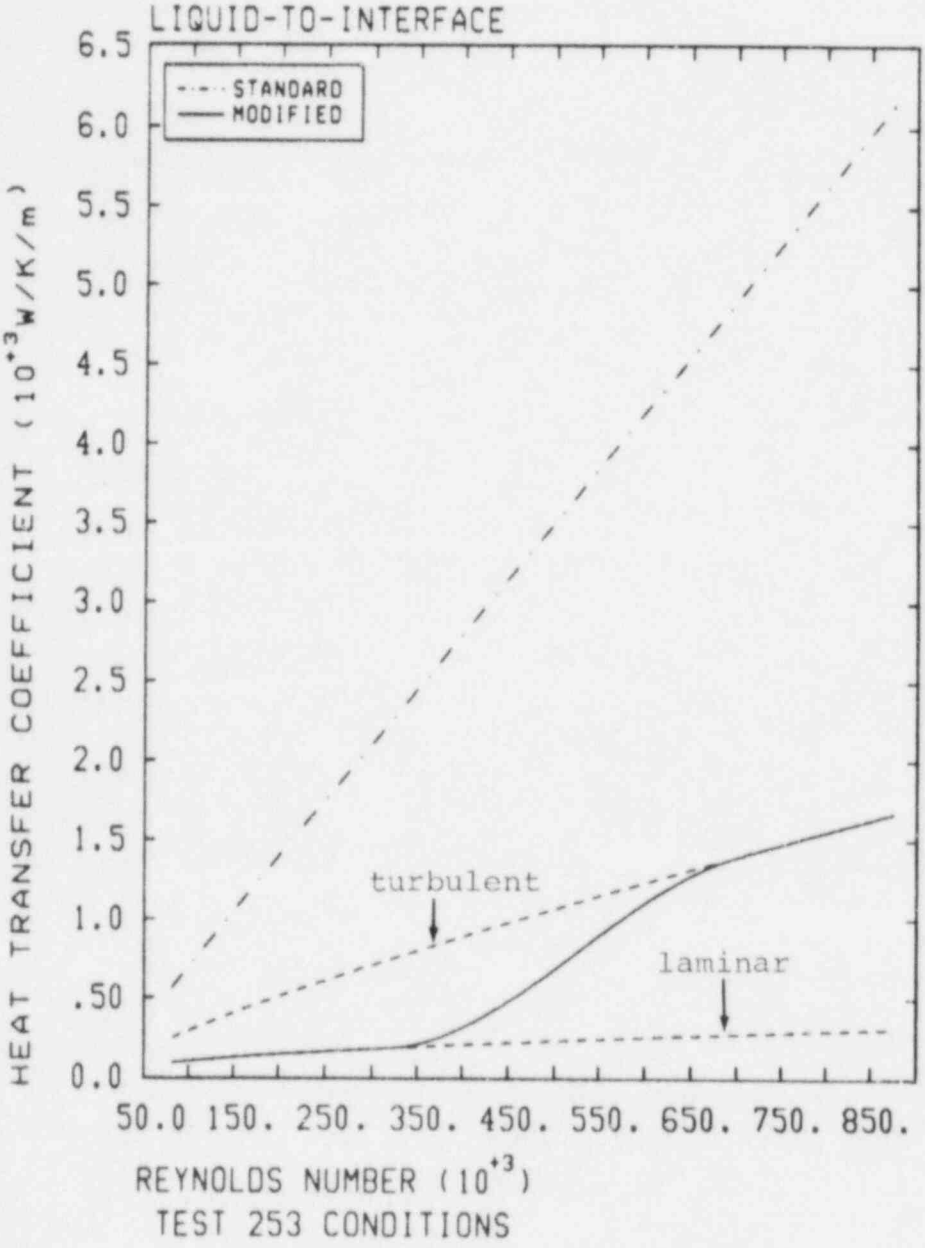

Figure 4.2.1 Standard and Modified Interfacial Heat Transfer Coefficients

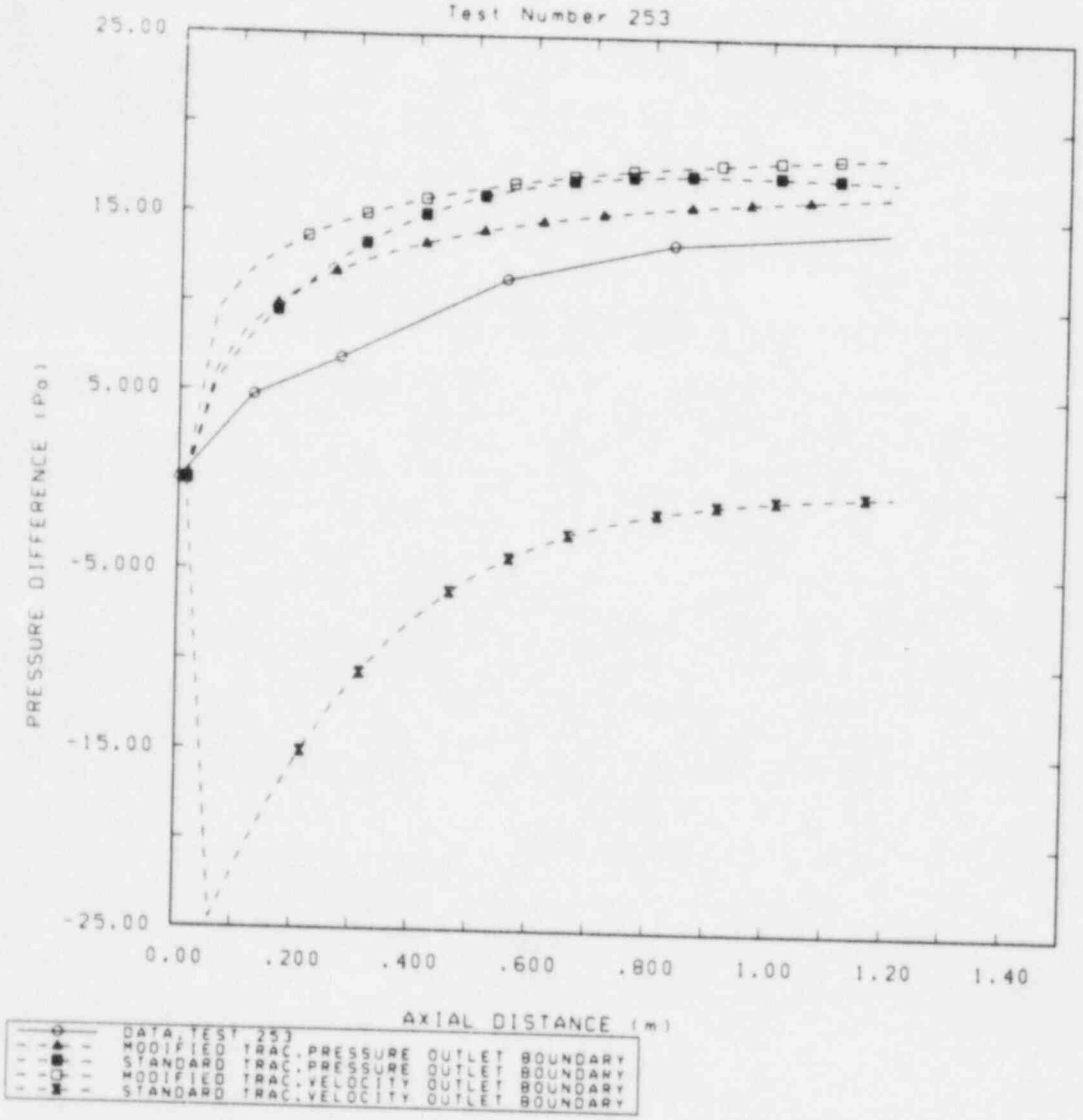

Figure 4.2.2 Differential Pressure Profiles for Test 253 with Two Outlet Boundary Conditions; Effect of Modified Interfacial Energy and Momentum Transfer Models

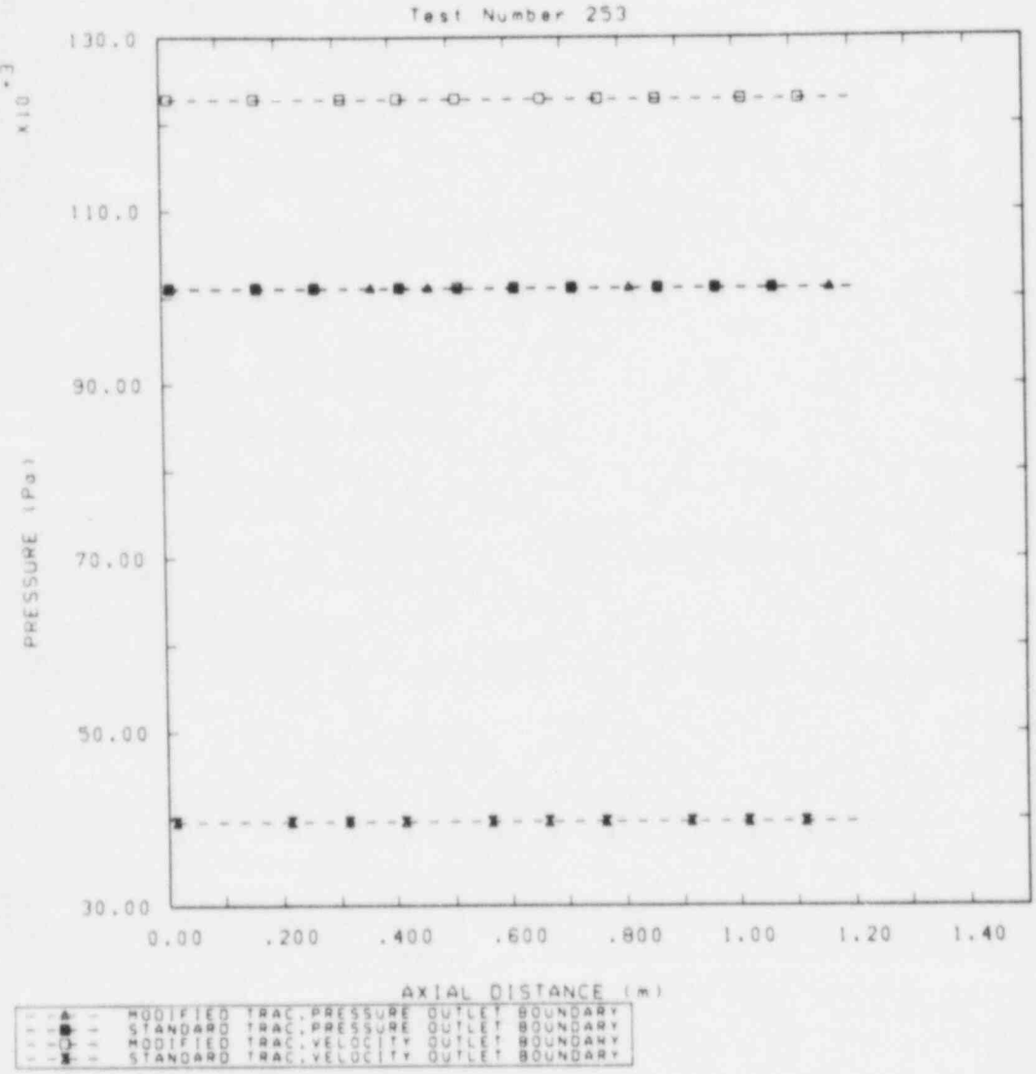

Figure 4.2.3 Pressure Profiles for Test 253 with Two Outlet Boundary Conditions; Effect of Modified Interfacial Energy and Momentum Transfer Models

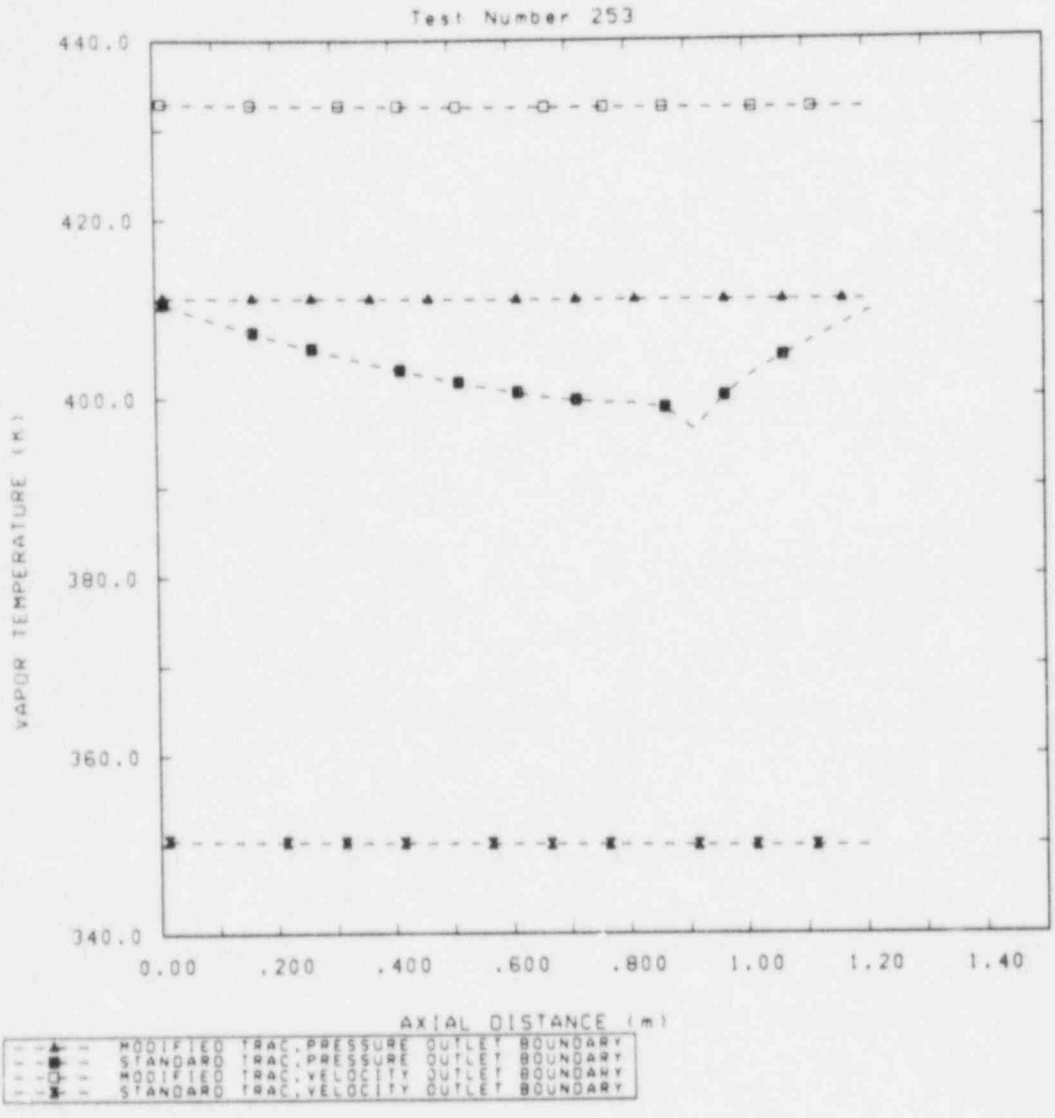

Figure 4.2.4 Vapor Temperature Profiles for Test 253 with Two Outlet Boundary Conditions; Effect of Modified Interfacial Energy and Momentum Transfer Models

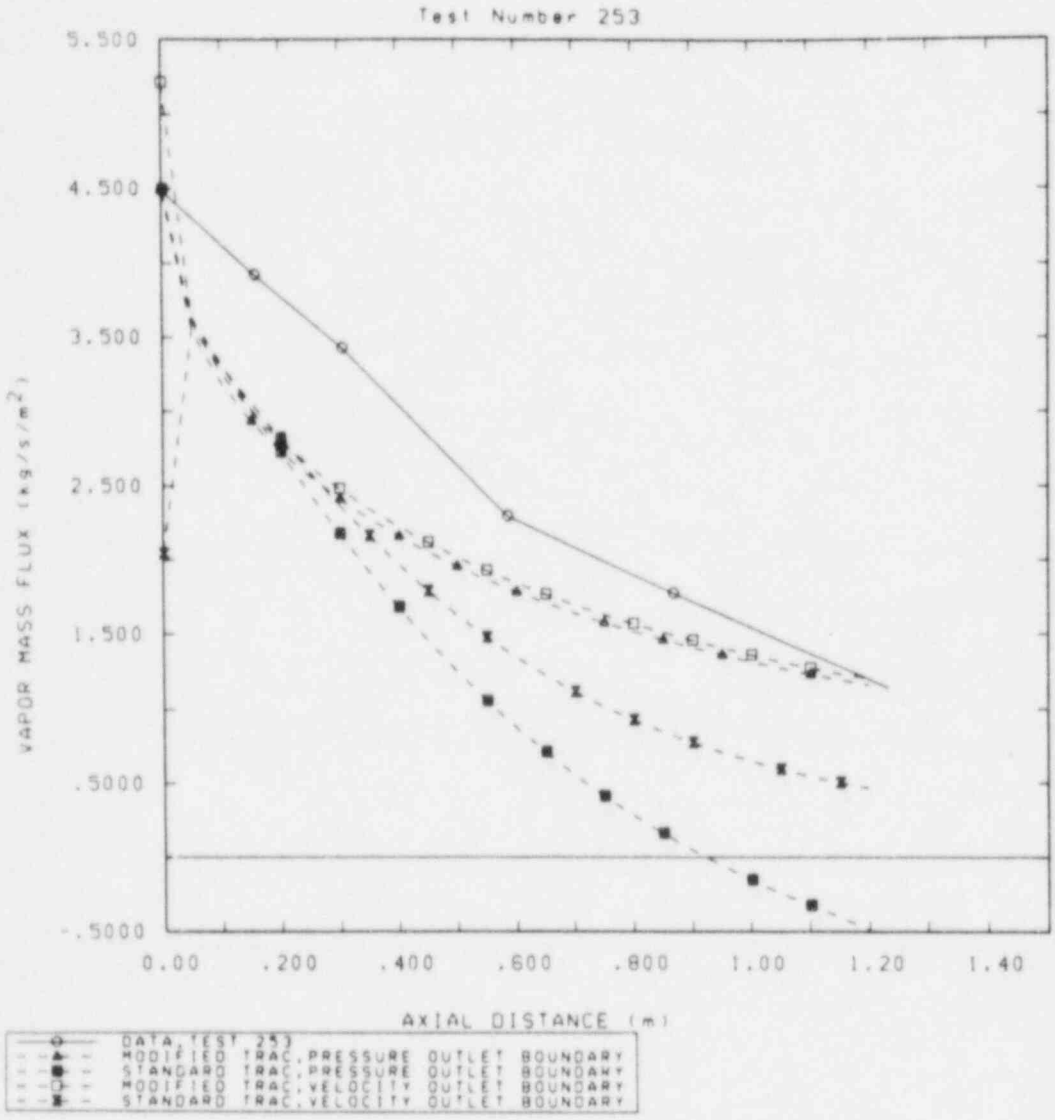

Figure 4.2.5 Vapor Flux Profiles for Test 253 with Two Outlet Boundary Conditions; Effect of Modified Interfacial Energy and Momentum Transfer Models

5.0 Results of Variations in Inlet Conditions

As mentioned above, direct quantitative comparison of TRAC and experimental results is impossible because of geometric differences. For this reason, we decided early in the study to perform calculations for only a few of the experiments described in Reference 2, with the primary goal of assessing the qualitative effects of changes in the inlet conditions. Further, variations in inlet volume fractions would only complicate the difficulty with the geometry of the flow channel. Because of the inlet liquid temperature discrepancy alluded to earlier, we excluded the experiments with the lowest flow rates. We chose, therefore, to consider combinations of low and high values of inlet flow rates and liquid subcooling, arriving at Tests 253, 259, 293, and 459 (the solid symbols in Figure 2.1); boundary conditions for these tests may be found in Table 5.1. The data report did not provide pressure information for any of the tests with elevated liquid inlet temperature, so we chose outlet pressure for Test 459 equal to the 259 value. We also examined the effects of including air in the vapor. Where test data appear in the discussions and figures in this Section, the reader should remember that strict quantitative comparisons with calculated results are inappropriate.

Table 5.1

Boundary Conditions for the TRAC Analyses [2]

Test	Δp (Pa)	T_v (K)	T_ℓ^I (K)	W_v^I (g/s)	W_ℓ^I (kg/s)	T_ℓ^O (K)	W_v^O (g/s)	α_v^{O*}
253	14.3	411.3	294.8	65.1	0.657	331.7	17.7	0.81
259	71.5	415.5	297.4	159.3	0.765	349.0	72.3	0.91
293	17.9	410.2	298.1	65.2	1.439	319.5	8.6	0.70
459	71.5**	415.5	325.3	156.4	0.709	357.8	101.4	0.90

*All inlet vapor volume fractions are 0.75

**Arbitrarily chosen the same as Test 259 (not tabulated in data report)

5.1 Variation in Inlet Vapor Flow Rate

Test 259 had approximately 2.5 times the vapor mass flow rate at the inlet as did Test 253, and about the same values of liquid inlet flow rate and temperature. As the relative velocity between the phases increases, so should the interfacial heat transfer (hence the condensation rate). The momentum and mass balance equations at a steady state show that an increase in condensation rate corresponds to an increase in pressure gradient, to the extent that changes in wall friction and momentum fluxes are less important.

The pressure profiles in Figure 5.1.1 display the relationship described in the previous paragraph, both with respect to differing experimental conditions and

differing models for interfacial heat transfer. As may be seen in Figure 5.1.2, the difference between vapor flows with the standard and modified treatments was less for the higher inlet vapor flow. Total condensation increased with vapor flow for both models, but the standard treatment yielded a smaller increase.

Figure 5.1.3 shows that, for Test 253, the interface-to-liquid heat transfer terms in the two models differed by a factor nearly as large as 5, while Test 259 results were slightly more equal. Because the difference between saturation and average liquid temperature was smaller for the high-flow case, the condensation rates (Figure 5.1.4) did not display such large disparities as did the heat transfer terms.

5.2 Variation in Inlet Liquid Flow Rate

A comparison of results for Tests 253 and 293 is essentially an assessment of the effects of an increase in inlet liquid flow rate. In this case, the relative velocity between the phases is not much affected, but increased turbulence in the liquid should enhance the transfer of energy from the interface. Both standard and modified models showed an increase in condensation with liquid flow, as may be inferred from Figure 5.2.1. As expected, the low vapor flow, high liquid flow case showed even more "over-condensation" and countercurrent flow with the standard interfacial heat transfer coefficients; the standard liquid-to-interface term is simply proportional to the liquid velocity, and is the most dominant term for this case.

The liquid wall friction coefficients for Tests 253 and 293 (Figure 5.2.2) were virtually the same with the modified treatment, while the standard model coefficients differed for the differing inlet conditions. The pressure profiles, shown in Figure 5.2.3, clearly showed the expected effects of changing the liquid flow rate only for the modified calculation method. Pressure profiles for the standard analyses were fairly similar, with the exception that, for Test 293, the liquid momentum flux became large enough to effect a negative pressure gradient for about the last fifth of the flow path. Quantitative differences between the results with the standard models do not appear very significant, and this seems to support our expectation that changes in interfacial heat transfer would be more important than changes in wall friction.

The standard model calculation for Test 293 was the only one which showed vapor volume fractions between 0.5 and 0.75, and these results exposed some rather peculiar features in the computational model for the vapor-to-interface energy transfer term (the product of the heat transfer coefficient and the area). In this situation, TRAC performs a cubic interpolation (in the vapor volume fraction) between the annular or annular-mist and bubbly slug flow regimes to arrive at an interfacial area term. The heat transfer coefficient for the bubbly regime is set to one thousand (ten thousand if the vapor is subcooled), and the coefficient-area product combined with the corresponding term for the annular regime. If the vapor is not superheated, -- whether or not the interpolation was made -- the final result (in SI units) is required to be no less than the larger of one thousand times the flow area and ten million times the cell volume. Single-timestep increases and decreases in the interface terms are also limited to factors of two and one-tenth, respectively. Thus, the cell size in a calculation can have an unexpected (and probably unreasonable) effect on the results.

With the standard interface treatment for Test 293, the vapor temperature dropped rapidly to saturation, then repeatedly increased and returned to, or below, saturation. Figure 5.2.4 demonstrates this behavior for a cell at the midpoint of the flow path. As may be seen more clearly in the vapor superheat history in Figure 5.2.5, this situation seemed not to have disappeared by the time of the last record on the graphics output file. That file does not contain results from the cycle on which the coding determines that a steady state has been reached. The vapor-to-interface heat transfer term shown in Figure 5.2.6 was also uncharacteristic of steady-state conditions, and displayed the results of the limiting procedures described in the previous paragraph. (The graphics edit frequency in this calculation was 2 s, and a cell volume approximately 4.8x10**-4 m**3.) We also observed that the signal-variable values of interface-related terms and wall friction were zero on the zeroth-cycle edit. The large changes from initial conditions, therefore, may not be entirely caused by the geometric dichotomy inherent in obtaining those conditions.

5.3 Variation in Inlet Liquid Temperature

Tests 259 and 459 have virtually the same inlet flows for both phases, but the liquid in Test 459 is approximately 27 K warmer at the inlet. Because the liquid-to-interface energy transfer dominates, and depends on the amount of liquid subcooling, Test 259 should have the higher condensation rates and higher overall condensation. Figures 5.3.1 and 5.3.2 show that both the standard and modified treatments yielded the proper relationship between these quantities.

As mentioned earlier, the only vapor temperatures that appear in the report are those at the inlet, which we assume means that any recorded temperatures were essentially constant for a given test. The experimenters' analysis of the data (see Appendix A) reinforces this assumption. Vapor-to-interface energy transfer had a very small effect on condensation rates, but the same is not true of its effects on vapor temperature. Figure 5.3.3 shows that the modified model did result in a virtually uniform temperature, while the standard version for both Tests 259 and 459 calculated the vapor to be cooled by about 30 K by the time it reached the outlet. Vapor-to-interface heat transfer terms (Figure 5.3.4) differed by nearly two orders of magnitude between the models.

5.4 Analyses with Air Included

According to the TRAC manual, the presence of noncondensable gas can effect a large reduction in the calculated amount of condensation. The vapor-to-interface contribution is multiplied by the ratio of the water partial pressure to the total pressure, and the liquid-to-interface term by a function of steam, liquid, and noncondensable densities. In order to assess the magnitude of this effect, we performed calculations for Tests 293 and 459, this time including air at a mass fraction of about 3 % (referred to the vapor) at the inlet. This number was chosen quite arbitrarily, since no data on this quantity are given in the report. Some time after these calculations were done, however, we became aware of a continuation [4] of the work described in Reference 2, using an improved version of the experimental apparatus and a wider range of flows. In the more recent publication, the steam supply is described as containing about 3 ppm of air and 20 ppm of an anticorrosion agent, diethylaminoethanol. Because we were interested principally in qualitative effects, we did not attempt to make use of the later information. As was the case with previous calculations, we used both the standard model and the modifications to wall shear and interfacial heat transfer.

For Test 293, the inclusion of a relatively large amount of air reduced the calculated amount of condensation with the standard TRAC model, as shown by the vapor mass flow and condensation rate profiles in Figures 5.4.1 and 5.4.2. Figures 5.4.3 and 5.4.4 respectively display the interfacial energy transfer terms for the four Test 293 calculations, and the large changes produced when air was included and the standard treatment used. Our modification has no explicit treatment for a noncondensable gas, so those results showed no significant differences. The interpolation and limiting procedures for vapor-to-interface energy transfer and its changes, described in the previous Section, are the source of the rather peculiar profile for the standard result without air in Figure 5.4.4. The high points in the figure are five and ten million times the value of the cell volume in our nodalization. Vapor temperatures (Figure 5.4.5) show that the standard treatment resulted in much more cooling of the vapor; even in the presence of air, the vapor temperature was unreasonably low.

In the case of Test 459, contrary to expectation, the standard treatment with air included yielded more condensation in the downstream four-fifths of the flow path, as shown in Figure 5.4.6. The standard condensation results were higher than the modified ones over most of the flow distance, whether or not air is included. However, condensation near the inlet with the modified treatment was large enough that vapor flows (Figure 5.4.7) were lower than those from either of the standard calculations, except very near the outlet. Figure 5.4.8 compares the vapor-to-interface heat transfer terms from the four calculations; the standard result with air was forced by a min/max limit in the coding to be 10**7 times the cell volume throughout the downstream 1 m of the channel. The consequent energy loss was sufficient to cause TRAC to predict subcooled vapor in that calculation, as shown in Figure 5.4.9. In the code model, a negative vapor-to-interface heat flux contributes to condensation, and this overcame the reduction in interface-to-liquid flux, producing the unexpectedly higher condensation rate.

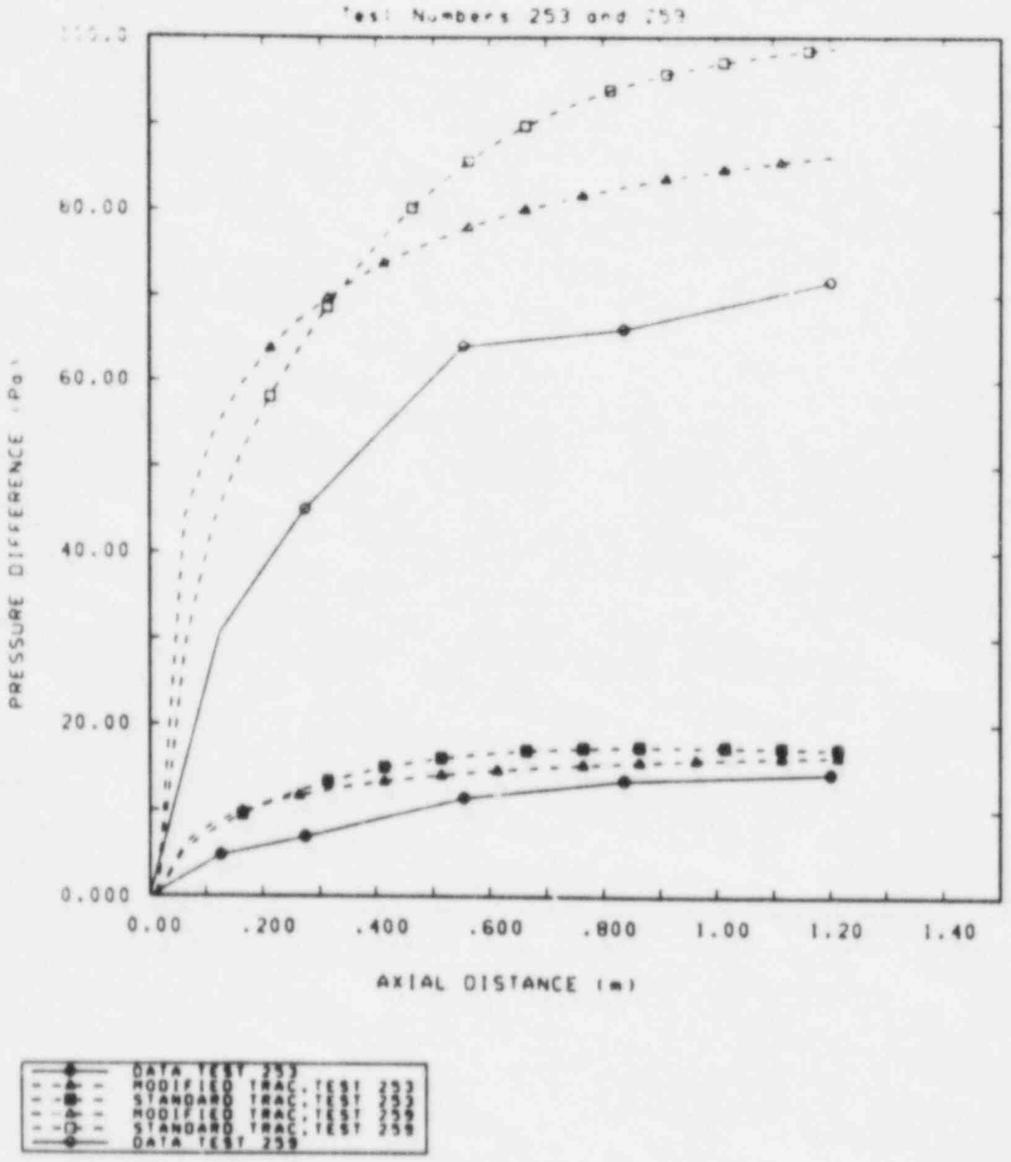

Figure 5.1.1 Differential Pressure Profiles for Tests 253 and 259

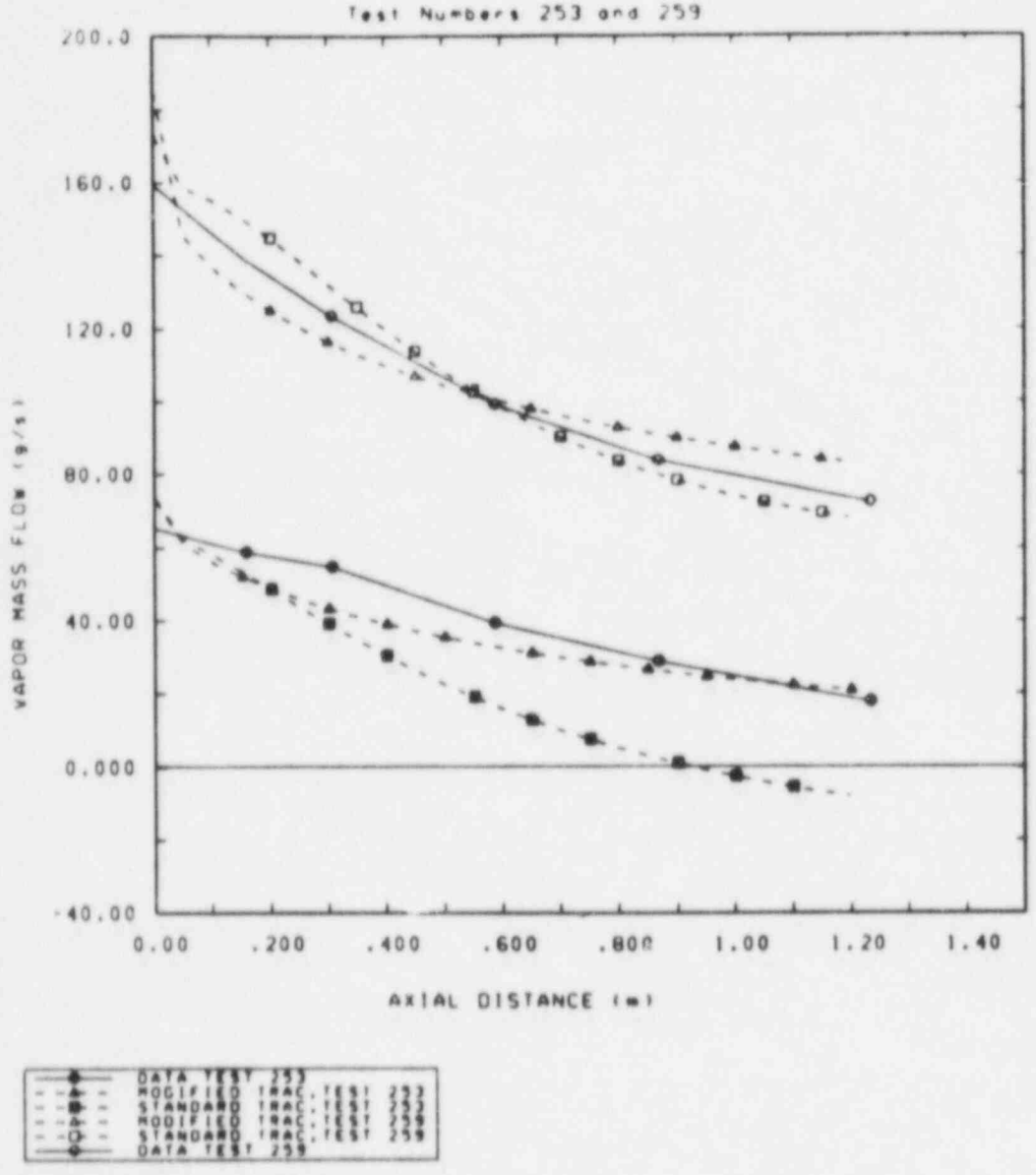

Figure 5.1.2 Vapor Flow Profiles for Tests 253 and 259

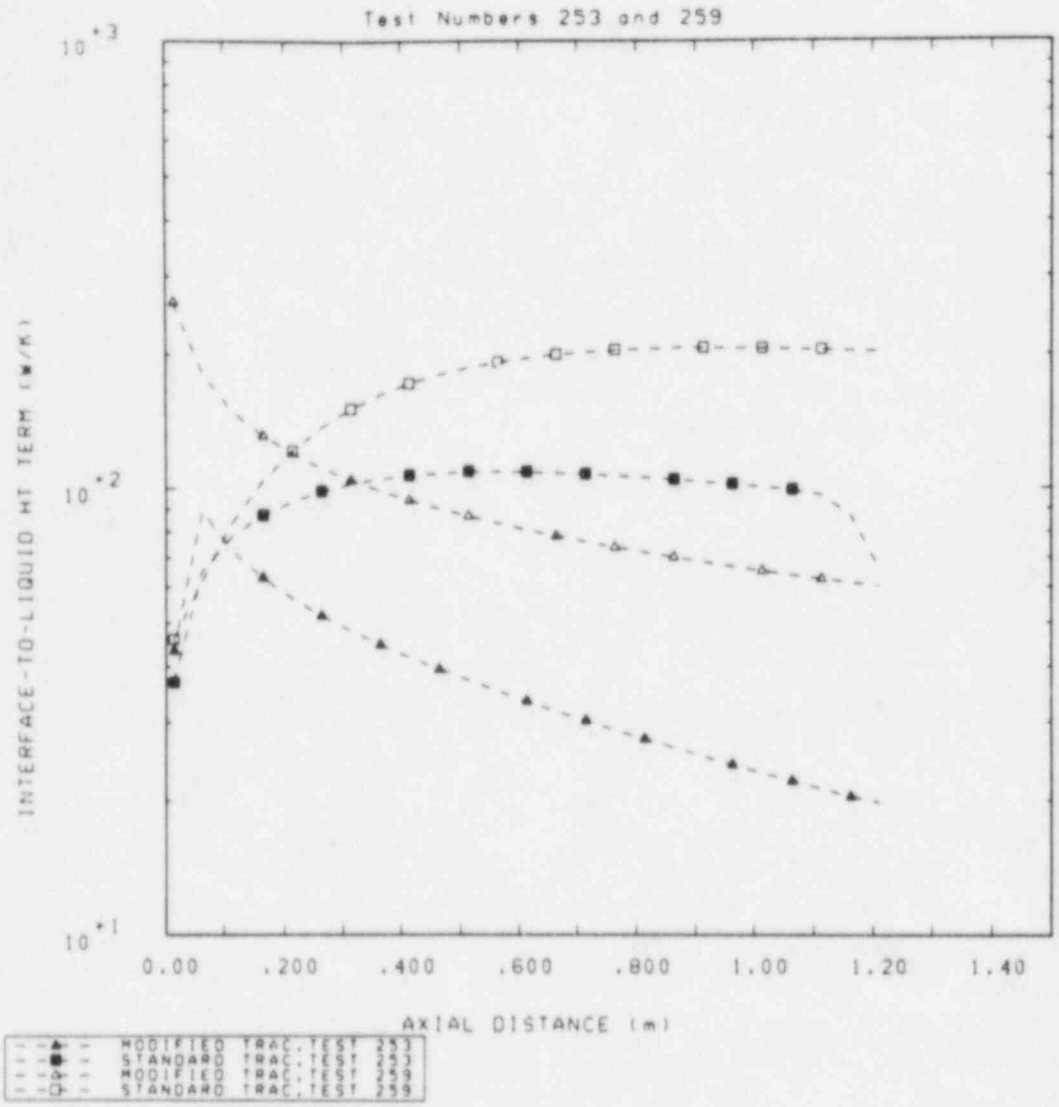

Figure 5.1.3 Interface-to-Liquid Heat Transfer Terms from Standard and Modified Calculations, Tests 253 and 259

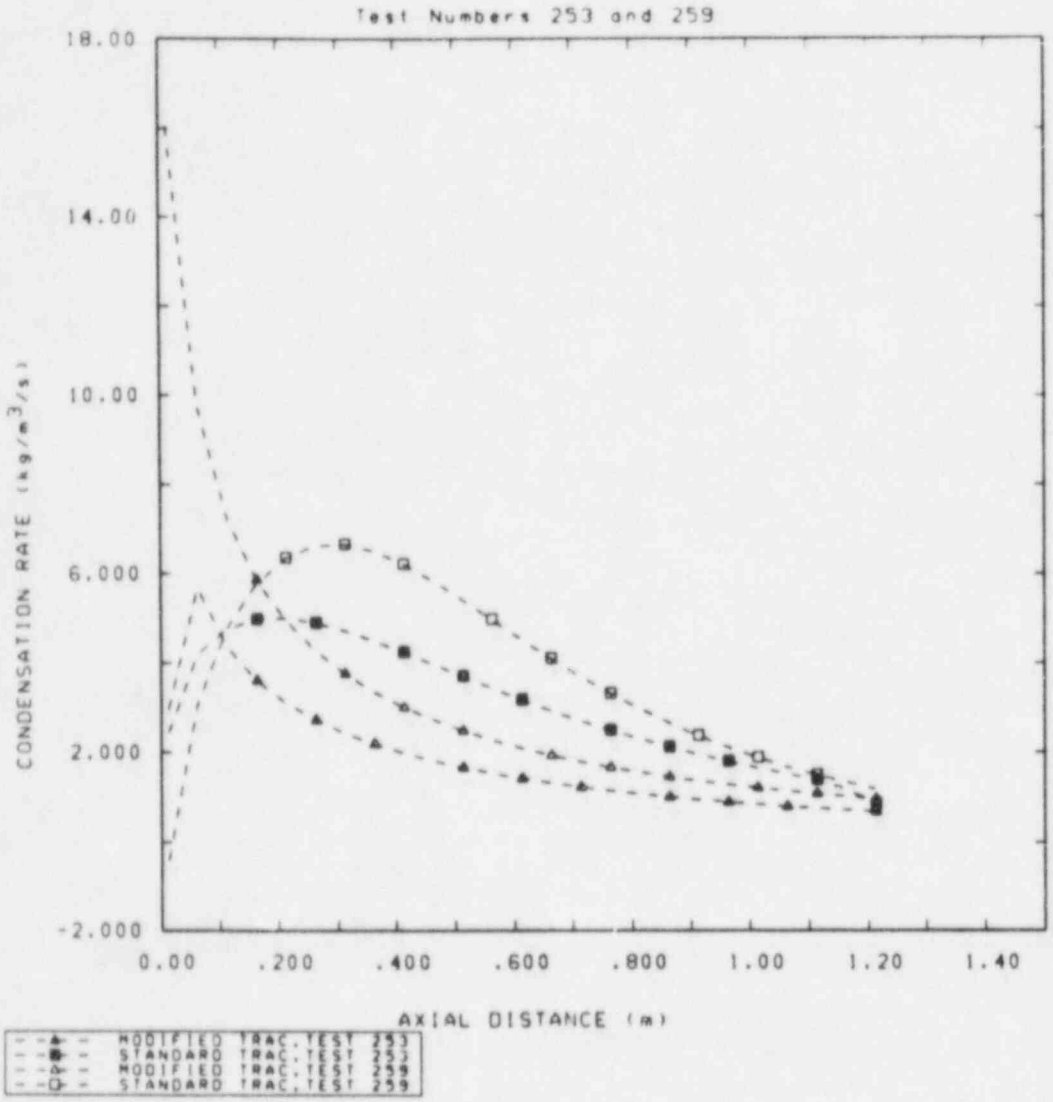

Figure 5.1.4 Condensation Rates from Standard and Modified Calculations, Tests 253 and 259

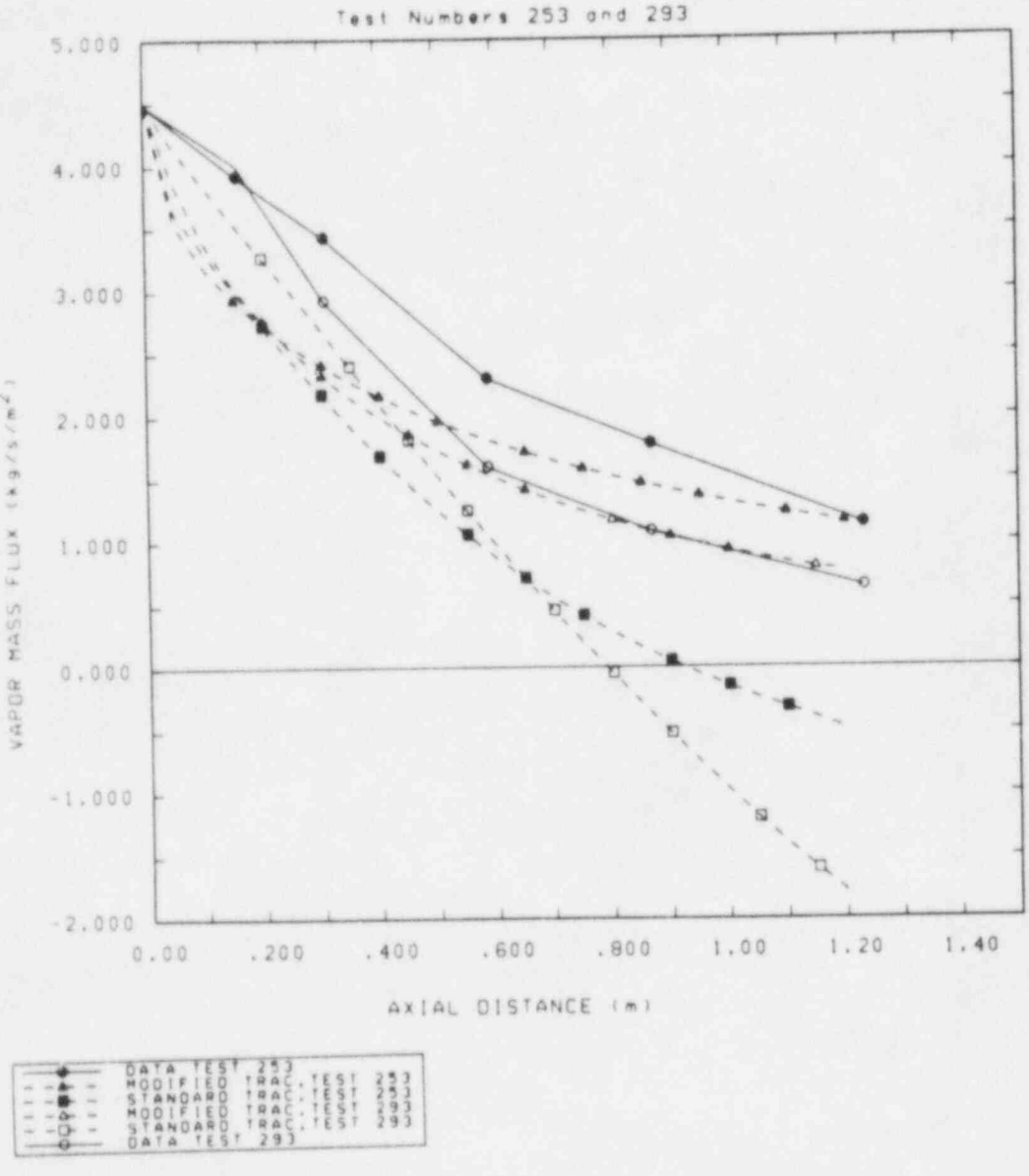

Figure 5.2.1 Vapor Mass Fluxes for Low Vapor Inlet Flow Cases (Tests 253 and 293)

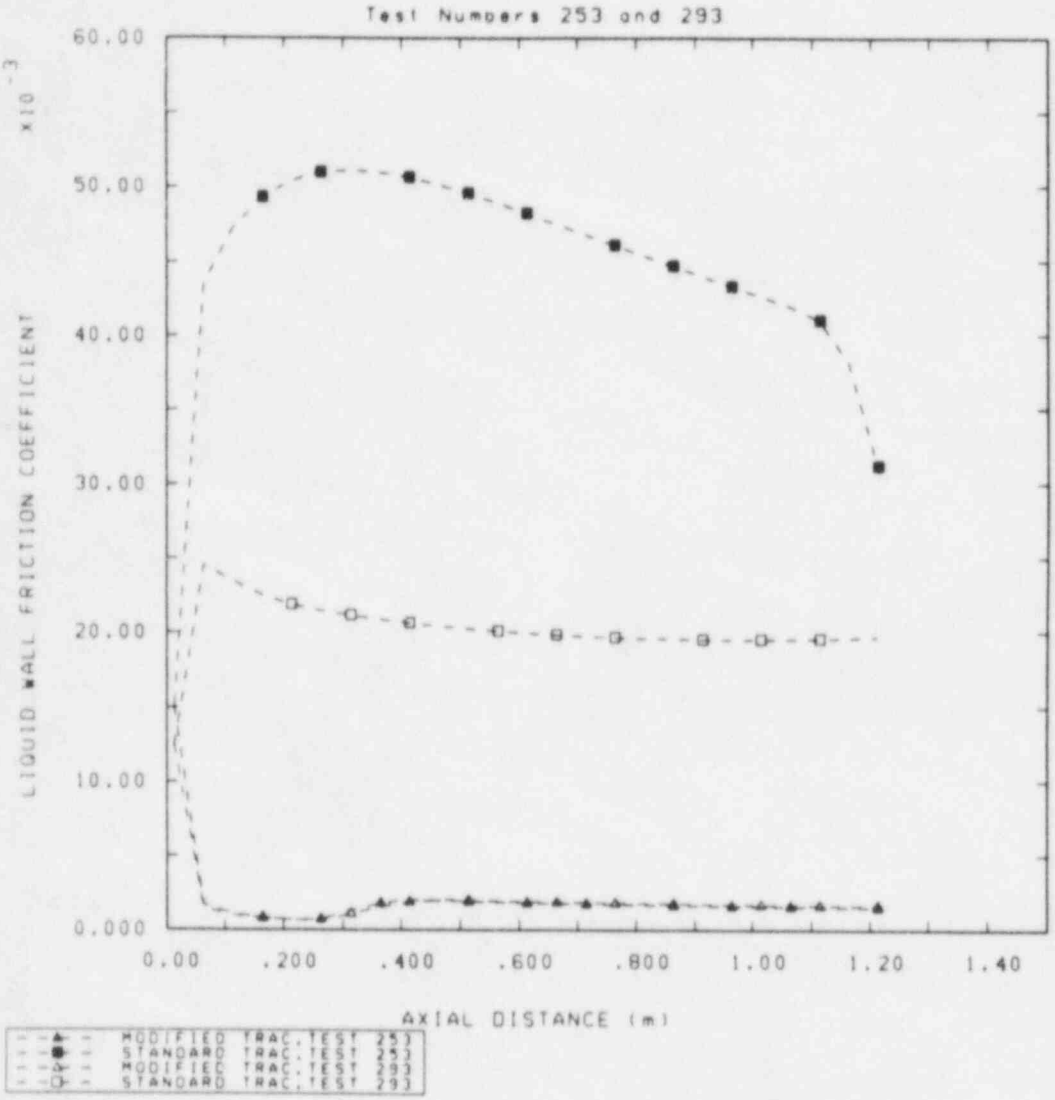

Figure 5.2.2 Liquid Wall Shear Coefficients for Tests 253 and 293

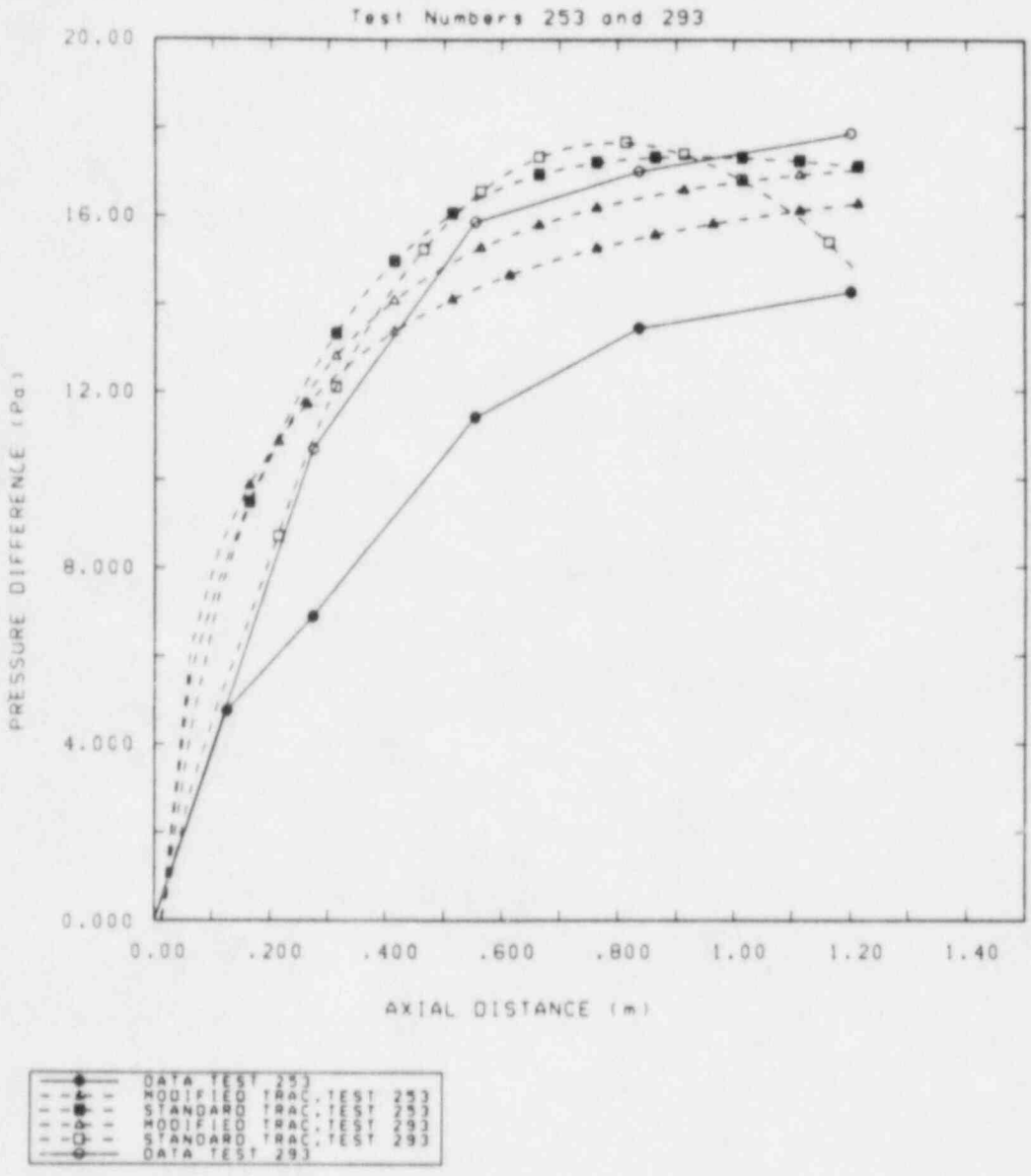

Figure 5.2.3 Differential Pressure Profiles for Tests 253 and 293

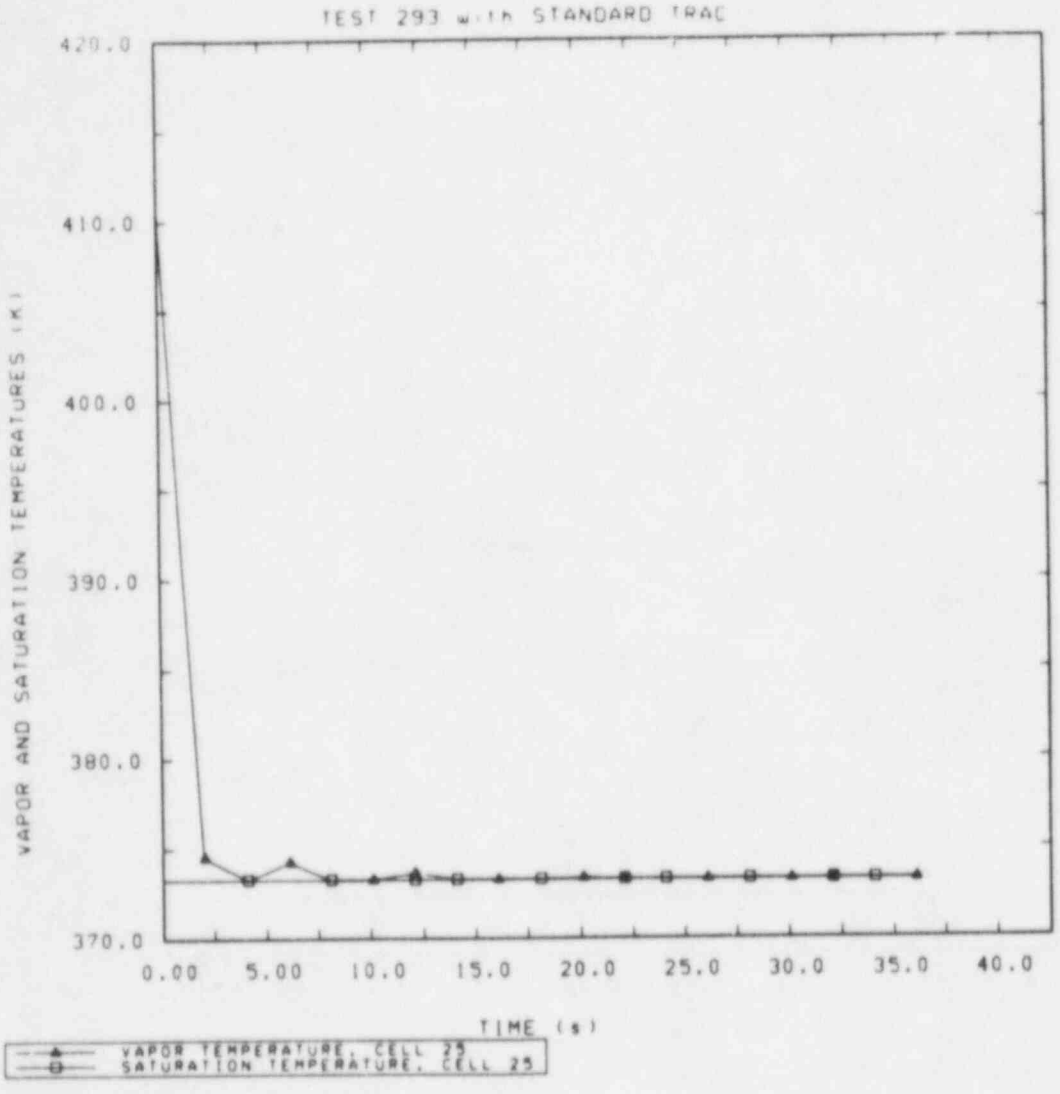

Figure 5.2.4 Vapor Temperature at Flow Path Midpoint (Test 293)

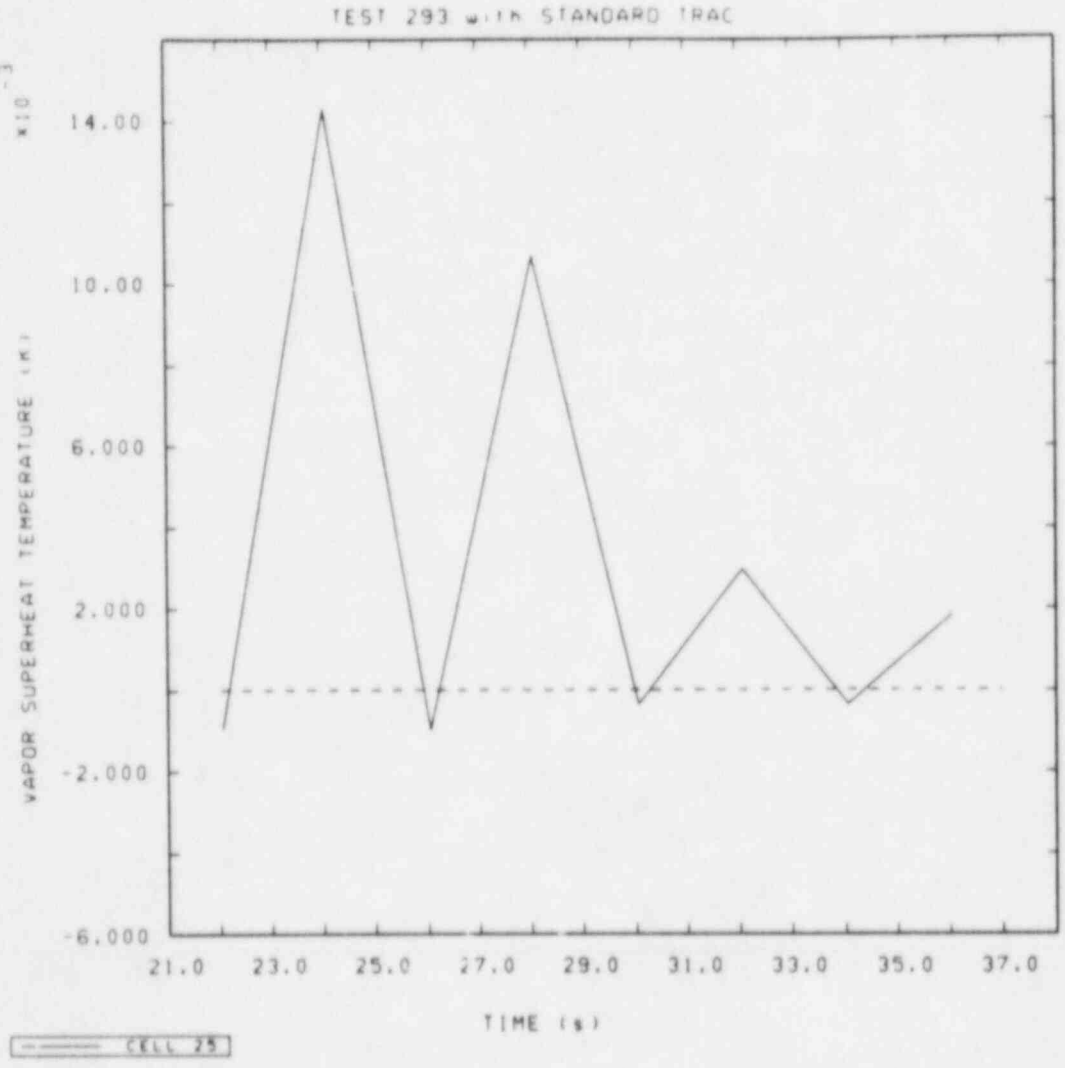

Figure 5.2.5 Vapor Superheat Temperature at Flow Path Midpoint (Test 293)

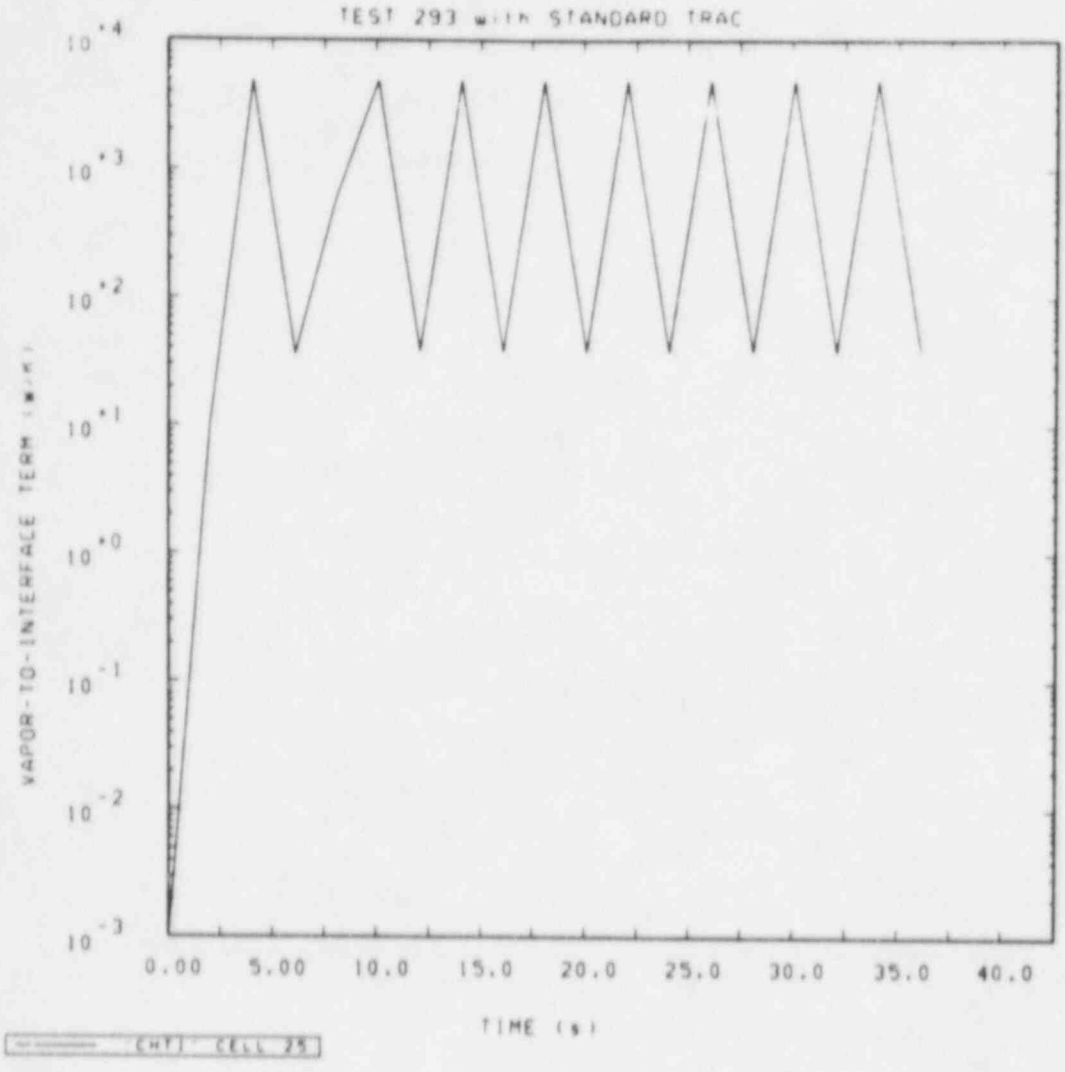

Figure 5.2.6 Vapor-to-Interface Heat Transfer Term (Test 293)

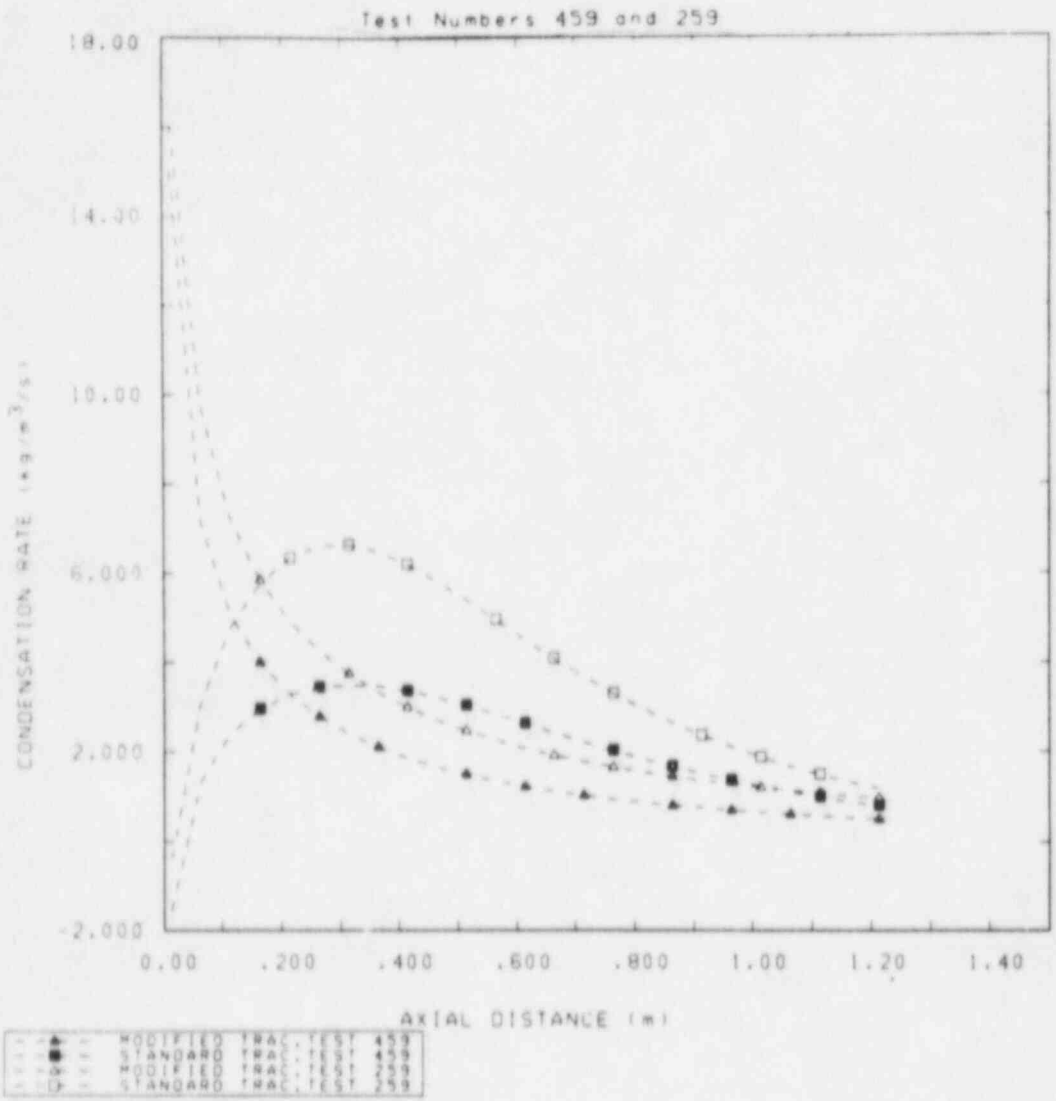

Figure 5.3.1 Condensation Rate Profiles for Tests 259 and 459

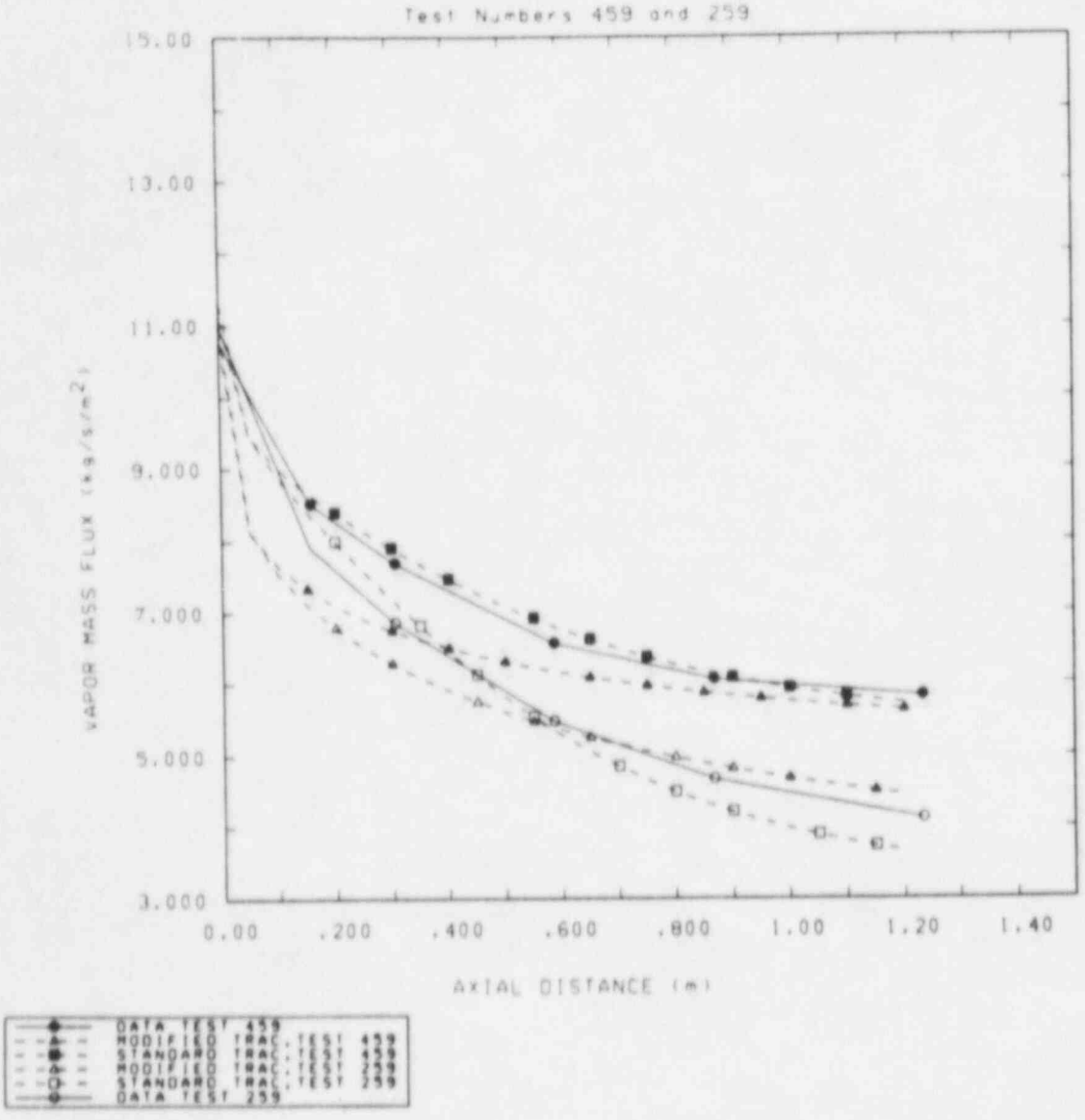

Figure 5.3.2 Vapor Mass Flux Profiles for Tests 259 and 459

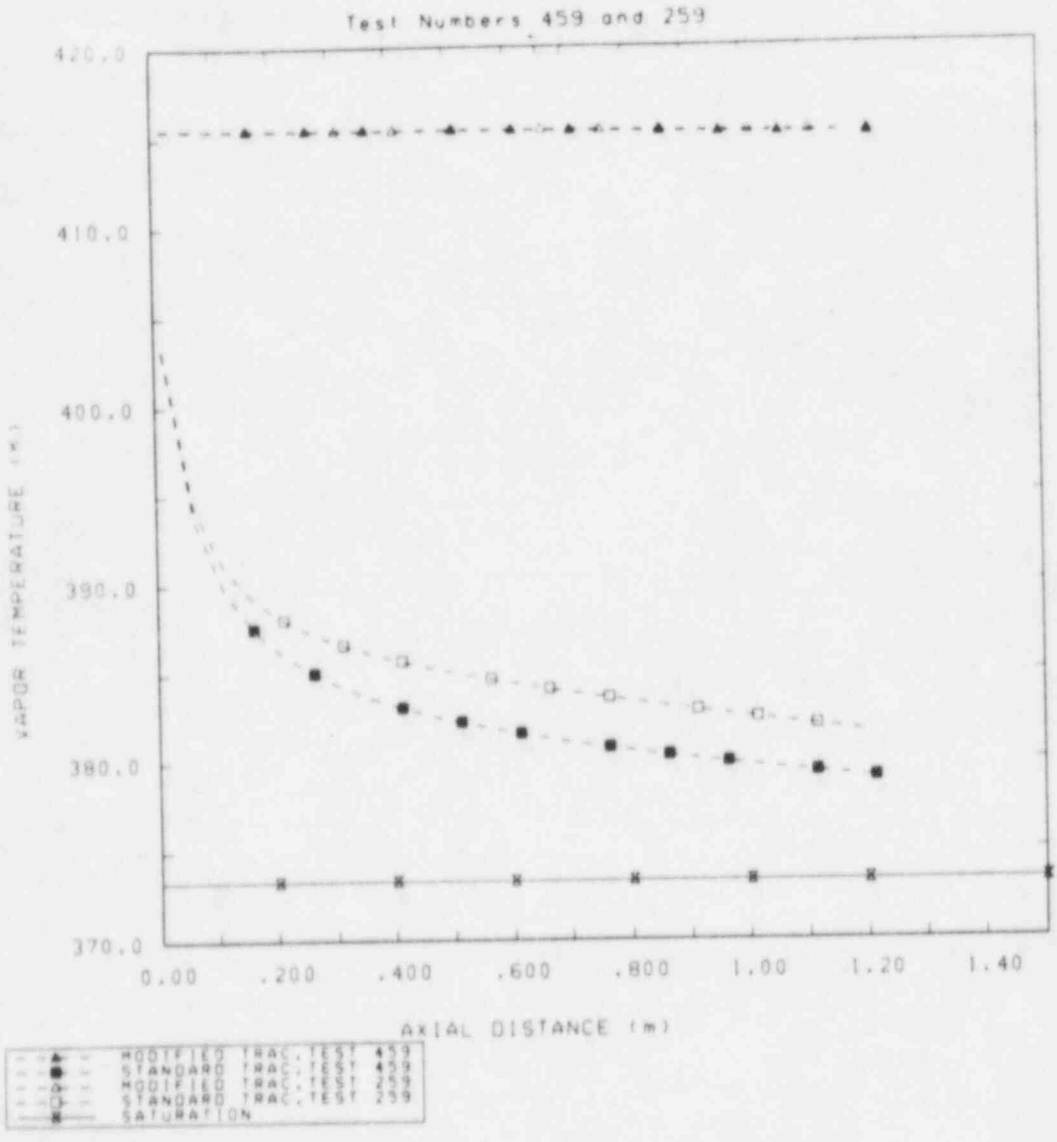

Figure 5.3.3 Vapor Temperatures for Tests 259 and 459

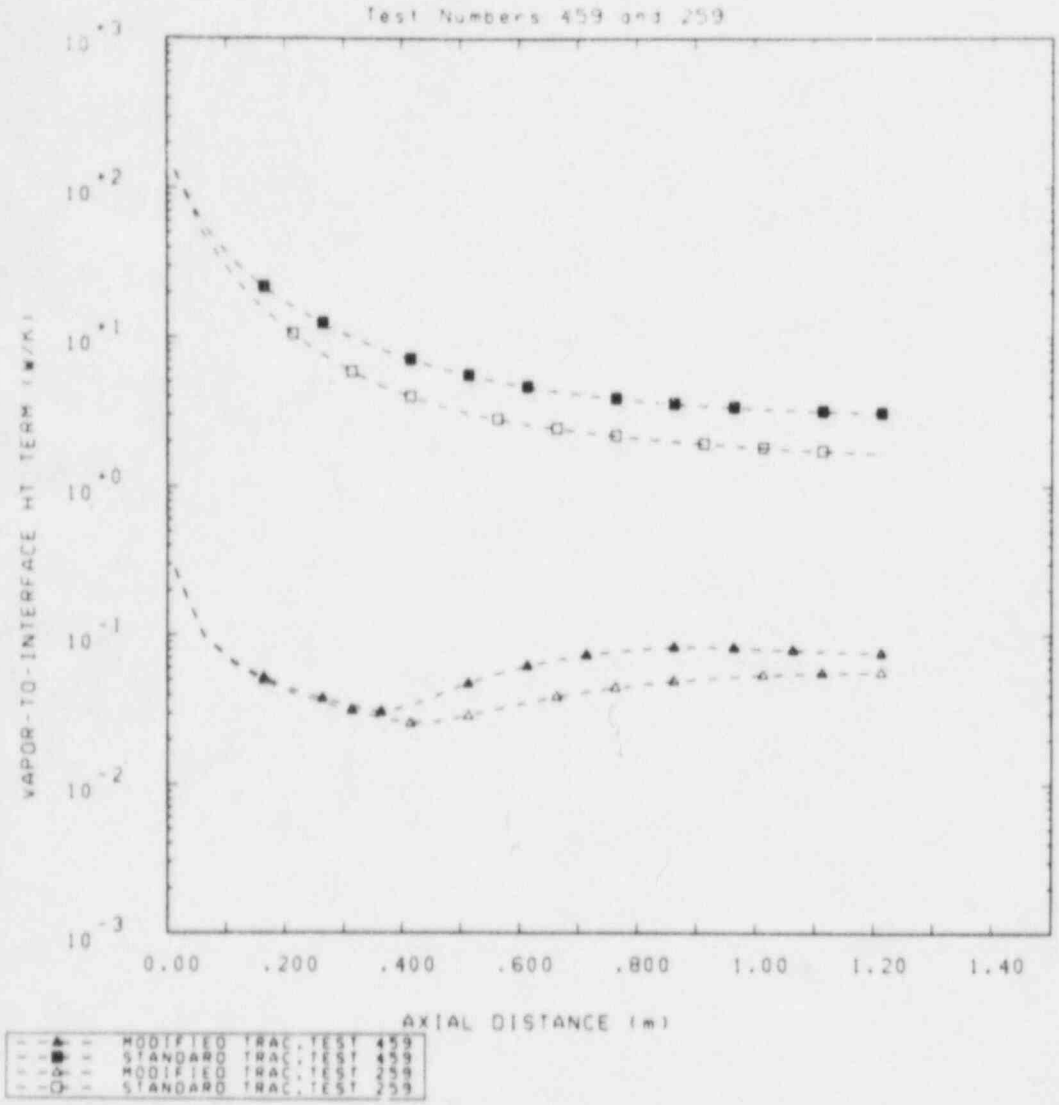

Figure 5.3.4 Vapor-to-Interface Heat Transfer Terms (Tests 259 and 459)

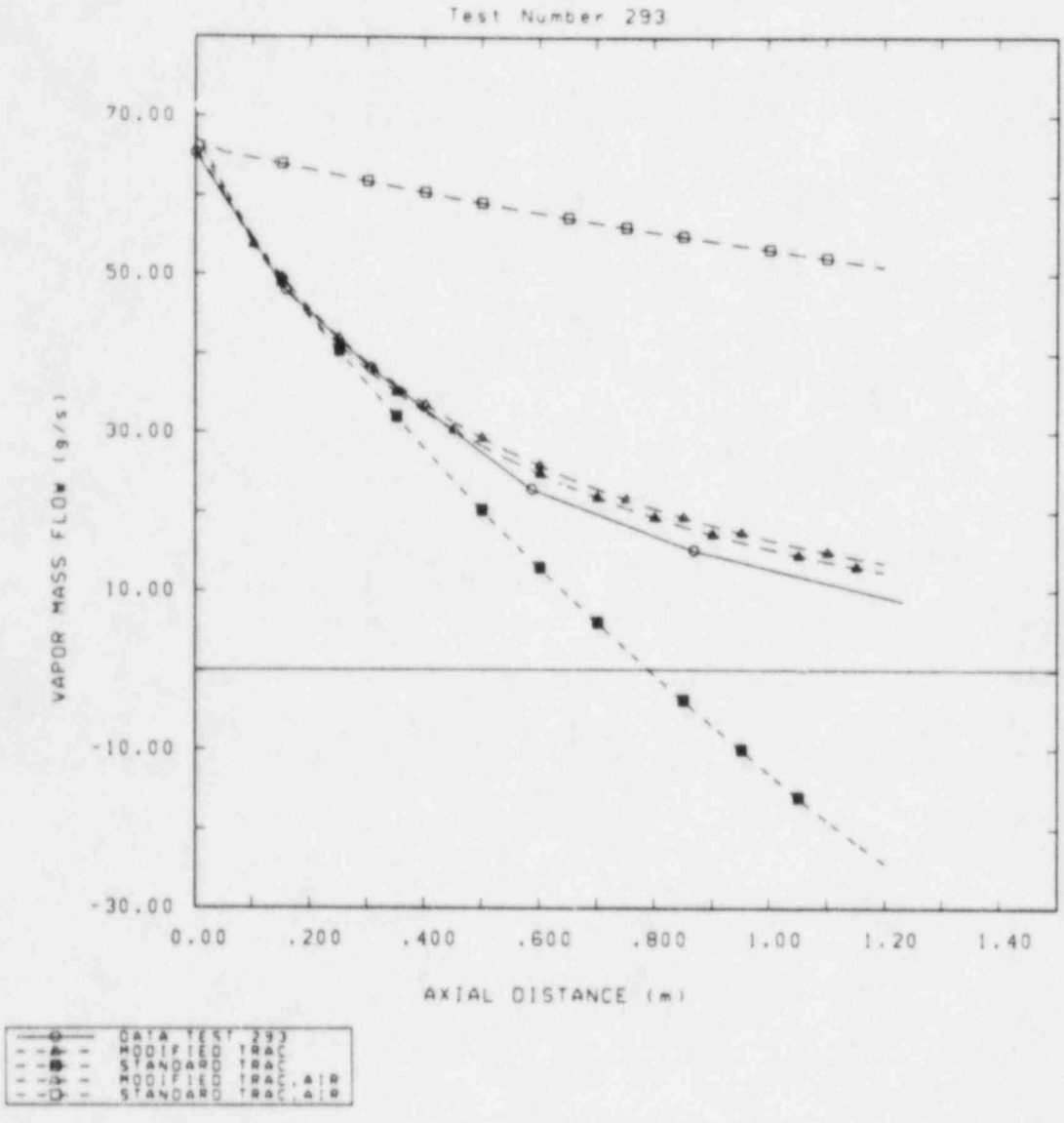

Figure 5.4.1 Vapor Mass Flows for Low Vapor Inlet Flow Case (Test 293), with and without Air in the Vapor

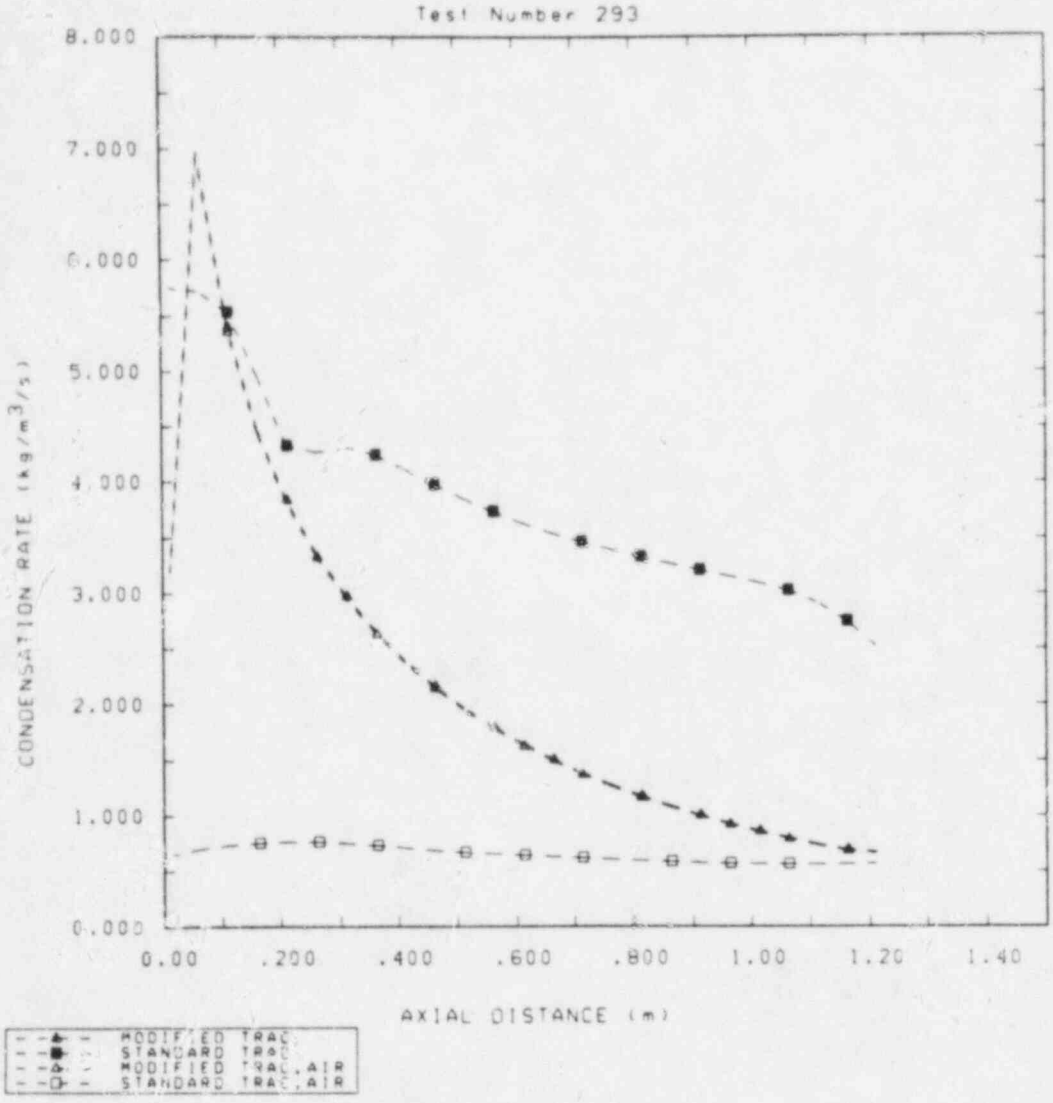

Figure 5.4.2 Condensation Rates for Low Vapor Inlet Flow Case (Test 293), with and without Air in the Vapor

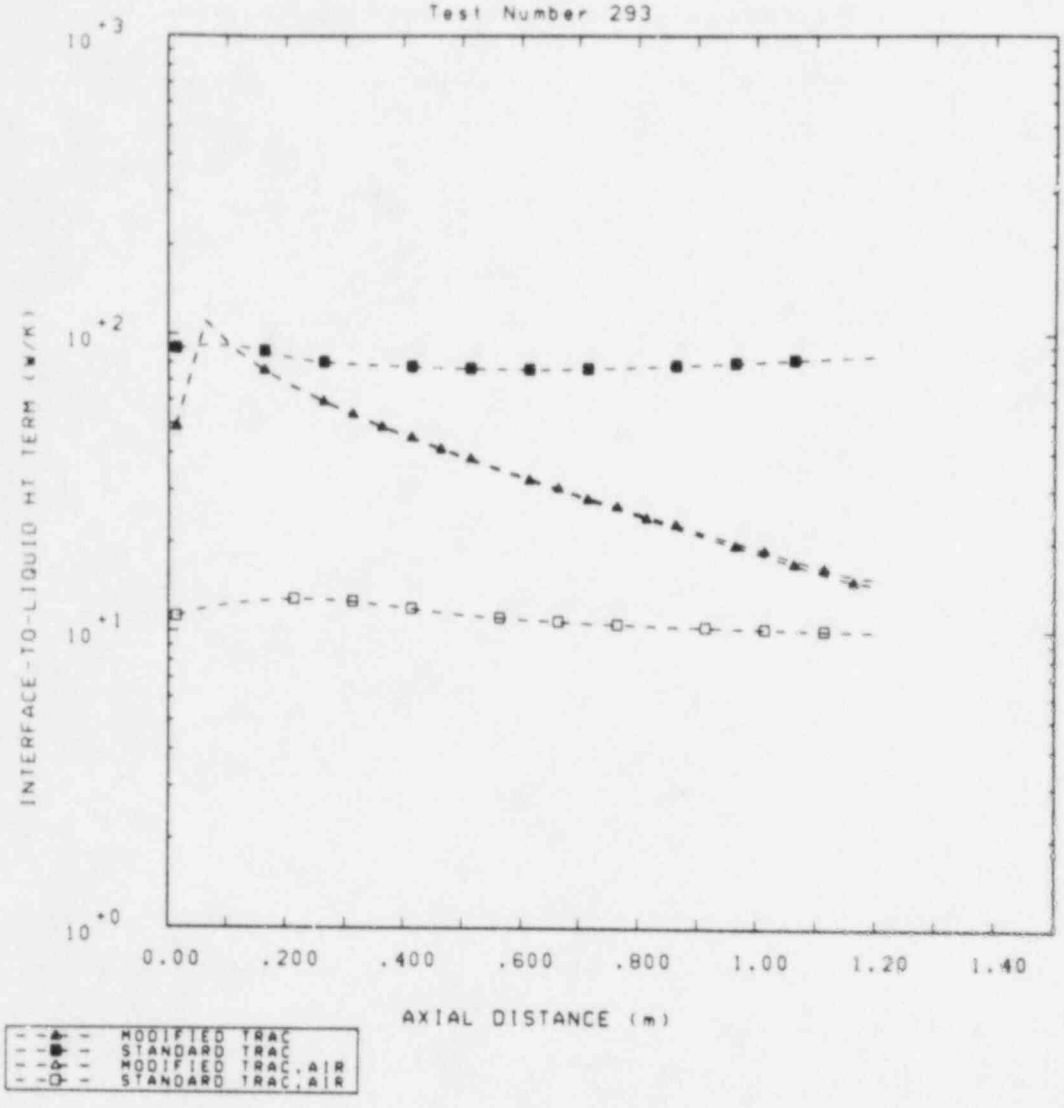

Figure 5.4.3 Interface-to-Liquid Heat Transfer Terms for Test 293, with and without Air

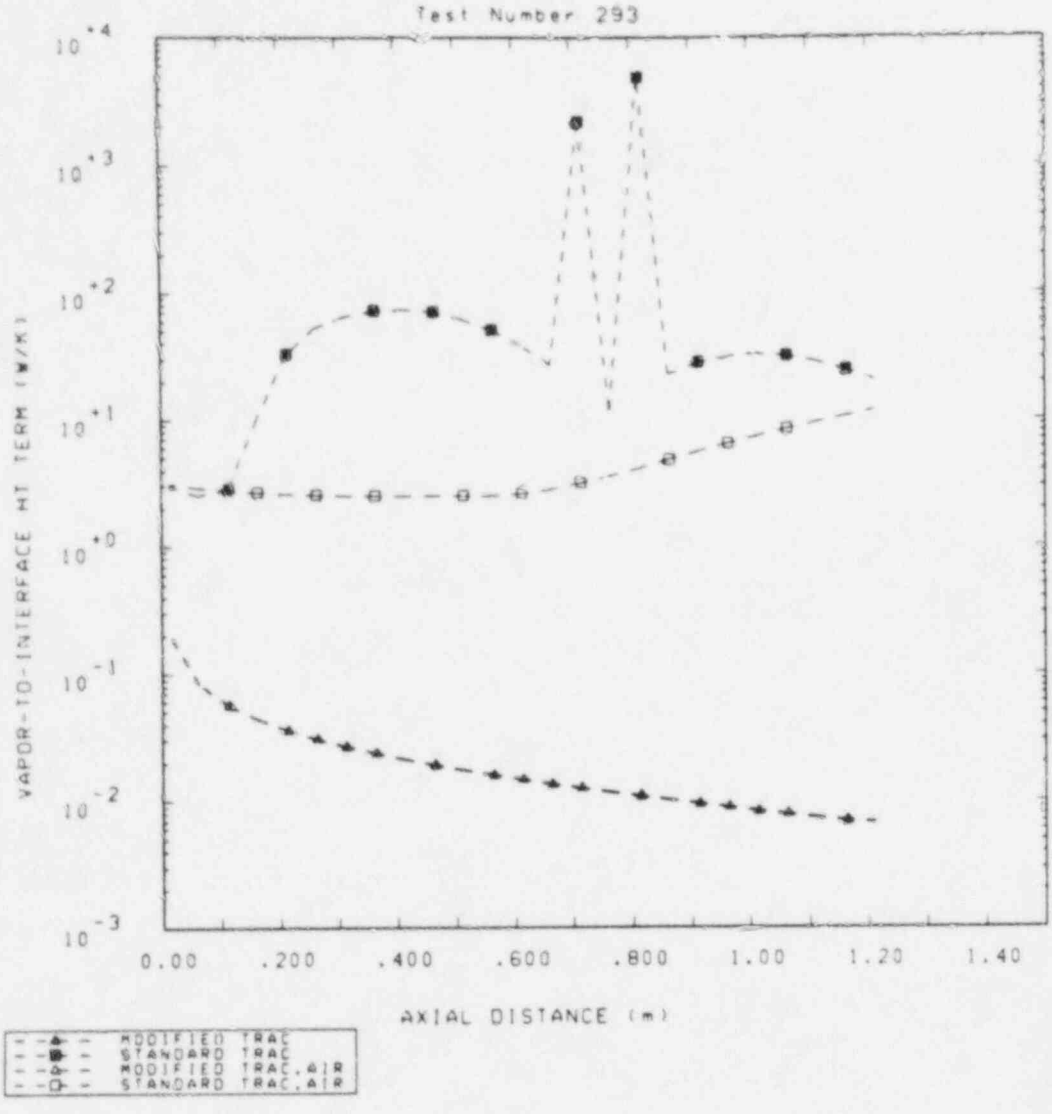

Figure 5.4.4 Vapor-to-Interface Heat Transfer Terms for Test 293, with and without Air

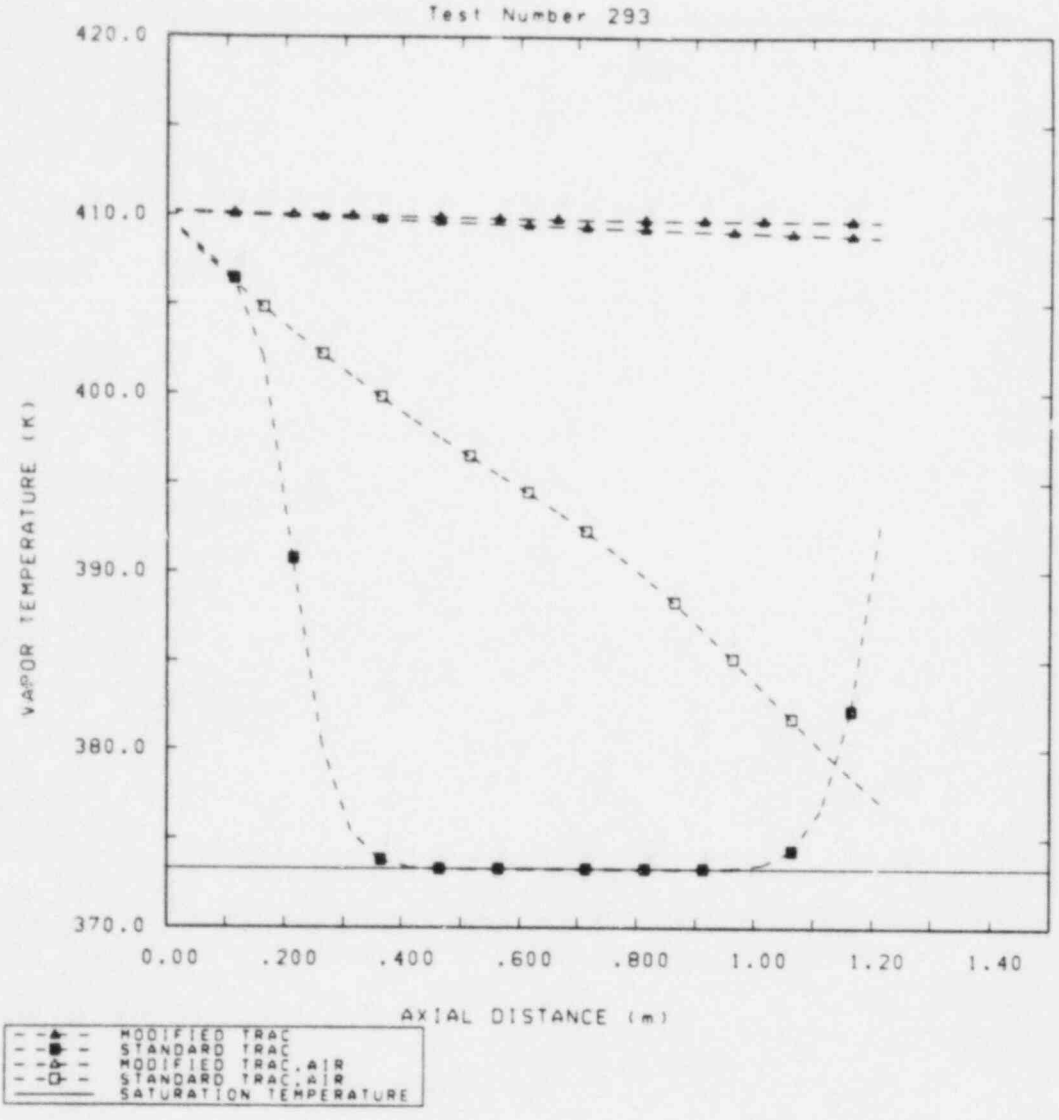

Figure 5.4.5 Vapor Temperatures for Test 293, with and without Air

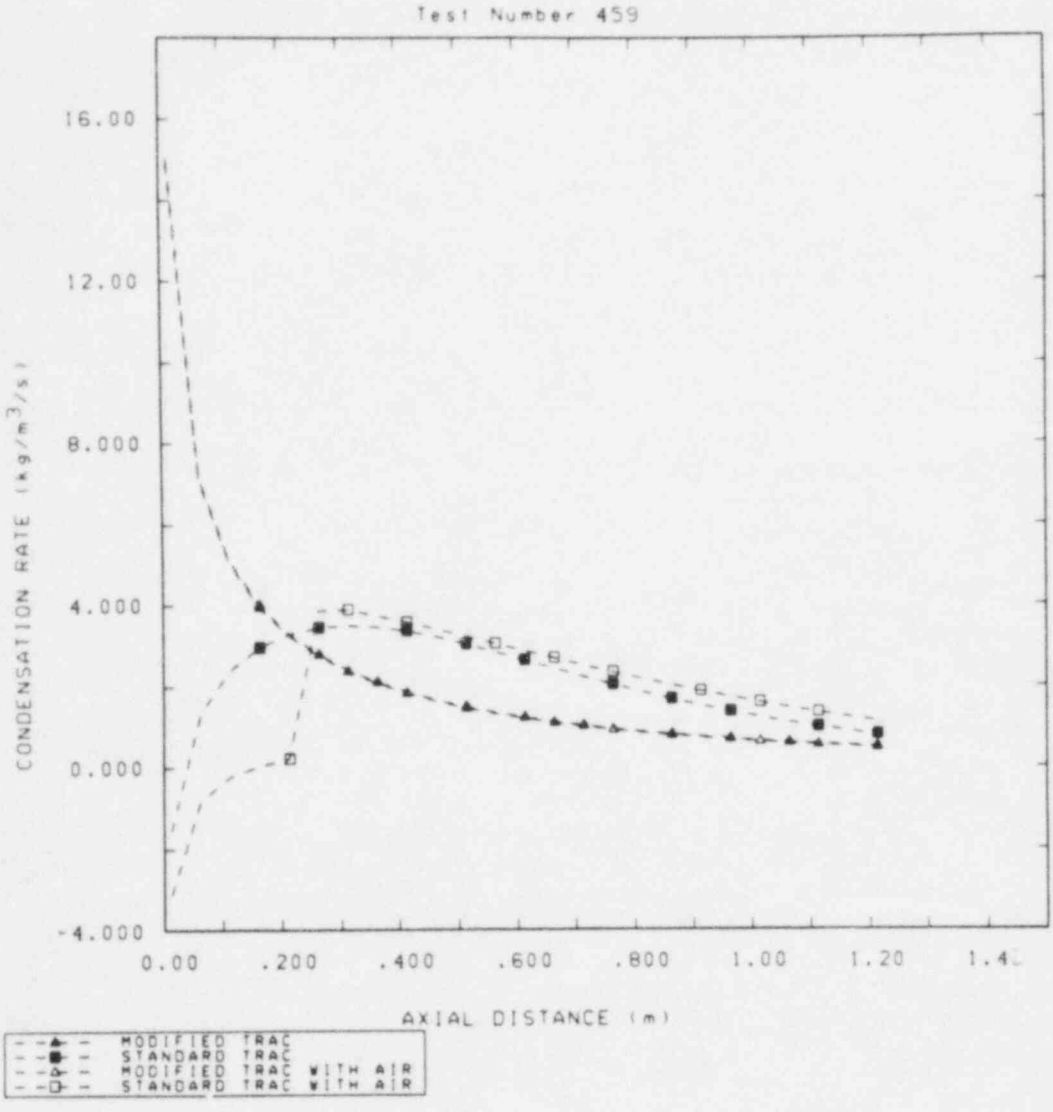

Figure 5.4.6 Condensation Rates for Test 459, with and without Air

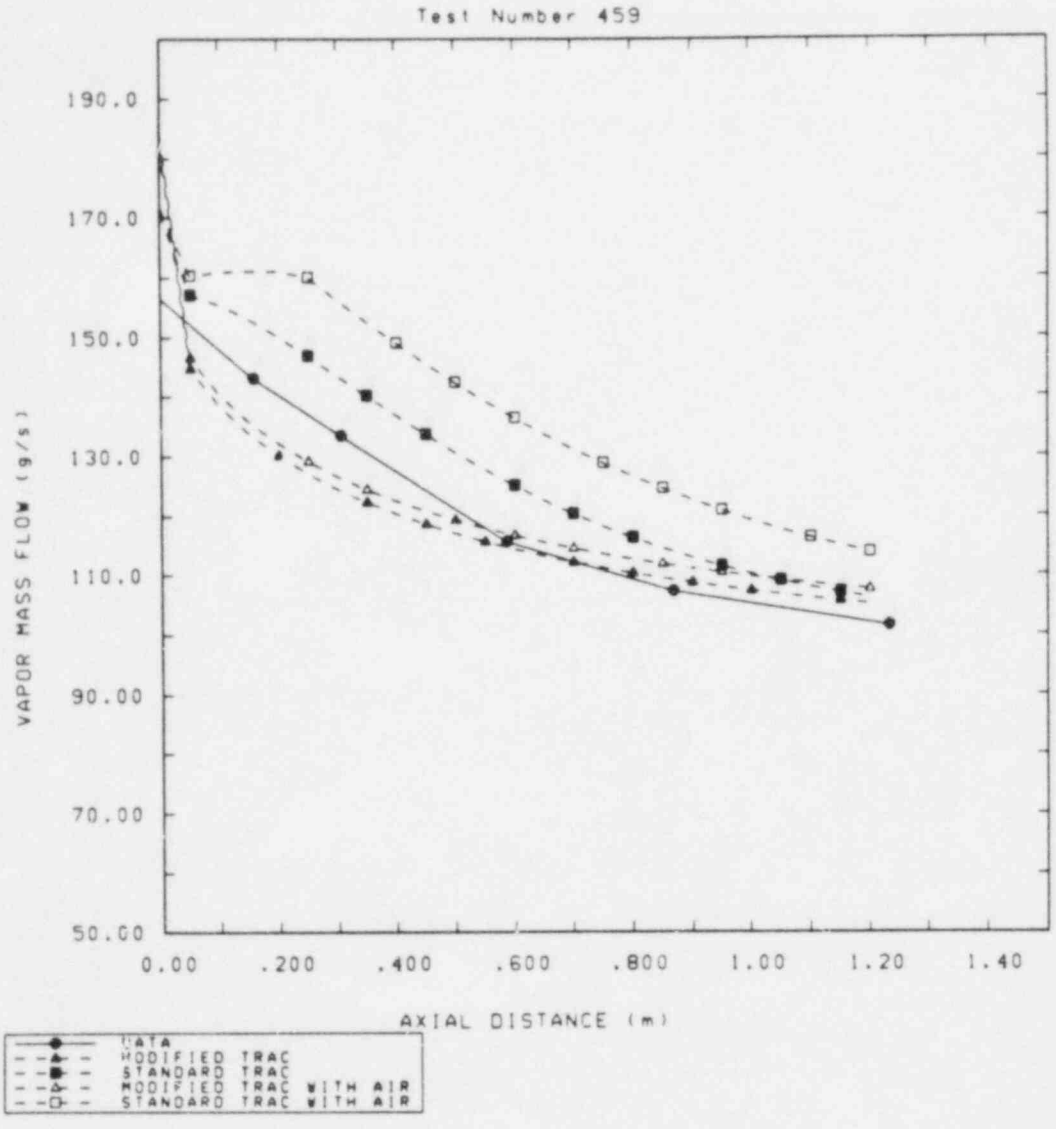

Figure 5.4.7 Vapor Mass Flows for Test 459, with and without Air

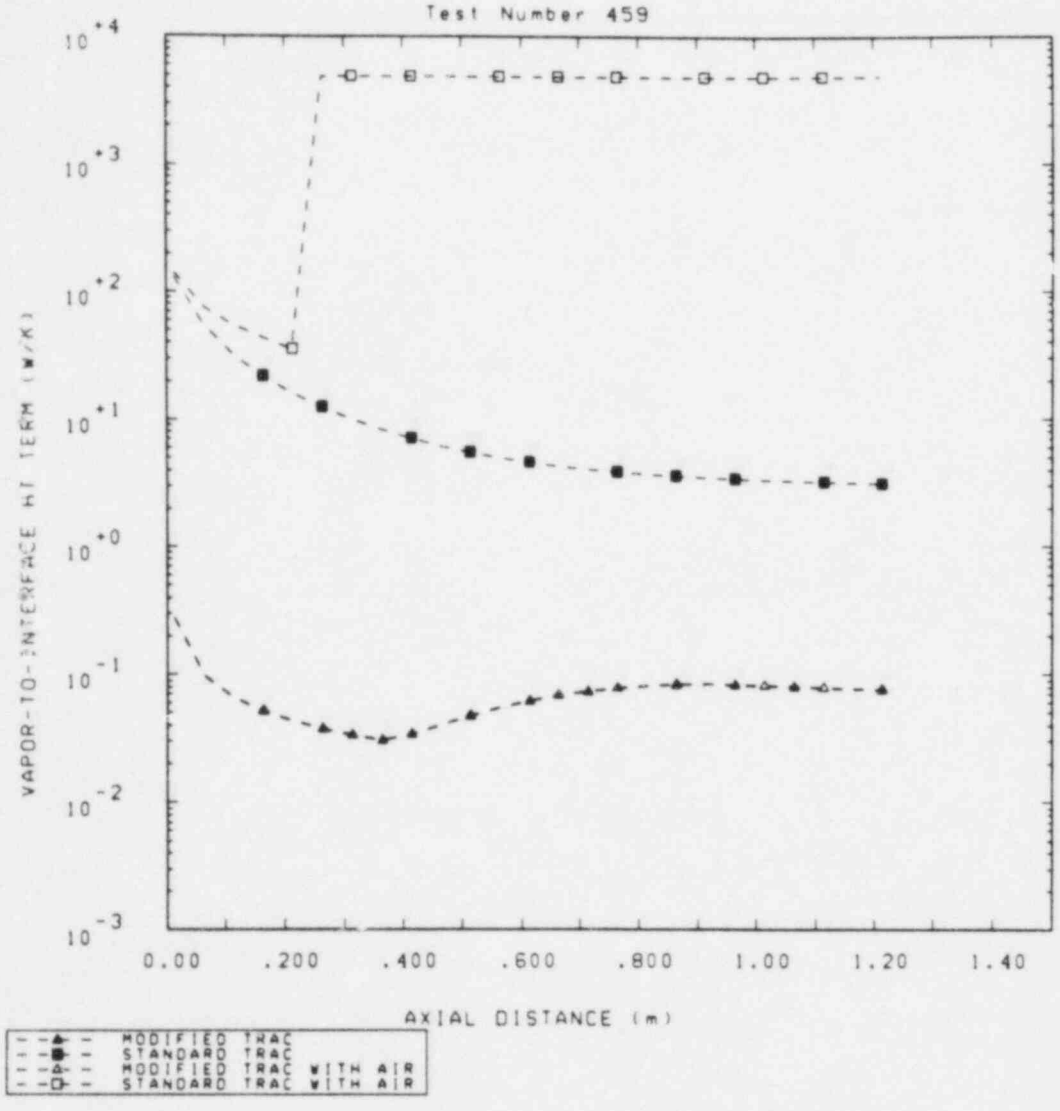

Figure 5.4.8 Vapor-to-Interface Heat Transfer Terms for Test 459, with and without Air

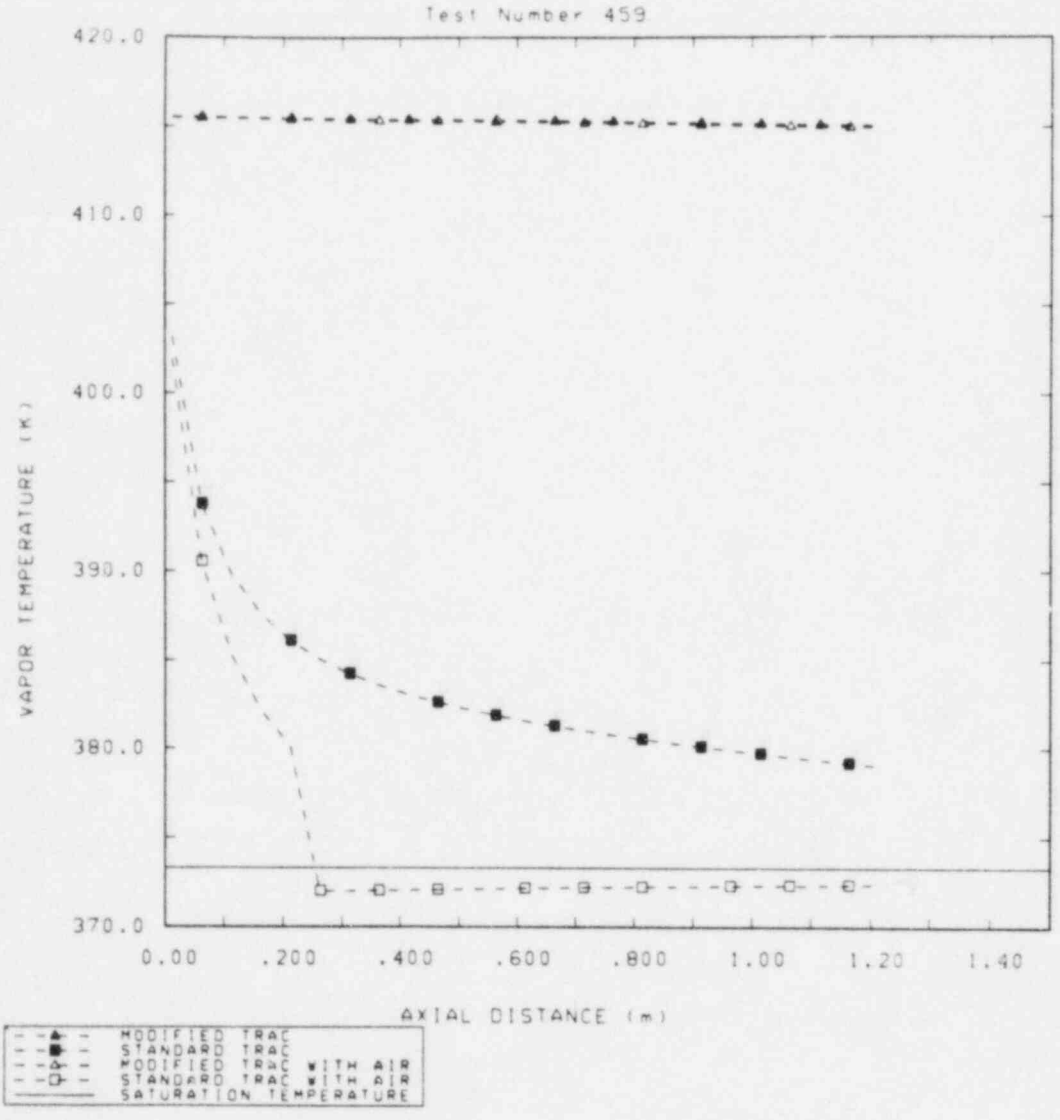

Figure 5.4.9 Vapor Temperatures for Test 459, with and without Air

6.0 Discussion and Conclusions

Since TRAC cannot model flow in a simple, horizontal, rectangular channel, there was no obvious choice of the way to use experiment conditions to specify TRAC input. We elected to approximate the test conditions for inlet mass flows and fluxes. The circular flow area of the PIPE in the calculations was made equal to the flow area of the rectangular test channel, and experimental volume fractions and mass flows, together with densities at the inlet and outlet pressures and temperatures, were used to specify the phase velocities.

On the basis of preliminary results, TRAC's timestep selection algorithm and initialization procedure appear to be inappropriate when steady, two-phase flow is the dominant feature. It is not surprising that a code whose original purpose was the analysis of large-break LOCAs in PWRs shows this property, and we have observed it elsewhere [5]. Experimentation with the user-supplied maximum timestep was required to achieve both convergence to a steady state in a reasonable amount of computer time, and assurance that the timestep size was not affecting the conditions attained when the criterion for a steady state was satisfied. Thus, our experience suggests that TRAC requires a more stringent criterion for convergence to a steady state; without such a criterion, it appears that a number of steady solutions with different timestep limits must be generated and the results compared for convergence to the "same answer".

Because detailed, direct, and quantitative comparison of calculated and experimental results was not possible, we performed calculations for only four test conditions. The character of the results was, in general, acceptable; in particular, the qualitative effects of changes in inlet flows and liquid temperature were consistent with experimental observations and with physical intuition. Interactions between outlet boundary conditions and the heat transfer models caused major discrepancies (e.g., two cases with regions of countercurrent flow). We implemented very simple modifications to the interfacial heat transfer coefficients, which had the overall effect of reducing the amount of condensation. With those modifications, the qualitative discrepancies were eliminated, showing that a more general correction, if desired, could probably be effected fairly easily. Trial calculations with air included in the vapor showed reductions in condensation rate computed with the standard models, with the exception of a case in which the code calculated a region of subcooled vapor.

The data as presented in the experiment report were difficult to use for the purpose of code assessment, for several reasons. The data may be analyzed in such a way as to infer heat transfer coefficients, and we have demonstrated (in Appendix A) such a procedure for data corresponding to the four sets of calculations we performed. However, this type of analysis requires values for the axial gradients of the mass flows. With only six points along the flow path, the results of such an analysis can be significantly influenced by the details of fitting the profile. Further, both the choice of a fitting method and any search for correlations for the heat transfer coefficients would be aided by knowledge of the character of the interface, as and if it changed along the flow path; no quantitative information on that question was reported. Liquid temperature profiles did not appear in the report, and this required some otherwise unnecessary assumptions to be made in analyzing the data. The experimenters did use all their data to obtain correlations defining heat

transfer coefficients as functions of various thermodynamic and dimensionless quantities. However, those correlations were for axially-averaged values (with not all quantities averaged in the same way); in order to be useful in TRAC, heat transfer coefficients must be local quantities.

Data from separate effects tests of the sort addressed in this study can be very valuable as the basis for models treating the phenomena under scrutiny. When a code can directly describe the experimental configuration, such data may also be used to measure the accuracy of calculations which exercise those models. The latter of these objectives could not be achieved here, because none of TRAC's available components can model the geometry and orientation of the test apparatus. An effort to develop models based on the full test matrix, and the extensive interpretation of the measured data that would require, were clearly outside the purposes of this investigation. We believe, however, that such an undertaking could be fruitful.

7.0 References

1. Safety Code Development Group, TRAC-PF1/MOD1: An Advanced Best-Estimate Computer Program for Pressurized Water Reactor Analysis (Draft), Los Alamos National Laboratory Report, Los Alamos, NM, 1983.

2. I. S. Lim et al., Cocurrent Steam/Water Flow in a Horizontal Channel, NUREG/CR-2289, Northwestern University, August 1981.

3. W. H. Giedt, Principles of Engineering Heat Transfer, Van Nostrand, Princeton, NJ, 1957.

4. I. S. Lim, R. S. Tankin, and M. C. Yuen, Condensation Measurement of Horizontal Cocurrent Steam/Water Flow, Transactions of the ASME, Journal of Heat Transfer v. 106, p425, May 1984.

5. L. N. Kmetyk, RELAP5 Assessment: Conclusions and User Guidelines, NUREG/CR-3936, SAND84-1122, Sandia National Laboratories, October 1984.

Appendix A

Analysis of Reported Data for Comparison with the Models used in TRAC

As has been stated, there seems to be no easy way to use the experimental data to compare directly with results from TRAC. However, the quantities of interest - principally interfacial heat transfer coefficients - are most frequently analyzed in terms of dimensionless heat and mass transport parameters, and with some effort, both experimental data and calculated results may be put on common ground. Data from separate effects tests like those considered in this report may be very useful in the development and verification of code models, but the way this is to be accomplished should be considered when deciding on a particular form in which to present those data. After a description of the methods used by the experimenters to interpret their data, we present a necessarily brief examination of a way in which those data can be used to investigate the TRAC models for the interfacial phenomena of interest. We carried out this procedure only for data from Tests 253, 259, 293, and 459.

Using the mass and energy balance equations for steady flow of each phase, neglecting the pressure gradient, and assuming that the vapor enthalpy is constant along the flow path, it is easy to arrive at an expression for the liquid enthalpy in terms of its inlet value, the vapor enthalpy, and mass flow:

$$h_\ell = h_v - (h_v - h_\ell^I) \cdot \frac{W_\ell^I}{W_\ell}$$

In Reference 2, the vapor enthalpy times the vapor flow gradient was equated to a vapor-to-liquid energy flow; the resulting heat transfer coefficient is

$$H_{v\ell} = \frac{h_v}{w(T_v - T_\ell)} \partial_z W_\ell$$

This expression is obviously derived on the assumption that interfacial area per unit length is simply the channel width, w; i.e., the interface is virtually smooth and horizontal. For the liquid temperature in this expression, it was assumed that the liquid constant-pressure specific heat was constant, and that its product with the temperature was equal to the enthalpy. The report's description of the experiment facility indicates that the means for measuring temperature profiles was available, but no such data appear in the document. The heat transfer coefficient was thus expressed entirely in terms of the flow, its gradient, and appropriate constants. Profiles of axial average coefficient, defined in the usual way as the integral to a position divided by the position, were also calculated; these quantities obviously depend only upon the flow, the position, and constants.

The process of obtaining the flow gradient for the local coefficient is described in [2] (p 31 ff) as follows: "Values of steam mass flow rate are plotted as a function of axial distance and a smooth curve is drawn which best fits the experimental data. Point values are then taken from the curve at an interval of 10 cm and the slopes are calculated by the quadratic function with three consecutive data points."

In [4], three of the authors of the experiment report analyzed a larger body of similar data using a slightly different technique. There, they chose to fit the flow data with two different functions, depending on whether the interface was locally smooth or wavy. These functions each contained two arbitrary constants determined by "best fit" of the data. Also, using the same thermodynamic assumptions, they considered energy flow from the interface (at saturation temperature) to the liquid, taking account of the enthalpy increase due to condensation. With that approach, they derived a local interface-to-liquid heat transfer coefficient given by

$$H_{i\ell} = \frac{h_v - h_{\ell s}}{w(T_s - T_\ell)} \partial_z W_\ell$$

In both of the works cited above, the authors obtained correlations over large bodies of data between Nusselt numbers, liquid Prandtl numbers, and liquid and vapor Reynolds numbers based on axial position. Unfortunately for our purposes, these correlations were formed with the axial average heat transfer coefficients; mass fluxes, viscosities, and Prandtl numbers were the arithmetic means of their values at the inlet and the axial position. Local heat transfer coefficients, which are of course what TRAC requires, were only presented graphically as profiles along the flow path.

We attempted to approximate the process of calculating heat transfer coefficients with a computer program, in which the flow data are fit with quadratic splines, with interpolation between overlapping splines where appropriate. The program then evaluates the average and local heat transfer coefficients using the expressions given above. As may be seen in Figure A.1, the axial average coefficient did not necessarily agree well with values obtained from a figure in the experiment report. Since this coefficient is merely an evaluation with given flows and presumably accepted values of thermodynamic constants, the discrepancy is puzzling. Figures A.2 and A.3 demonstrate that, even with a reasonably good fit to the flow data, local heat transfer coefficients computed from the flow do not agree with the graphically-presented values. In this case, the subjective nature of "drawing a curve which best fits the data" may be partly responsible. Because of these difficulties, we decided to try analyzing the flow data in a way similar to those described above, but more compatible with TRAC.

The "condensation model" in TRAC is simple and appealing: in the absence of wall heat transfer, a steady-state energy balance for each phase consists only of heat transfer to the interface and a term depending on the mass transfer rate. The sum of the energy changes for both phases must be zero, so the condensation rate may be calculated in terms of the heat transfer coefficients, the temperatures, the interfacial area, and the heat of vaporization. The complications arise, of course, in specifying the interfacial heat transfer coefficients and area as functions of Reynolds numbers, Prandtl numbers, etc. (As mentioned in Section 4, the definition of the area, even in completely stratified flow, is obvious in TRAC only for the interface-to-liquid term.)

We modified the data interpretations described above by including energy balance terms for both phases in a way consistent with TRAC's equations; the result for the interface-to-liquid heat transfer coefficient is identical to that already given. The coefficient for the vapor-to-interface term is

$$H_{vi} = \frac{C_{p_v}}{w} \partial_z W_\ell$$

We constructed another computer program which employs overlapping cubic splines to fit the experimental data for mass flows and liquid thicknesses. Interpolating cubic spline fits generally have superior interpolation properties in regions of overlap, compared to their quadratic counterparts. Fits to the flow rates for Tests 253, 259, 293, and 459 are shown in Figure A.4, and the resulting condensation rates (which are, of course, simply proportional to the flow gradients) appear in Figure A.5. Liquid enthalpy is calculated by the equation given earlier. The changes in pressure were too small to have a significant effect on the quantities of interest, and so were neglected. Enthalpy and pressure were used with routines which provide the thermodynamic and transport properties of water.

Using the information described in the previous paragraph, we calculated vapor-to-interface and interface-to-liquid heat transfer coefficients, mean phase velocities, and Nusselt, Reynolds, and Prandtl numbers for each phase. Interfacial energy and mass transfer terms from the TRAC models were also evaluated. In evaluating the vapor term for the standard model, the interpolating and limiting procedures described in Section 5.2 were not incorporated; only Test 293 results would have been affected.

Figures A.6 through A.9 display condensation rates calculated by fitting the data, and by using the standard and modified models with quantities obtained in the fitting process. Both models generally give higher condensation rates than those inferred from the data. For three of the tests, the modified condensation rate model yields a lower value in the downstream portion of the flow path, because of dependence on negative powers of axial position. For Test 459, however, the relative velocity (which appears in the model raised to a positive power) remains high enough that the rate from the modified model is higher throughout the flow distance.

As may be seen in Figure A.10, the interface-to-liquid heat fluxes inferred from Test 253 data, and calculated with the standard model, were roughly ten to a hundred times their vapor-to-interface counterparts; interface-to-liquid heat transfer was relatively much more dominant with the modified treatment. The conditions of Test 459 (Figure A.11) were such that the vapor-to-interface flux with the standard model dominated near the inlet, resulting in the small region of evaporation near X=0 in Figure A.9.

We also used the results of the data-fitting process described above in a brief investigation of possible correlations for local interfacial heat transfer coefficients. Stanton and Reynolds numbers are computed for each phase; either absolute or relative velocities may be used these calculations. These numbers, and Nusselt and Prandtl numbers, are normalized with their respective logarithmic mean values. We then found least-squares linear relations among the logarithms of these normalized numbers.

Figure A.12 shows the result of a least-squares linear fit for liquid Nusselt, Reynolds and Prandtl numbers, with absolute velocities used throughout, and using 25-point profiles from the data fits for all four tests. The Nusselt number resulting from this fit is plotted versus Reynolds number in Figure A.13. The graph also contains representative values which would result from the standard and modified TRAC models; these curves are only approximate, because the computer program used for these fitting calculations does not have all the information required to make them more accurate. The data do not seem to display any obvious trend for low Reynolds numbers, but at least hint at more coherent behavior for higher values. The choice of axial position to evaluate the Reynolds numbers results in relatively few data points for low values of that quantity.

The data in Figures A.12 and A.13 may also be fit by adding a dependence on vapor Reynolds number, with the result shown in Figure A.14. The standard deviation for this fit is about three quarters of that for the previous one, so, on that basis, it is somewhat better. If, on the other hand, the data are fit as in Figure A.12 but with Reynolds numbers based on relative velocity, the accuracy of the fit is reduced, as may be seen in Figure A.15.

Obviously, many ways could be chosen to analyze the data for good correlations for heat transfer coefficients. Because of insufficient linear independence of the variables used in the fits, some choices (e.g., relative velocities in all Reynolds and Stanton numbers) would give poor results, if any, but the list of possibilities is still fairly large. It should also be clear that the functional form used to fit the flow profiles has a significant influence on the coefficients inferred from the fit. In addition, reasonably good approximations to the data would need to be restricted in their range of application, in order to account for differing flow regimes. The "smooth/wavy" character of the interface was described in both [2] and [4], but no information was given that would allow a choice of fitting function based on local fluid conditions. For these reasons, and because of the quantity of data that would require processing to compare the accuracy of particular correlations, we did not pursue the matter further. However, it appears that by appropriate interpretation of the data, the geometric difficulty so often mentioned here could be overcome by comparing results inferred from the data with the output of the models in TRAC. We have studied examples of this process only for interfacial heat transfer coefficients, but it seems likely that a similar procedure could be carried out for frictional coefficients.

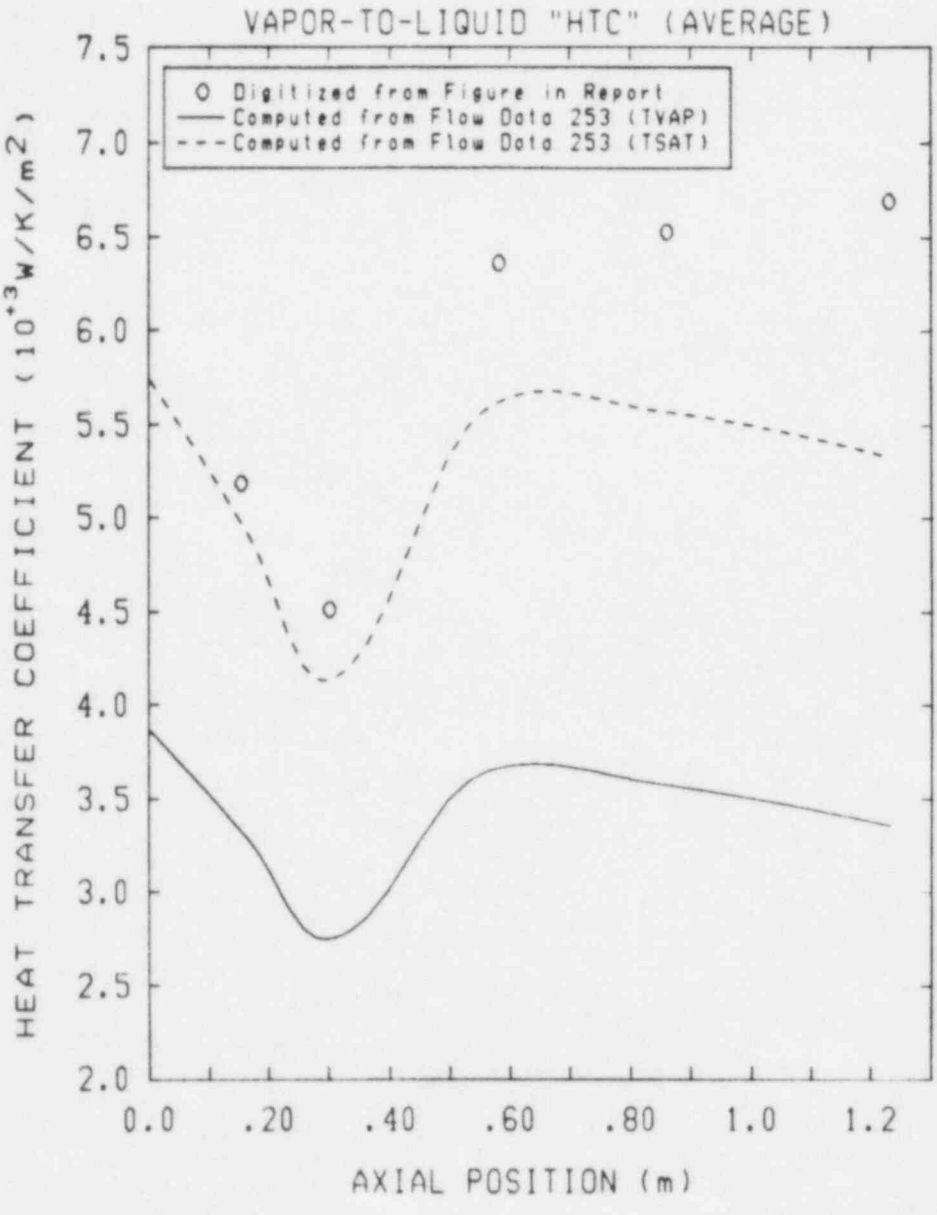

Figure A.1 Axial Average Heat Transfer Coefficients from Reference 2, and Computed from Flow Data

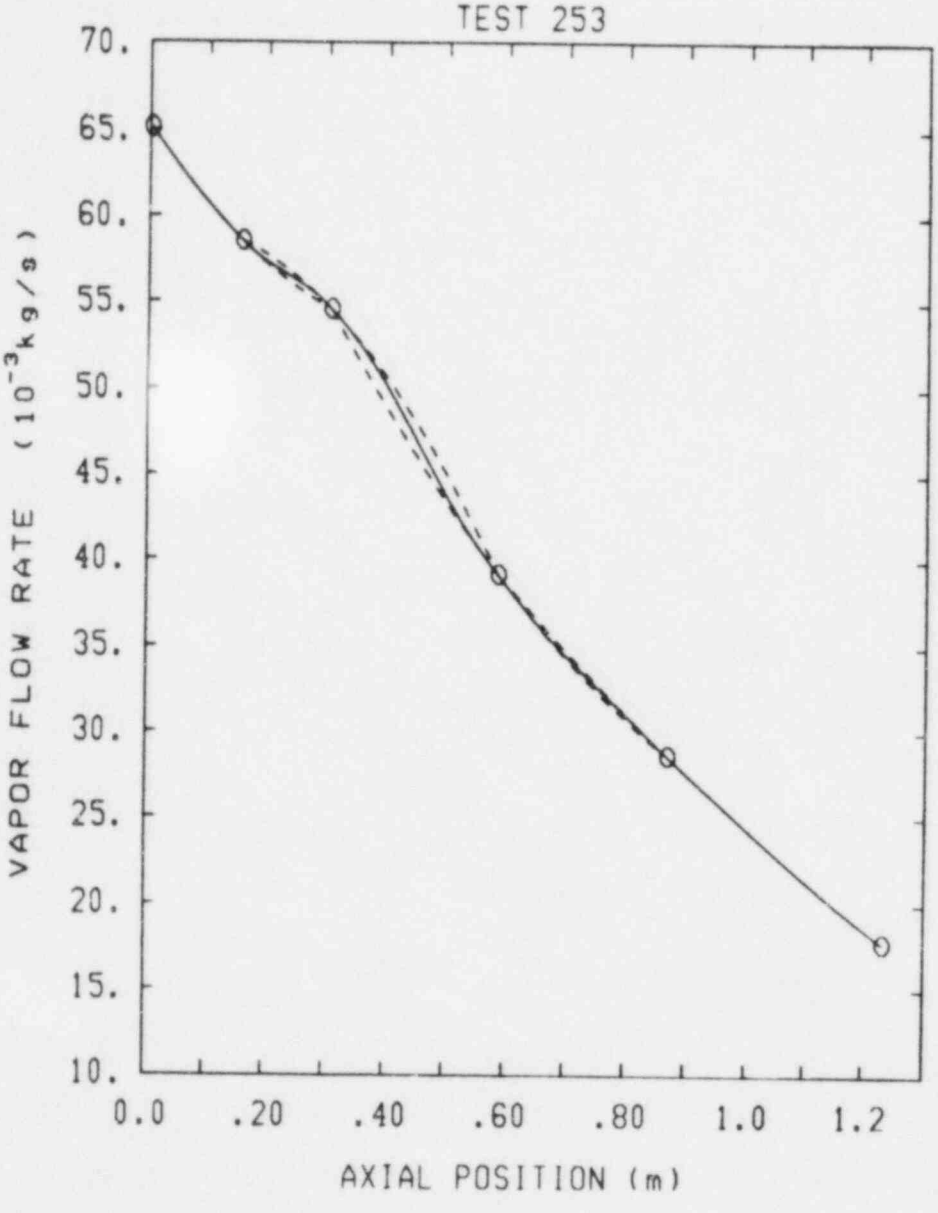

Figure A.2 Quadratic Spline Fit to Flow Data in Reference 2

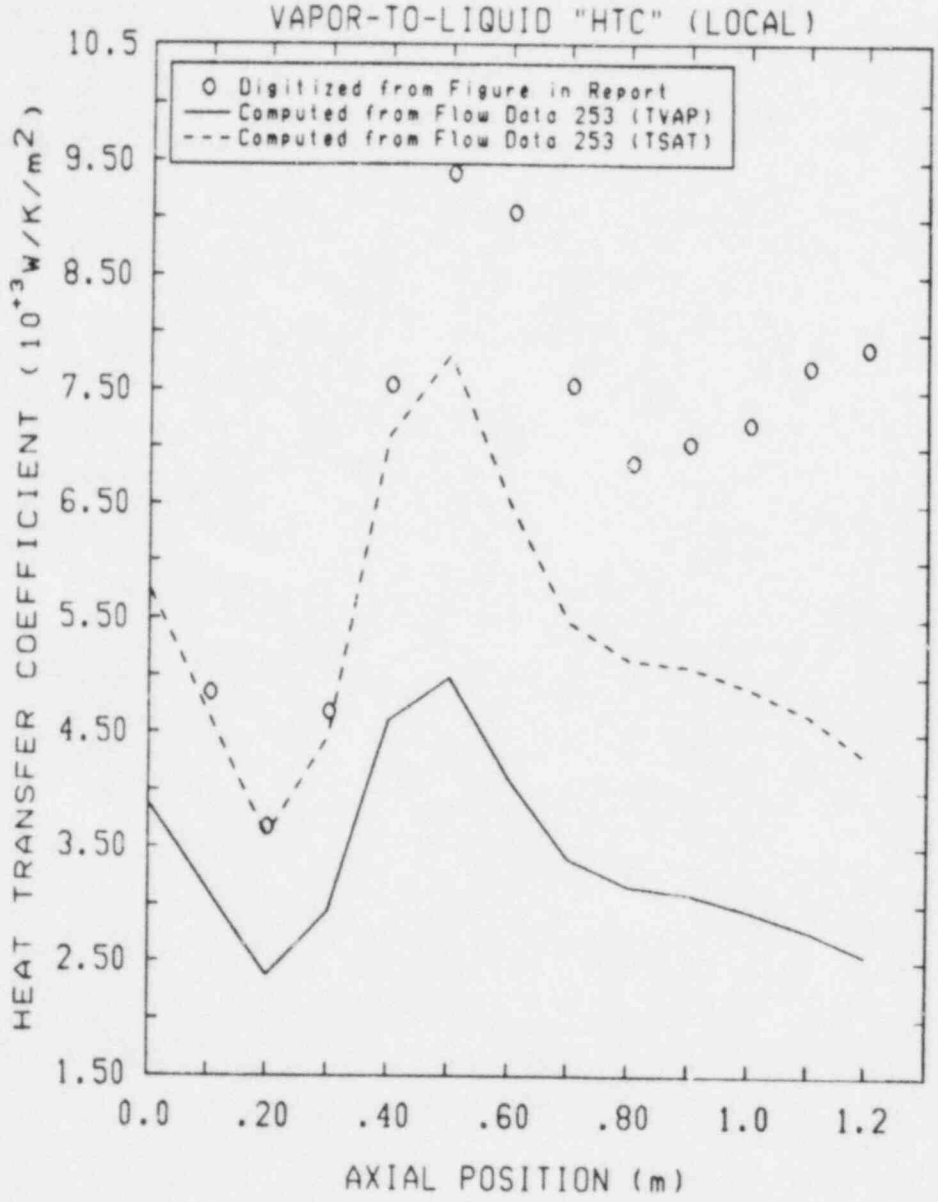

Figure A.3 Local Heat Transfer Coefficients from Reference 2, and Computed from Flow Data

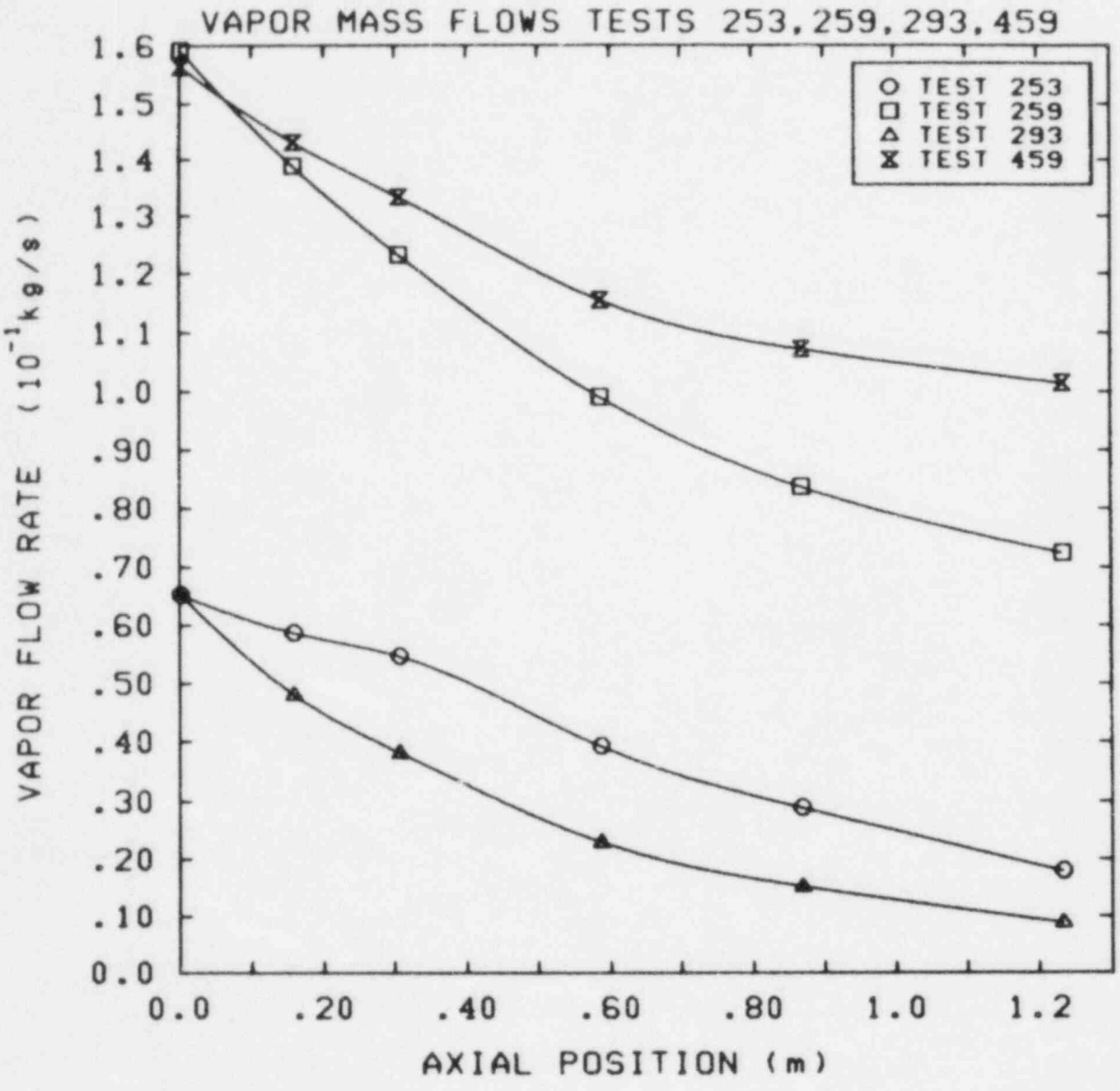

Figure A.4 Vapor Mass Flow Rates from Overlapping Cubic Spline Fits to Data

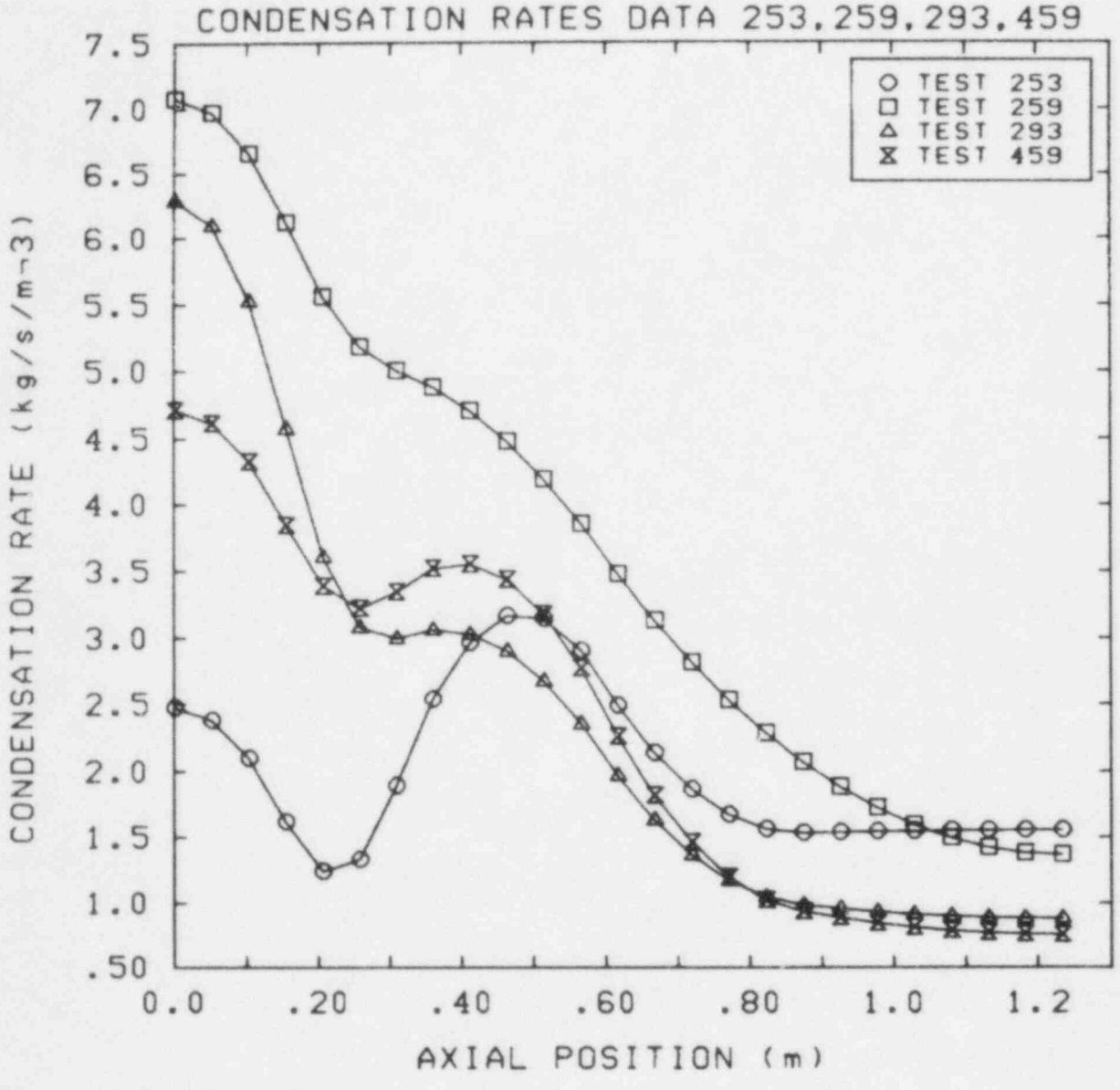

Figure A.5 Condensation Rates from Overlapping Cubic Spline Fits to Data

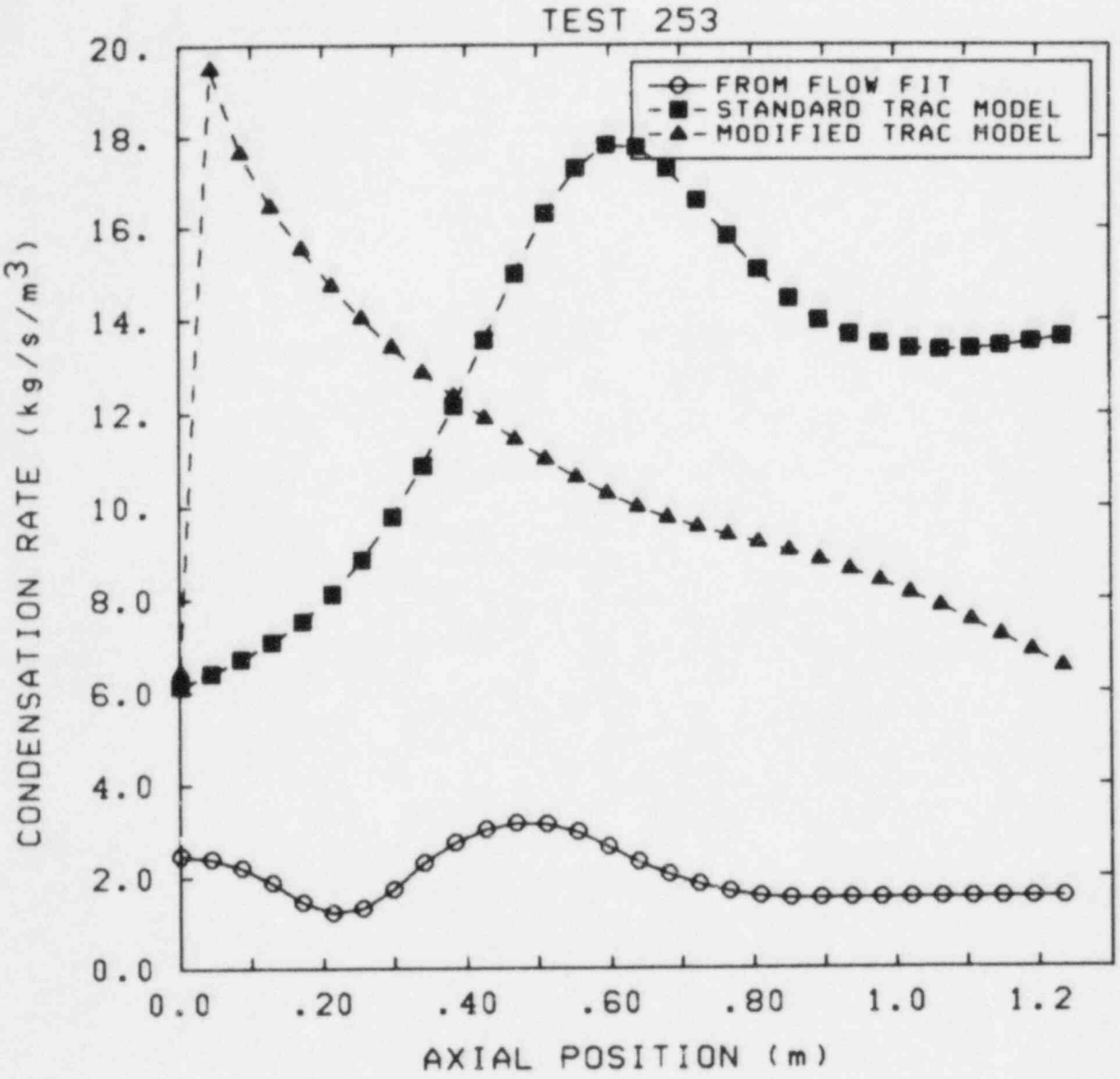

Figure A.6 Condensation Rates from Fit to Data, and Standard and Modified TRAC Models (Test 253)

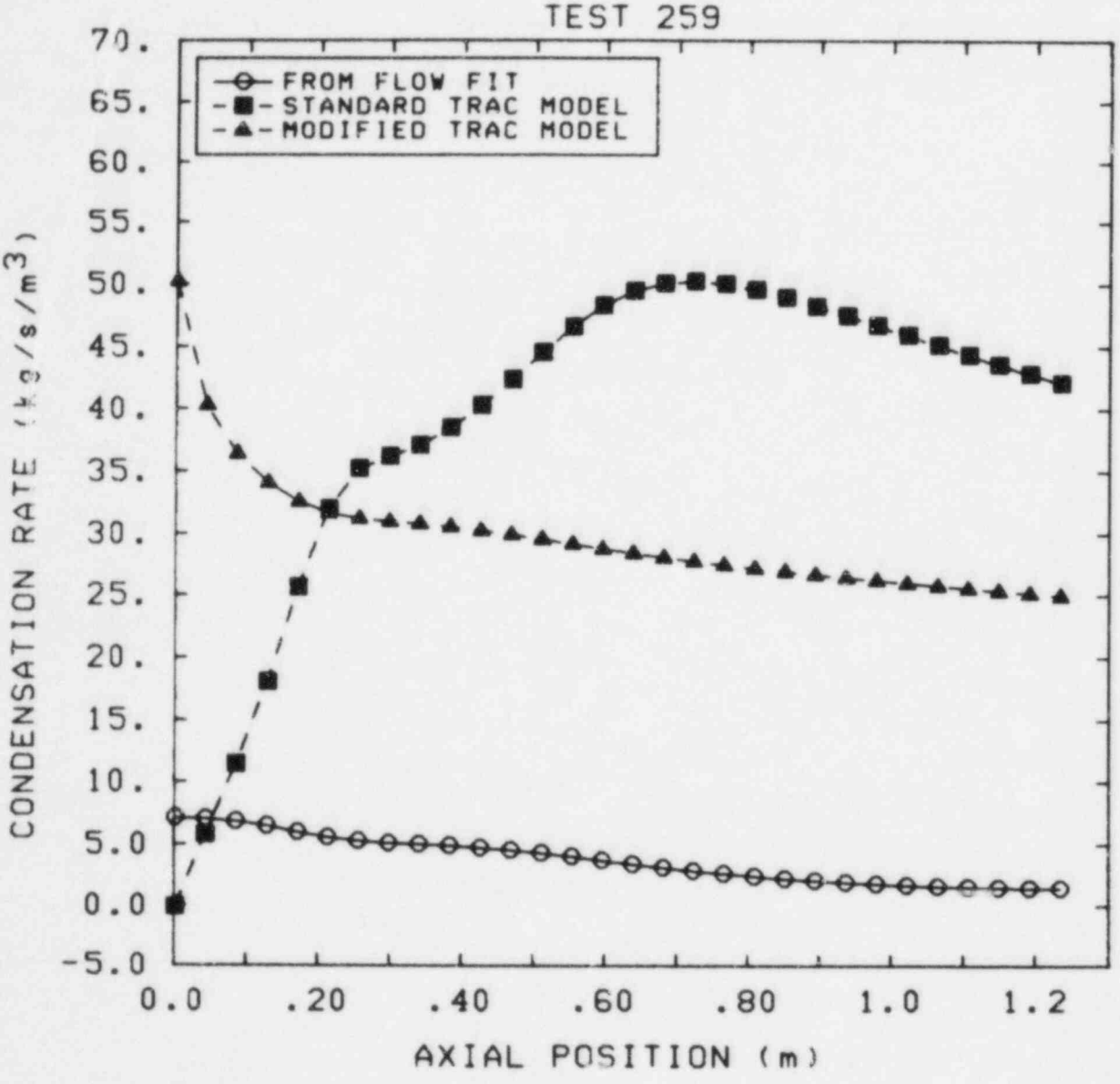

Figure A.7 Condensation Rates from Fit to Data, and Standard and Modified TRAC Models (Test 259)

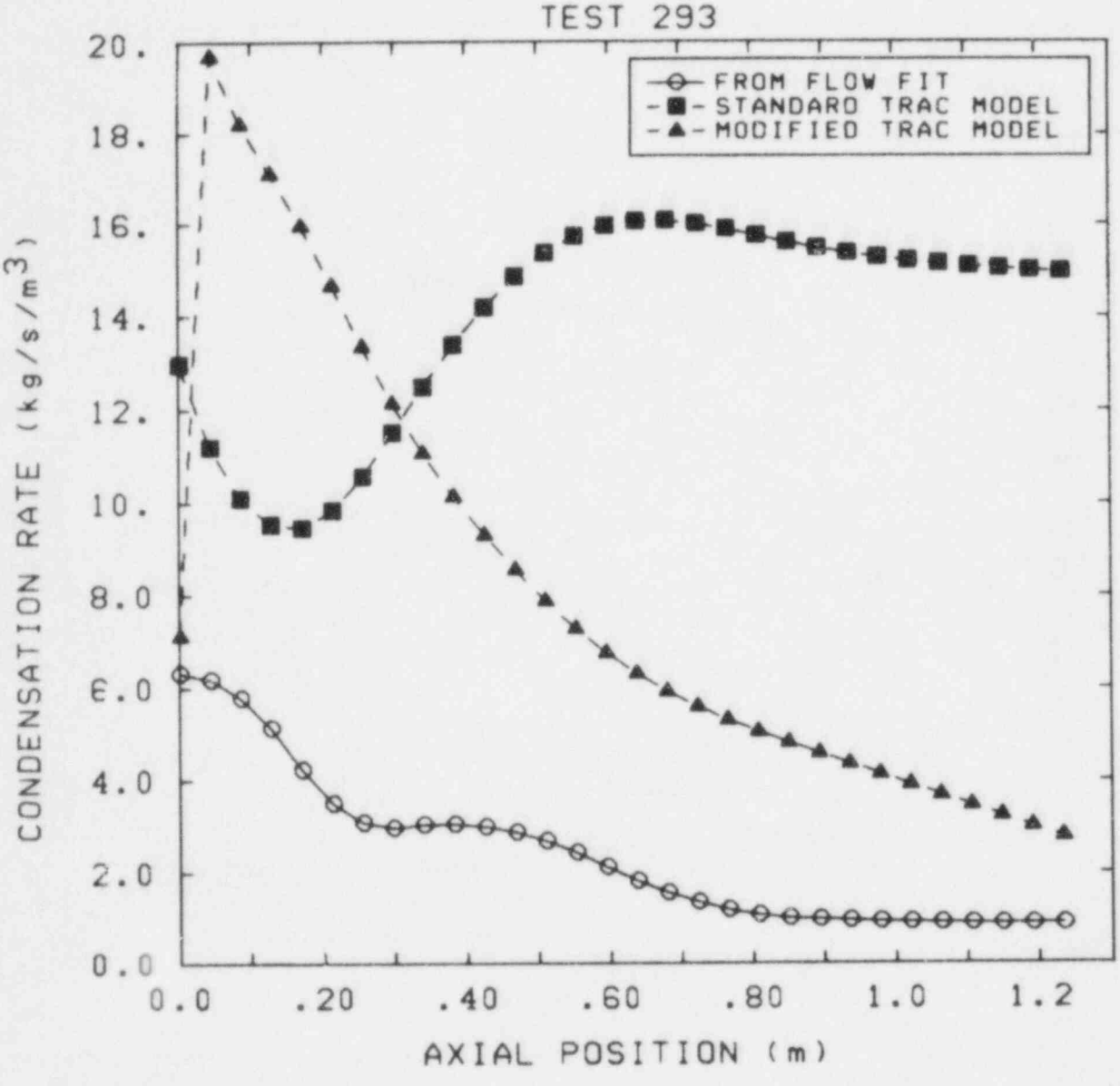

Figure A.8 Condensation Rates from Fit to Data, and Standard and Modified TRAC Models (Test 293)

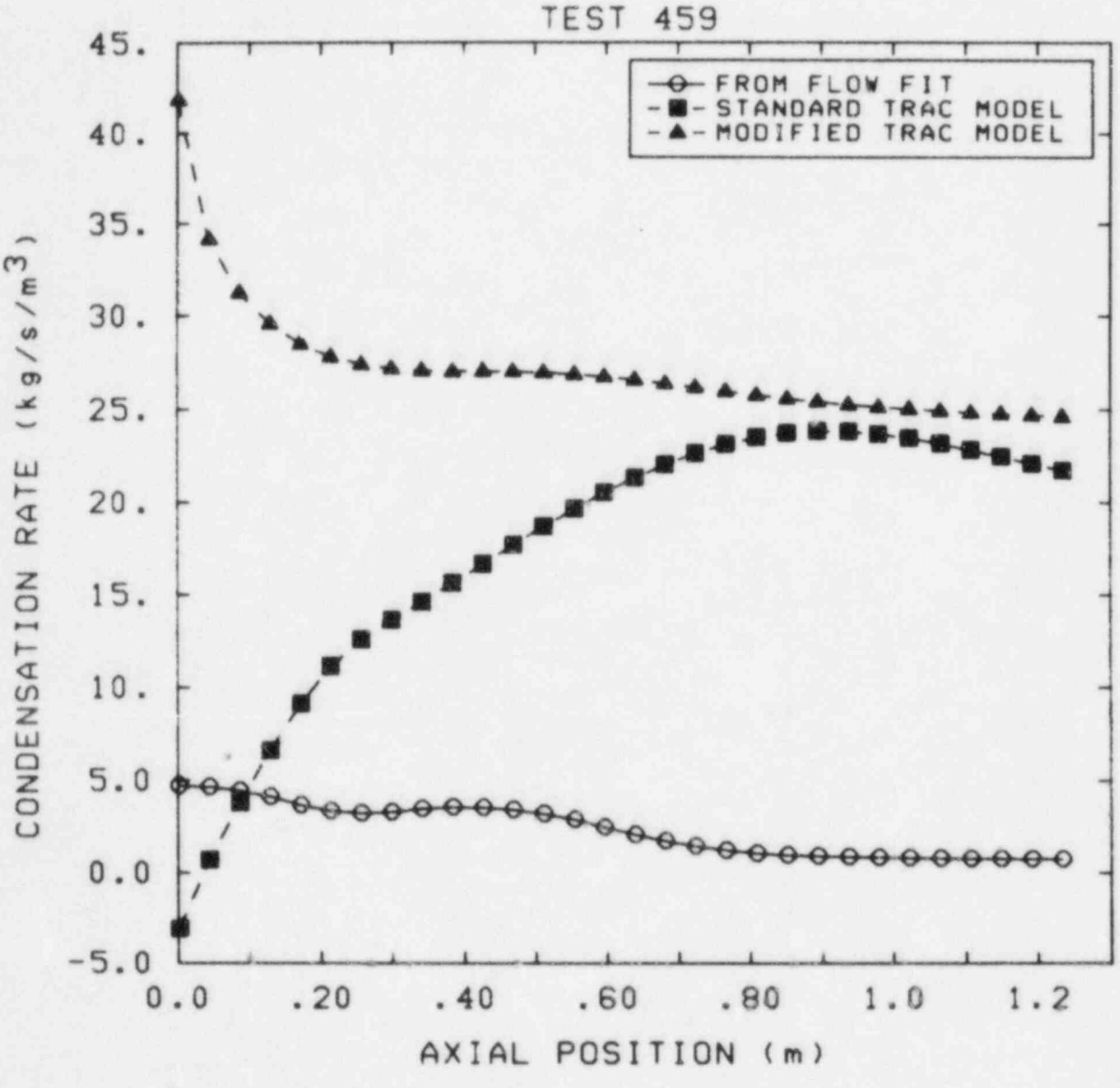

Figure A.9 Condensation Rates from Fit to Data, and Standard and Modified TRAC Models (Test 459)

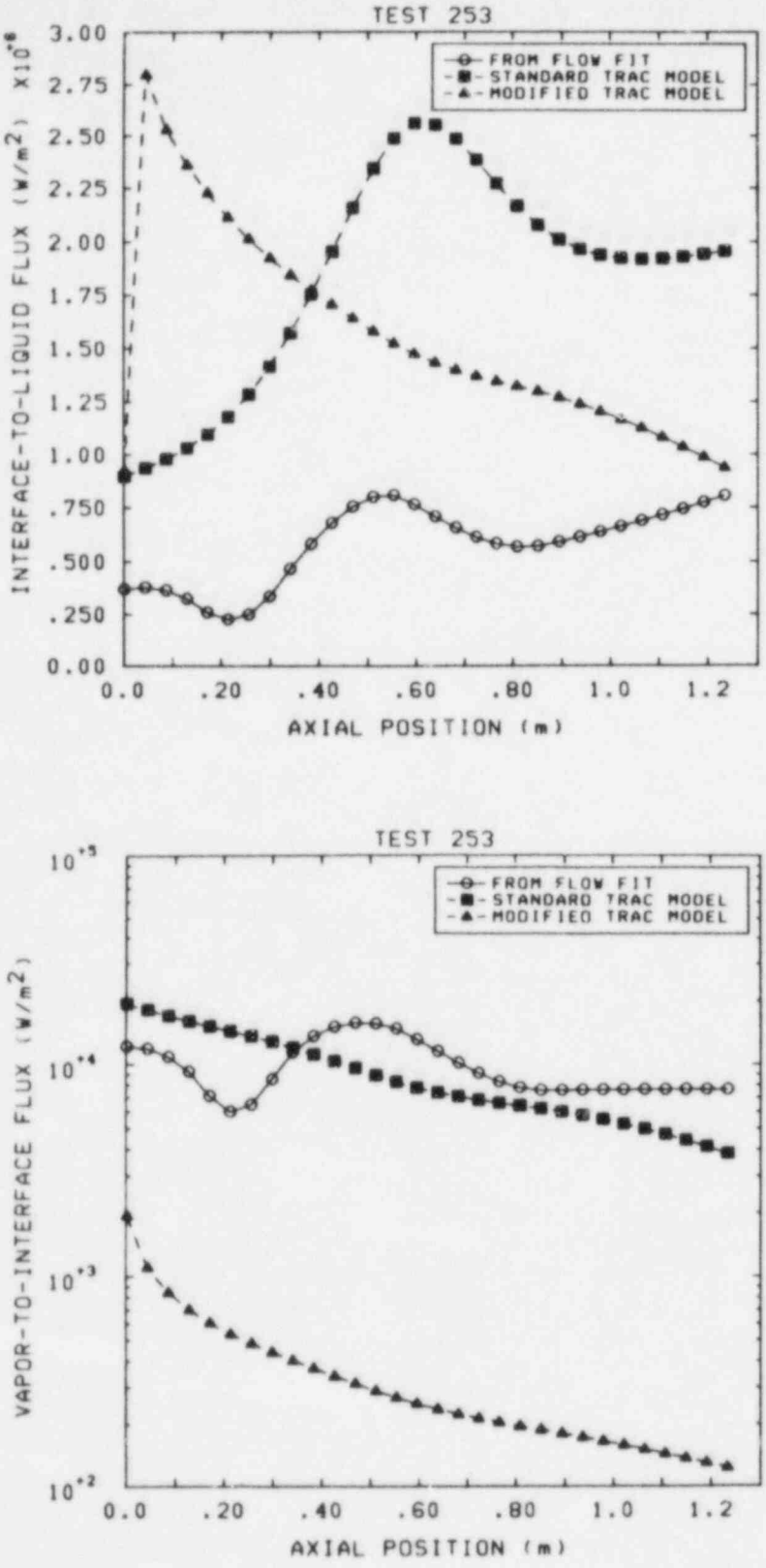

Figure A.10 Interface-to-Liquid (above) and Vapor-to-Interface (below) Heat Fluxes (Test 253)

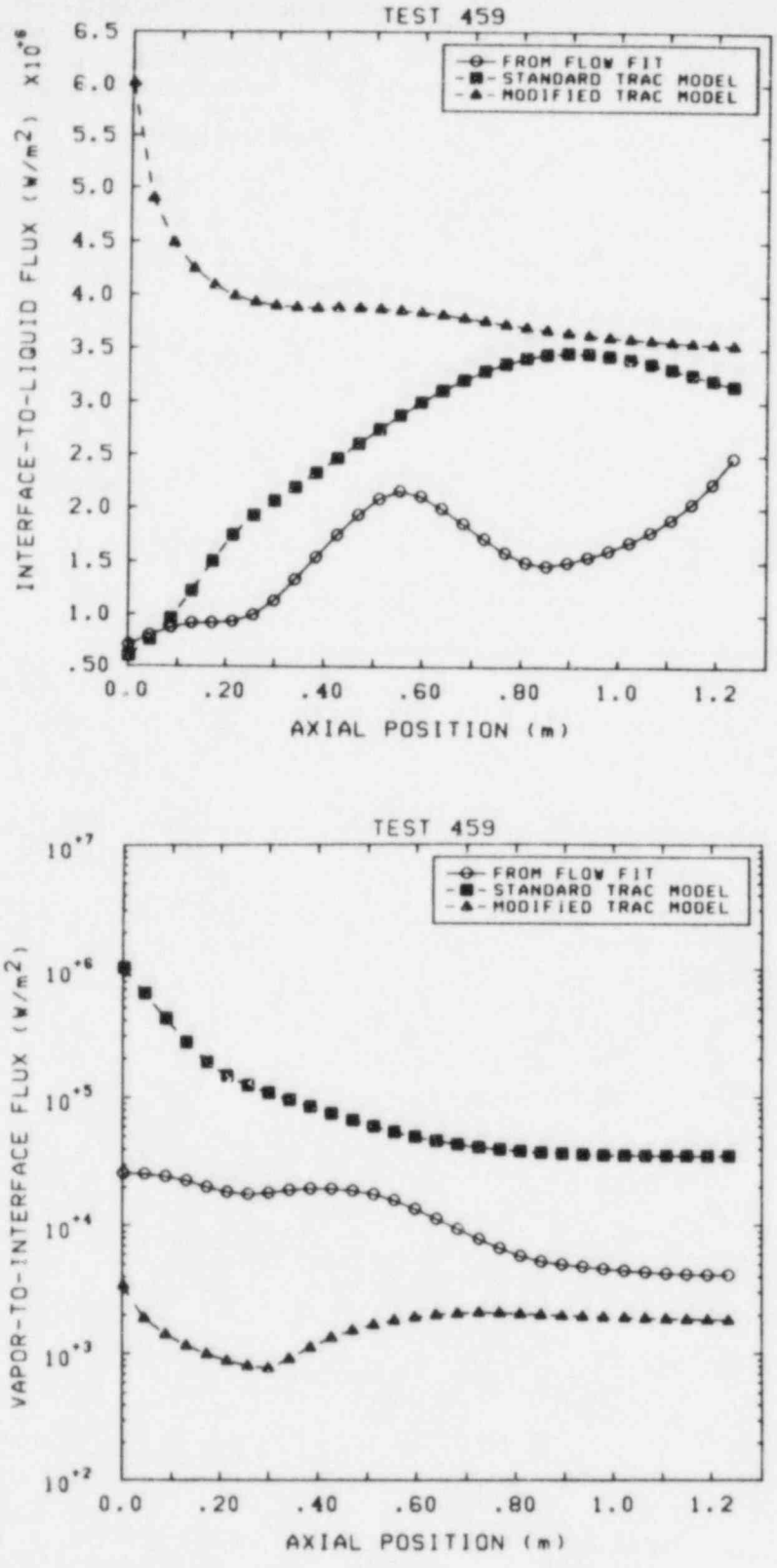

Figure A.11 Interface-to-Liquid (above) and Vapor-to-Interface (below) Heat Fluxes (Test 459)

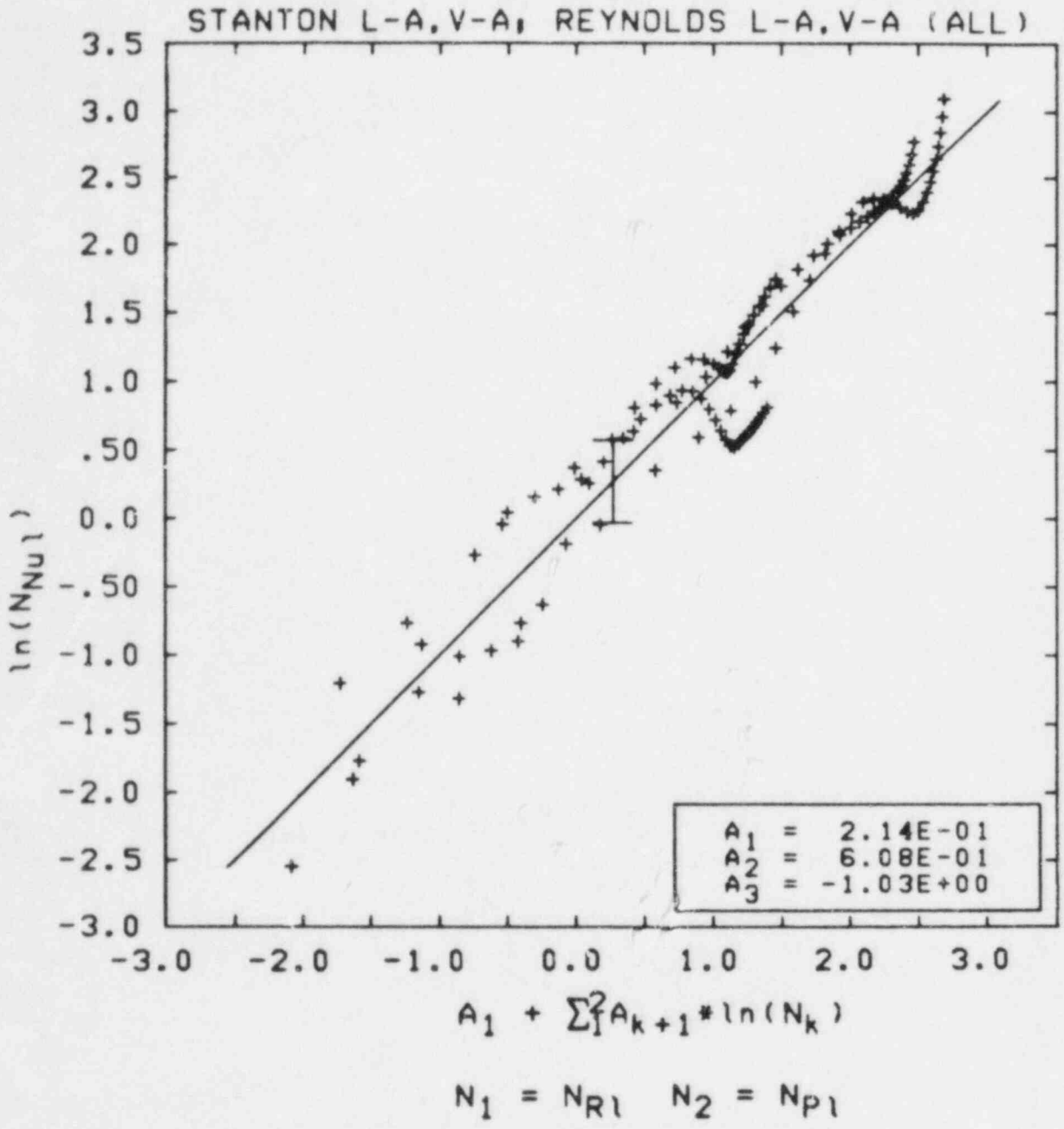

Figure A.12 Linear Fit for Logarithms of Normalized Liquid Nusselt, Reynolds, and Prandtl Numbers. (Absolute Velocities used in Stanton and Reynolds Numbers.) The "Error Bar" Represents 1 Standard Deviation for the Fit.

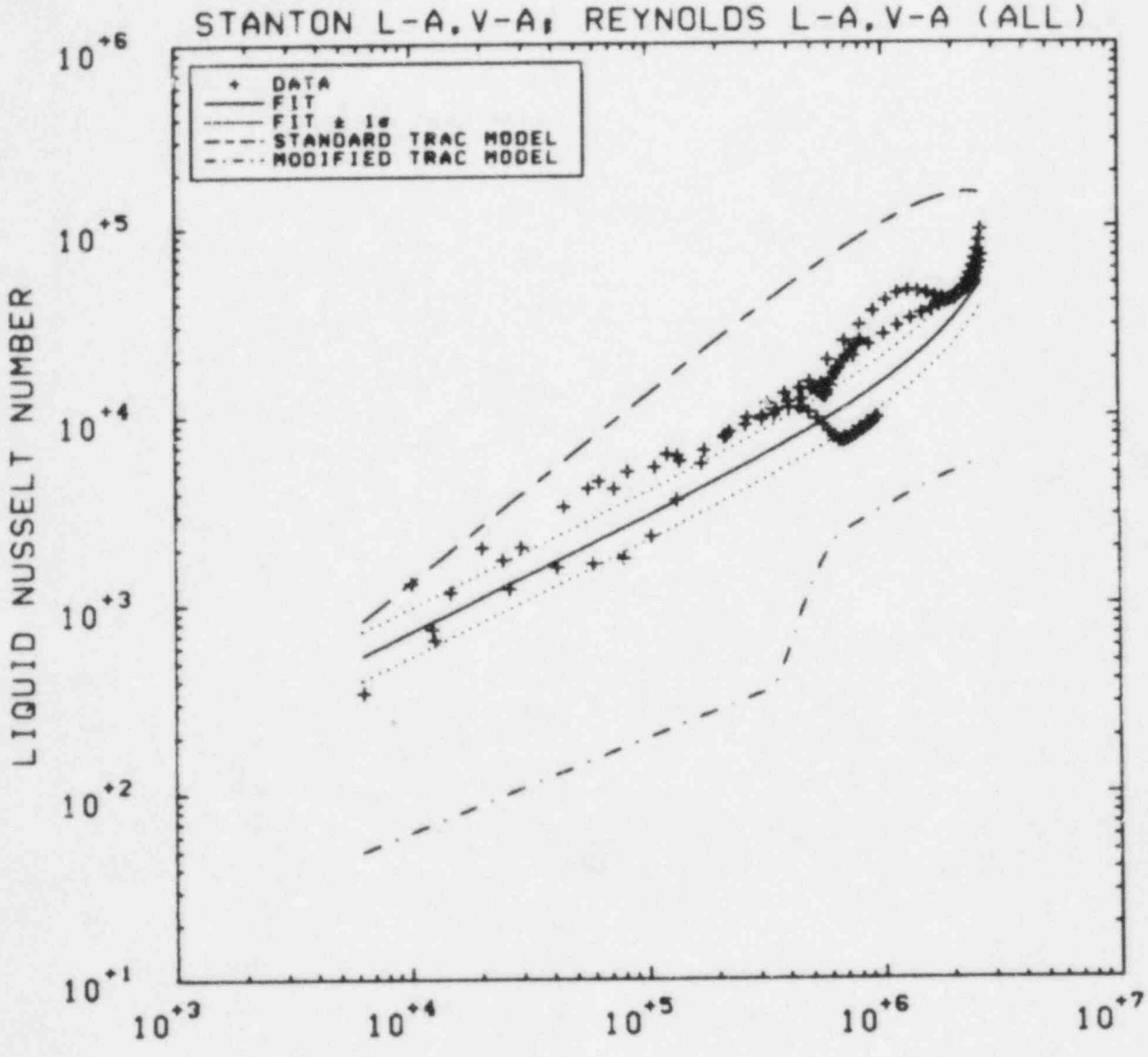

Figure A.13 Liquid Nusselt Number vs Reynolds Number. (Absolute Velocities used in Stanton and Reynolds Numbers)

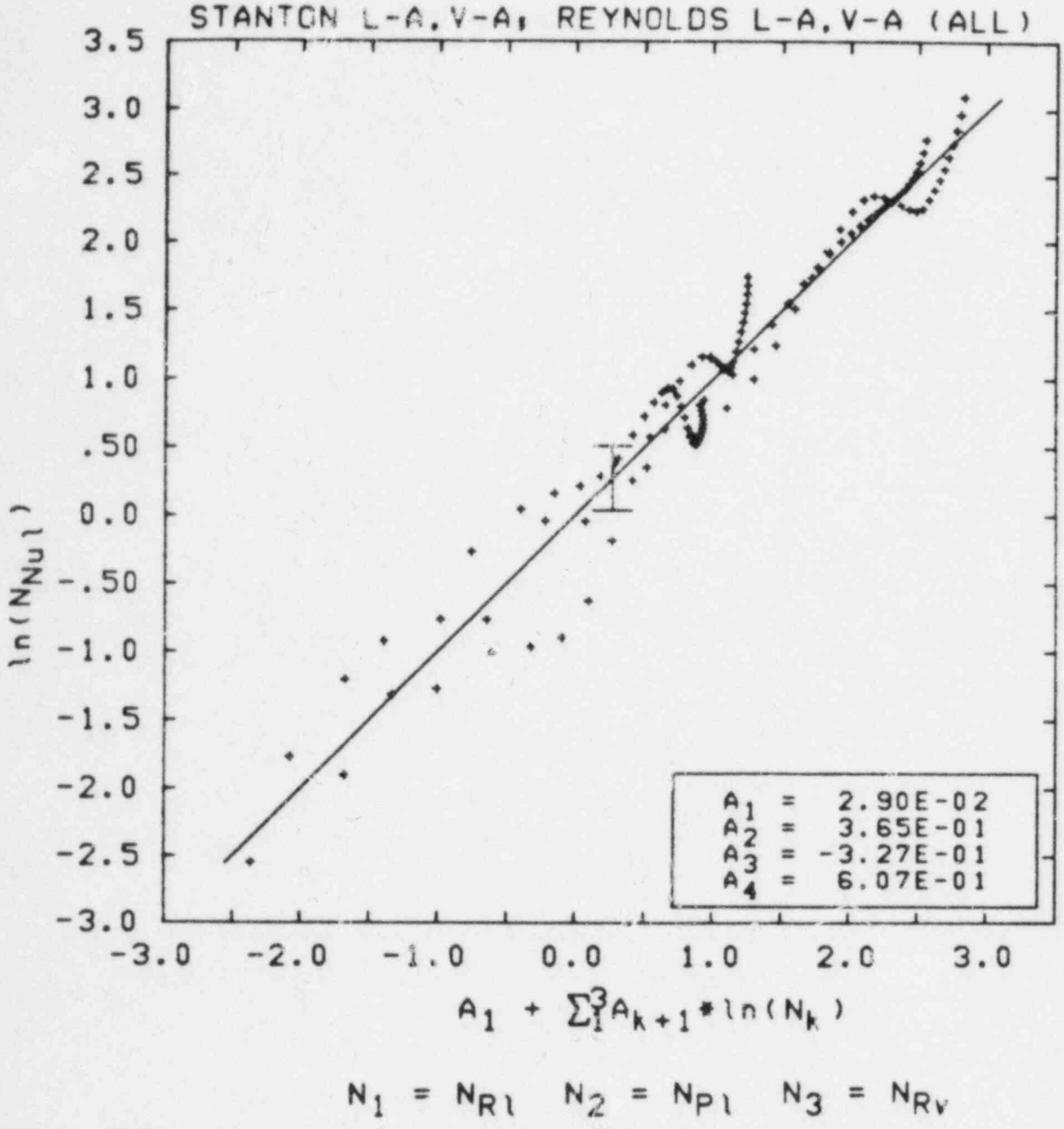

Figure A.14 Linear Fit for Logarithms of Normalized Liquid Nusselt, Reynolds, and Prandtl Numbers, and Vapor Reynolds Number. (Absolute Velocities used in Stanton and Reynolds Numbers.) The "Error Bar" Represents 1 Standard Deviation for the Fit.

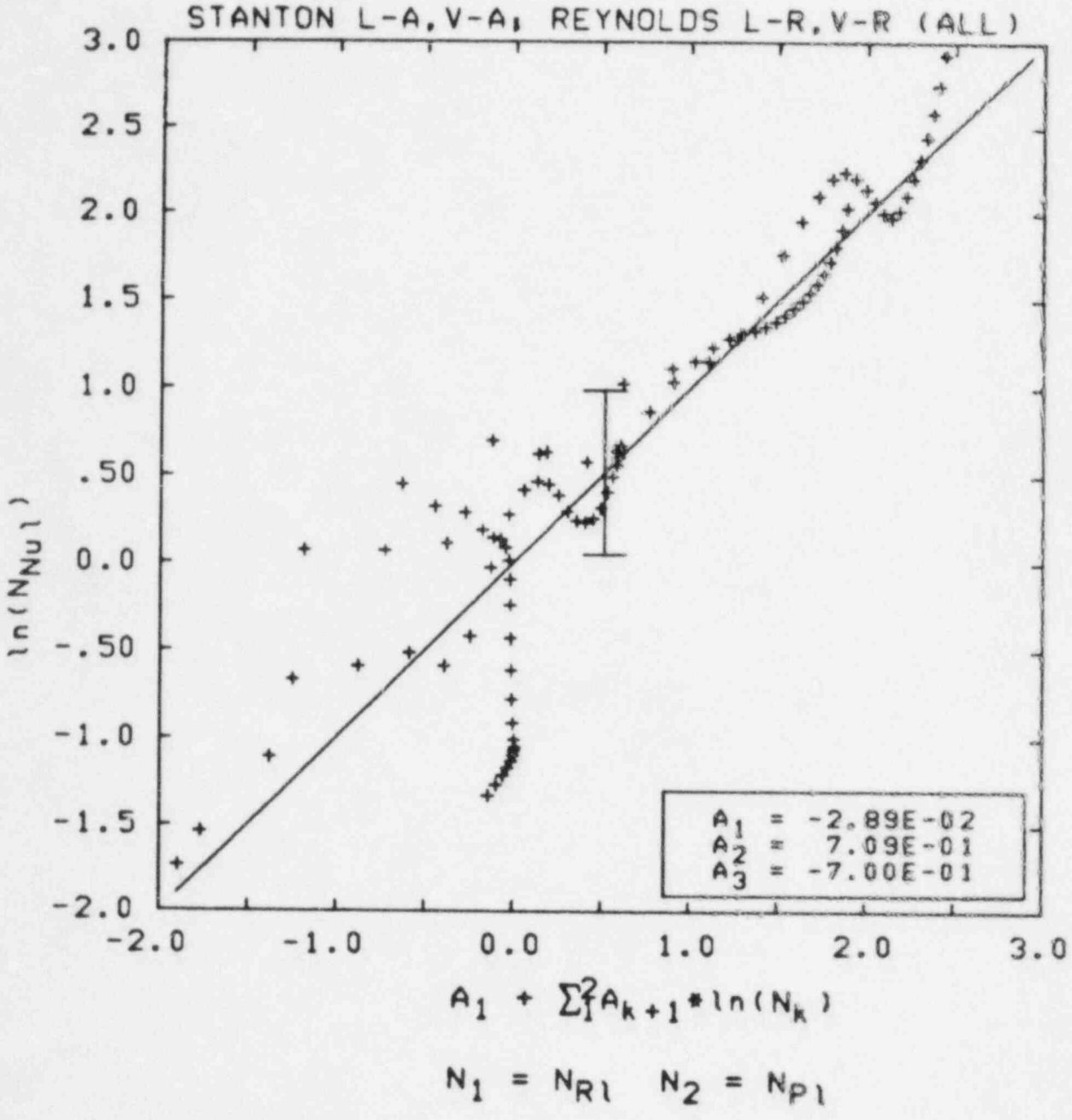

Figure A.15 Linear Fit for Logarithms of Normalized Liquid Nusselt, Reynolds, and Prandtl Numbers. (Absolute Velocities used in Stanton and Relative Velocities in Reynolds Numbers.) The "Error Bar" Represents 1 Standard Deviation for the Fit.

```
*/
*/
*/  UPDATES TO CHANGE STEADY STATE CHECK, ADD TO EDIT,
*/  FIX MINOR BREAK ERROR, AND CHANGE SOME SIGNAL VARIABLES
*/
*ID TSTCONS
*/ PERFORM SS CONVERGENCE TEST EVERY TIMESTEP
*/
*D STEADY.138,140
*D TF1DS3.496,498
*C STEADY,TF1DS3
*/
*ID TSTBAL
*/ CONVERGENCE TESTS ON MASS,MOMENTUM, AND ENERGY FLUXES
*/
*D TF1D.86
     A  A(LPA),A(LPAN),A(LEAN),A(LROAN),A(LTSSN),A(LDX)
     B  ,A(LROL),A(LROV),A(LEL),A(LEV),A(LROA))
*C TF1D
*D TF1DS3.8
     6  PA,PAN,EVAN,ROVAN,TSSN,DX
     7  ,ROL,ROV,EL,EV,ROVA)
*I TF1DS3.21
      DIMENSION ROL(1),ROV(1),EL(1),EV(1),ROVA(1)
*D TF1DS3.482,539
*I TF1DS3.544
 9000  FORMAT(* TF1DS3 *,I3,6(2X,1PE13.5))
      IF(ISTDY .EQ. 0) GO TO 738
      RDELT = 1./DELT
      DO 737 J=1,NCELLS
      GVAP = ALP(J)*ROV(J)*VV(J)
      GVAPN = ALPN(J)*ROVN(J)*VVN(J)
      GLIQ = (1.-ALP(J))*ROL(J)*VL(J)
      GLIQN = (1.-ALPN(J))*ROLN(J)*VLN(J)
      GAIR = ALP(J)*ROVA(J)*VV(J)
      GAIRN = ALPN(J)*ROVAN(J)*VVN(J)
      DGV = GVAPN-GVAP
      DGL = GLIQN-GLIQ
      DGAIR = GAIRN-GAIR
      VGVAP = GVAP*VV(J)
      VGVAPN = GVAPN*VVN(J)
      VGLIQ = GLIQ*VL(J)
      VGLIQN = GLIQN*VLN(J)
      DGVGV = VGVAPN - VGVAP
      DGVGL = VGLIQN - VGLIQ
      EGVAP = GVAP*(EV(J)+0.5*VV(J)**2)
      EGVAPN = GVAPN*(EVN(J)+0.5*VVN(J)**2)
      EGLIQ = GLIQ*(EL(J)+0.5*VL(J)**2)
      EGLIQN = GLIQN*(ELN(J)+0.5*VLN(J)**2)
```

```
      DGGEV = EGVAPN - EGVAP
      DGGEL = EGLIQN - EGLIQ
      XBCT = 0.
      IF(ABS(GVAPN) .GT.MAXFLN) XBCT = DGV*RDELT/GVAPN
      IF(ABS(XBCT) .LE. FMAX(1)) GO TO 731
      FMAX(1) = XBCT
      LOK(1,1) = NUM
      LOK(1,2) = J
  731   XBCT = 0.
      IF(ABS(GLIQN) .GT.MAXFLN) XBCT = DGL*RDELT/GLIQN
      IF(ABS(XBCT) .LE. FMAX(2)) GO TO 732
      FMAX(2) = XBCT
      LOK(2,1) = NUM
      LOK(2,2) = J
  732   XBCT = 0.
      IF(ABS(VGVAPN) .GT.MAXFLN) XBCT = DGVGV*RDELT/VGVAPN
      IF(ABS(XBCT) .LE. FMAX(3)) GO TO 733
      FMAX(3) = XBCT
      LOK(3,1) = NUM
      LOK(3,2) = J
  733   XBCT = 0.
      IF(ABS(VGLIQN) .GT.MAXFLN) XBCT = DGVGL*RDELT/VGLIQN
      IF(ABS(XBCT) .LE. FMAX(4)) GO TO 734
      FMAX(4) = XBCT
      LOK(4,1) = NUM
      LOK(4,2) = J
  734   XBCT = 0.
      IF(ABS(EGVAPN) .GT.MAXFLN) XBCT = DGGEV*RDELT/EGVAPN
      IF(ABS(XBCT) .LE. FMAX(5)) GO TO 735
      FMAX(5) = XBCT
      LOK(5,1) = NUM
      LOK(5,2) = J
  735   XBCT = 0.
      IF(ABS(EGLIQN) .GT.MAXFLN) XBCT = DGGEL*RDELT/EGLIQN
      IF(ABS(XBCT) .LE. FMAX(6)) GO TO 736
      FMAX(6) = XBCT
      LOK(6,1) = NUM
      LOK(6,2) = J
  736   XBCT = 0.
      IF(ABS(GAIRN) .GT.MAXFLN) XBCT = DGAIR*RDELT/GAIRN
      IF(ABS(XBCT) .LE. FMAX(7)) GO TO 737
      FMAX(7) = XBCT
      LOK(7,1) = NUM
      LOK(7,2) = J
  737   CONTINUE
  738   CONTINUE
*C TFIDS3
*D EDIT.49,59
 2000   FORMAT(/28H STEADY STATE TIME STEP NO. ,I5,/,
     1  29H LAST TIME STEP CONVERGED IN ,I3,
     2  12H ITERATIONS./8H TIME = ,1PE13.5,14H      DELT = ,E13.5/
     2  52H     VARIABLE     MAX CHANGE RATIO  COMP   CELL /
```

```
     3  21H VAPOR MASS FLUX     ,3X,E12.5,2I8/
     3  21H LIQUID MASS FLUX    ,3X,E12.5,2I8/
     3  21H VAPOR MOMENTUM FLUX ,3X,E12.5,2I8/
     3  21H LIQUID MOMENTUM FLUX,3X,E12.5,2I8/
     3  21H VAPOR ENERGY FLUX   ,3X,E12.5,2I8/
     3  21H LIQUID ENERGY FLUX  ,3X,E12.5,2I8/
     3  21H AIR MASS FLUX       ,3X,E12.5,2I8)
*C EDIT
*ID RKBBRK
*I RBREAK.222
      IF(ISAT .EQ. 2) A(LTL) = TLOFF
*C RBREAK
*ID RKBPRT
*D ECOMP.75
 520   CONTINUE
*D ECOMP.95,97
 600   FORMAT(/,11X,4HALV ,7X,4HCHTI,7X,6HENTHVL,5X,6HVAPGEN,4X,
    1  7HAINT ST,4X,4HHLIQ,7X,4HCIF 2,7X,5HDALVA /5H CELL)
*D ECOMP.82,83
C LIQUID LEVEL FOR HORIZONTAL STRATIFICATION
      IVS1 = N + LVOL
      IVS2 = IVS1 + LDX -LVOL
      IVS3 = IVS1 +LH(2) - LVOL
      V1 = 2.*A(IVS1)/(ASIN(1.)*A(IVS2))
      V1 = SQRT(V1)
      V2 = A(IVS3)/(V1*A(IVS2))
      V3 = 0.
      IF(V2 .LE. 1.) V3 = SQRT(1.-V2**2)
      IF(A(IVS1-LVOL+LALPN) .LT. 0.5) V3 = -V3
      HLIQ = 0.5*V1*(1.-V3)
      WRITE(IOUT,700) K,A(LALVN+N),A(LHLVN+N),A(LHFG+N),
     1  A(LGAMN+N),A(LH(2)+N),HLIQ,A(LCIFN+N+1),A(LDALVA+N)
  5   CONTINUE
*C ECOMP
*ID RKBSVCH
*D SVSET1.96
C LIQUID LEVEL FOR HORIZONTAL STRATIFICATION (TYPE 20)
      IVS1 = IA(KPT+4) -1 +LVOL
      IVS2 = IVS1 + LDX -LVOL
      IVS3 = IVS1 +LH(2) - LVOL
      V1 = 2.*A(IVS1)/(ASIN(1.)*A(IVS2))
      V1 = SQRT(V1)
      V2 = A(IVS3)/(V1*A(IVS2))
      V3 = 0.
      IF(V2 .LE. 1.) V3 = SQRT(1.-V2**2)
      IF(A(IVS1-LVOL+LALPN) .LT. 0.5) V3 = -V3
      A(KPT+7) = 0.5*V1*(1.-V3)
*B SVSET1.14
*CALL IOUNITS
*D SVSETC.145
C     INTERFACE AREA FOR STRATIFIED FLOW (TYPE 65)
      L = LH(2) - 1
      IF(NSVN .EQ. 9) GO TO 880
```

```
C
C     VAPOR-TO-LIQUID HTC  (TYPE 66)
C       - - NO WALL HEAT TRANSFER - -
C       - - COMPUTE AS IN APP.2,NUREG/CR-2289 - -
C
C        OR VAPOR ENTHALPY (TYPE 67)
C
      ICELSM = ICELLS - 1
      L = LHLV - 1
      DO 591 I = 1,ICELSM
      HVCELL = A(LEVN+I-1) + A(LPN+I-1)/A(LROVN+I-1)
      A(L+I) = HVCELL
      IF(NSVN .EQ. 11) GO TO 591
      ILIN = I - 1
      ILOUT = I
      IF(A(LVVN+I-1) .LT. 0.) ILIN = I
      IF(A(LVVN+I) .LT. 0.) ILOUT = I + 1
      ETIN = A(LEVN+ILIN-1) + A(LPN+ILIN-1)/A(LROVN+ILIN-1)
      ETOUT = A(LEVN+ILOUT-1) + A(LPN+ILOUT-1)/A(LROVN+ILOUT-1)
      EFIN = A(LALPN+ILIN-1)*A(LVVN+I-1)*A(LROVN+ILIN-1)*ETIN
      EFOUT = A(LALPN+ILOUT-1)*A(LVVN+I)*A(LROVN+ILOUT-1)*ETOUT
      AINT = A(LH(2) + I -1)
      IVS1 = I -1 +LVOL
      IVS2 = IVS1 + LDX -LVOL
      V1 = 2.*A(IVS1)/(ASIN(1.)*A(IVS2))
      V1 = SQRT(V1)
      IF(AINT .EQ. 0.) AINT = V1*A(IVS2)
      A(L+I) = A(LFA+I-1)*(EFIN-EFOUT)/
     1 (AINT*(A(LTVN+I-1)-A(LTLN+I-1)))
  591   CONTINUE
*/ MODS FOR REYNOLDS AND PRANDTL NUMBERS
*D SVSETC.48
      IF (ISVN .EQ. 35) GO TO 880
C      ISVN = 34 - VAPOR REYNOLDS NO/UNIT LENGTH
      L = LVV - 1
      L1 = LROVN
      L3 = LVISV
C        OR = 36 - VAPOR PRANDTL NUMBER
      IF(ISVN .EQ. 34) GO TO 322
      L1 = LVISV
      L2 = LCPV
      L3 = LCV
      GO TO 324
*I SVSET1.232
      IF(ISVN .EQ. 38) GO TO 880
      L = LVL - 1
C      ISVN = 37 - LIQUID REYNOLDS NO/UNIT LENGTH
      L1 = LROLN
      L3 = LVISL
C        OR = 39 - LIQUID PRANDTL NUMBER
      IF(ISVN .EQ. 37) GO TO 322
```

```
      L1 = LVISL
      L2 = LCPL
      L3 = LCL
      GO TO 324
  322   DO 323 I=1,ICELLS
C      USE RELATIVE VELOCITY FOR COMPARISON WITH HTC STUFF
      A(L+I) = A(L1+I-1)*ABS(A(LVVN+I-1)-A(LVLN+I-1))/A(L3+I-1)
  323   CONTINUE
      GO TO 880
  324   DO 325 I=1,ICELLS
      A(L+I) = A(L1+I-1)*A(L2+I-1)/A(L3+I-1)
  325   CONTINUE
*I SVSETC.332
*/MODS FOR WALL FRICTION TERMS- 97 (LIQUID) OR 99 (VAPOR)
*I SVSETC.350
      IF(ISVN .EQ. 98) GO TO 8001
      LWALLF = LWFL
      IF(ISVN .EQ. 99) LWALLF = LWFV
      DO 801 I=1,NCELLT
      A(L+I) = A(LWALLF+I-1)
  801   CONTINUE
      GO TO 880
 8001   CONTINUE
*D SVSETC.156
      L = LVM - 1
      DO 611 I = 1,NCELLT
      VVAP = 0.5*(A(LVVN+I-1) + A(LVVN+I))
      VLIQ = 0.5*(A(LVLN+I-1) + A(LVLN+I))
      A(L+I) = A(LROVN+I-1)*A(LALPN+I-1)*A(LFA+I-1)*VVAP
      A(L+I) = A(L+I)
     1  + A(LROLN+I-1)*(1.-A(LALPN+I-1))*A(LFA+I-1)*VLIQ
  611   CONTINUE
*C SVSET1
*/
*/
*/  UPDATES TO MODIFY WALL FRICTION AND INTERFACE HEAT TRANSFER
MODELS
*/
*ID RKBUCR
*/ VAPOR VELOCITY LIMIT FOR H.S. FLOW CHECK MISSING SOMETHING
*I FEMOM.528
      UG = UG*SQRT(PI)
*ID WALLF
*/ MODIFY WALL FRICTION TERMS (AD HOC CODING)
*I FEMOM.682
CONSTANT SPATIAL INCREMENTS
      ZPJ = (J-0.5)*DX(J)
      REYL = 2.*RL*AVLJ*ZPJ/VSCL
      REYV = 2.*RV*AVVJ*ZPJ/VSCV
      REYLAM = 3.2E5
      REYTUR = 7.0E5
```

```
      CONLAM = 0.332
      CONTUR = 0.0296
      XLAM = - 0.5
      XTUR = - 0.2
      XRETL = XLAM
      CONL = CONLAM
      IF(REYL .GE. REYTUR) XRETL = XTUR
      IF(REYL .GE. REYTUR) CONL = CONTUR
      IF(REYL.LE.REYLAM .OR. REYL.GE.REYTUR) GO TO 3000
      VRLAM = REYLAM*AVLJ/REYL
      VRTUR = REYTUR*AVLJ/REYL
      GLAM = VRLAM*RL
      GTUR = VRTUR*RL
C  STAR(A,B) = A**B
      WFLLAM = CONLAM*GLAM*VRLAM*STAR(REYLAM,XLAM)
      WFLTUR = CONTUR*GTUR*VRTUR*STAR(REYTUR,XTUR)
      ARG = (AVLJ - VRLAM)/(VRTUR - VRLAM)
      BETAL = (2.-XLAM)*WFLLAM/VRLAM
      BETAT = (2.-XTUR)*WFLTUR/VRTUR
      BETA2 = 3.*(VRTUR-VRLAM)*(BETAT+BETAL) - 6.*(WFLTUR-WFLLAM)
      BETA1 = (VRTUR-VRLAM)*(BETAT-BETAL) - BETA2
      WFLJT = WFLLAM+BETAL*(AVLJ-VRLAM)+0.5*BETA1*ARG**2
     1  +(BETA2*ARG**3)/3.
      WFLJ = WFLJT/(RL*AVLJ**2)
      GO TO 3001
 3000  WFLJ = CONL*STAR(REYL,XRETL)
 3001        CONTINUE
      CONV = CONLAM
      XRETV = XLAM
      IF(REYV .GE. REYTUR) XRETV = XTUR
      IF(REYV .GE. REYTUR) CONV = CONTUR
      IF(REYV.LE.REYLAM .OR. REYV.GE.REYTUR) GO TO 3030
      VRLAM = REYLAM*AVVJ/REYV
      VRTUR = REYTUR*AVVJ/REYV
      GLAM = VRLAM*RV
      GTUR = VRTUR*RV
C  STAR(A,B) = A**B
      WFVLAM = CONLAM*GLAM*VRLAM*STAR(REYLAM,XLAM)
      WFVTUR = CONTUR*GTUR*VRTUR*STAR(REYTUR,XTUR)
      ARG = (AVVJ - VRLAM)/(VRTUR - VRLAM)
      BETAL = (2.-XLAM)*WFVLAM/VRLAM
      BETAT = (2.-XTUR)*WFVTUR/VRTUR
      BETA2 = 3.*(VRTUR-VRLAM)*(BETAT+BETAL) - 6.*(WFVTUR-WFVLAM)
      BETA1 = (VRTUR-VRLAM)*(BETAT-BETAL) - BETA2
      WFVJT = WFVLAM+BETAL*(AVVJ-VRLAM)+0.5*BETA1*ARG**2
     1  +(BETA2*ARG**3)/3.
      WFVJ = WFVJT/(RV*AVVJ**2)
      GO TO 3031
 3030  WFVJ = CONV*STAR(REYV,XRETV)
 3031        CONTINUE
*C FEMOM
*ID RBCHTI
```

```
*I TF IDS1.232
*/ MODIFY INTERFACE ENERGY TRANSFER TERMS (AD HOC CODING)
*I TF IDS1.336
      GLIQS = 2.*ROL(J)*VRT
      GVAPS = 2.*ROV(J)*VRT
CONSTANT SPATIAL INCREMENTS
      ZPJ = (J-0.5)*DX(J)
      REYL = GLIQS*ZPJ/CMUL
      REYV = GVAPS*ZPJ/CMUV
      PRL = CMUL*DR(JDR+3)/TCONL
      PRV = CMUV*DR(JDR+4)/TCONV
      XPRT = -2./3.
      REYLAM = 3.2E5
      REYTUR = 7.0E5
      CONLAM = 0.332
      CONTUR = 0.0296
      XLAM = - 0.5
      XTUR = - 0.2
      XRETL = XLAM
      CONL = CONLAM
      IF(REYL .GE. REYTUR) XRETL = XTUR
      IF(REYL .GE. REYTUR) CONL = CONTUR
      IF(REYL.LE.REYLAM .OR. REYL.GE.REYTUR) GO TO 3000
      VRLAM = REYLAM*VRT/REYL
      VRTUR = REYTUR*VRT/REYL
      GLAM = VRLAM*GLIQS/VRT
      GTUR = VRTUR*GLIQS/VRT
C  STAR(A,B) = A**B
      ALVLAM = CONLAM*DR(JDR+3)*GLAM*STAR(PRL,XPRT)
     1  *STAR(REYLAM,XLAM)
      ALVTUR = CONTUR*DR(JDR+3)*GTUR*STAR(PRL,XPRT)
     1  *STAR(REYTUR,XTUR)
      ARG = (VRT - VRLAM)/(VRTUR - VRLAM)
      BETAL = (1.-XLAM)*ALVLAM/VRLAM
      BETAT = (1.-XTUR)*ALVTUR/VRTUR
      BETA2 = 3.*(VRTUR-VRLAM)*(BETAT+BETAL) - 6.*(ALVTUR-ALVLAM)
      BETA1 = (VRTUR-VRLAM)*(BETAT-BETAL) - BETA2
      ALVJ = ALVLAM+BETAL*(VRT-VRLAM)+0.5*BETA1*ARG**2
     1  +(BETA2*ARG**3)/3.
      GO TO 3001
 3000  ALVJ = CONL*DR(JDR+3)*GLIQS*STAR(PRL,XPRT)*STAR(REYL,XRETL)
 3001         ALVJ = ALVJ*SIDX(J)
      CONV = CONLAM
      XRETV = XLAM
      IF(REYV .GE. REYTUR) XRETV = XTUR
      IF(REYV .GE. REYTUR) CONV = CONTUR
      IF(REYV.LE.REYLAM .OR. REYV.GE.REYTUR) GO TO 3030
      VRLAM = REYLAM*VRT/REYV
      VRTUR = REYTUR*VRT/REYV
      GLAM = VRLAM*GVAPS/VRT
      GTUR = VRTUR*GVAPS/VRT
```

```
C  STAR(A,B) = A**B
      CHTLAM = CONLAM*DR(JDR+4)*GLAM*STAR(PRV,XPRT)
     1  *STAR(REYLAM,XLAM)
      CHTTUR = CONTUR*DR(JDR+4)*GTUR*STAR(PRV,XPRT)
     1  *STAR(REYTUR,XTUR)
      ARG = (VRT - VRLAM)/(VRTUR - VRLAM)
      BETAL = (1.-XLAM)*CHTLAM/VRLAM
      BETAT = (1.-XTUR)*CHTTUR/VRTUR
      BETA2 = 3.*(VRTUR-VRLAM)*(BETAT+BETAL) - 6.*(CHTTUR-CHTLAM)
      BETA1 = (VRTUR-VRLAM)*(BETAT-BETAL) - BETA2
      CHTIJ = CHTLAM+BETAL*(VRT-VRLAM)+0.5*BETA1*ARG**2
     1  +(BETA2*ARG**3)/3.
      GO TO 3031
 3030  CHTIJ = CONV*DR(JDR+4)*GVAPS*STAR(PRV,XPRT)*STAR(REYV,XRETV)
 3031         CHTIJ = CHTIJ*SIDX(J)
*C TFIDS1
```

Appendix C

Input Listing

```
FREE
 3 0 1 0
COCURRENT HORIZONTAL STRATIFIED FLOW TEST
TEST 253 - VELOCITY UPSTREAM,BREAK DOWNSTREAM BOUNDARY
 MAXIMUM DT = 0.125 S
*
$INOPTS
ICFLOW=0,
$END
************
* FOR CALCULATIONS WITH AIR :
*  NOAIR = 0 IN NAMELIST INPUT
************
 0 0.
 1 0 3 2 0
 1.0E-03 1.E-05 1.0E-04
 10 0 10 0
*  SIGNALS,CONTROLS,CONTROL TABLES,TRIPS,CONTROL PASSES
 500 0 0 0 1
 1 2 3 E
*
*  SIGNALS
*
* LIQUID LEVELS (MOD)
     1    20    2    1
     2    20    2    3
     3    20    2    5
     4    20    2    7
     5    20    2    9
     6    20    2   11
     7    20    2   13
     8    20    2   15
     9    20    2   17
    10    20    2   19
    11    20    2   21
    12    20    2   23
    13    20    2   25
    14    20    2   27
    15    20    2   29
    16    20    2   31
    17    20    2   33
    18    20    2   35
    19    20    2   37
    20    20    2   39
    21    20    2   41
    22    20    2   43
    23    20    2   45
    24    20    2   47
    25    20    2   49
```

```
* PRESSURE DIFFERENCES
   26    -21     2     1     1
   27    -21     2     3     1
   28    -21     2     5     1
   29    -21     2     7     1
   30    -21     2     9     1
   31    -21     2    11     1
   32    -21     2    13     1
   33    -21     2    15     1
   34    -21     2    17     1
   35    -21     2    19     1
   36    -21     2    21     1
   37    -21     2    23     1
   38    -21     2    25     1
   39    -21     2    27     1
   40    -21     2    29     1
   41    -21     2    31     1
   42    -21     2    33     1
   43    -21     2    35     1
   44    -21     2    37     1
   45    -21     2    39     1
   46    -21     2    41     1
   47    -21     2    43     1
   48    -21     2    45     1
   49    -21     2    47     1
   50    -21     2    49     1
* STEAM MASS FLOWS
   51     29     2     1
   52     29     2     3
   53     29     2     5
   54     29     2     7
   55     29     2     9
   56     29     2    11
   57     29     2    13
   58     29     2    15
   59     29     2    17
   60     29     2    19
   61     29     2    21
   62     29     2    23
   63     29     2    25
   64     29     2    27
   65     29     2    29
   66     29     2    31
   67     29     2    33
   68     29     2    35
   69     29     2    37
   70     29     2    39
   71     29     2    41
   72     29     2    43
   73     29     2    45
   74     29     2    47
   75     29     2    49
```

```
* VAPOR-TO-LIQUID HTCS (MOD)
    76    66    2    2
    77    66    2    4
    78    66    2    6
    79    66    2    8
    80    66    2    10
    81    66    2    12
    82    66    2    14
    83    66    2    16
    84    66    2    18
    85    66    2    20
    86    66    2    22
    87    66    2    24
    88    66    2    26
    89    66    2    28
    90    66    2    30
    91    66    2    32
    92    66    2    34
    93    66    2    36
    94    66    2    38
    95    66    2    40
    96    66    2    42
    97    66    2    44
    98    66    2    46
    99    66    2    48
   100    66    2    50
* VAPOR GENERATION RATES
   101   101    2    1
   102   101    2    3
   103   101    2    5
   104   101    2    7
   105   101    2    9
   106   101    2    11
   107   101    2    13
   108   101    2    15
   109   101    2    17
   110   101    2    19
   111   101    2    21
   112   101    2    23
   113   101    2    25
   114   101    2    27
   115   101    2    29
   116   101    2    31
   117   101    2    33
   118   101    2    35
   119   101    2    37
   120   101    2    39
   121   101    2    41
   122   101    2    43
   123   101    2    45
   124   101    2    47
   125   101    2    49
```

```
* LIQUID DENSITIES
   126    75     2     1
   127    75     2     3
   128    75     2     5
   129    75     2     7
   130    75     2     9
   131    75     2    11
   132    75     2    13
   133    75     2    15
   134    75     2    17
   135    75     2    19
   136    75     2    21
   137    75     2    23
   138    75     2    25
   139    75     2    27
   140    75     2    29
   141    75     2    31
   142    75     2    33
   143    75     2    35
   144    75     2    37
   145    75     2    39
   146    75     2    41
   147    75     2    43
   148    75     2    45
   149    75     2    47
   150    75     2    49
* VAPOR DENSITIES
   151    74     2     1
   152    74     2     3
   153    74     2     5
   154    74     2     7
   155    74     2     9
   156    74     2    11
   157    74     2    13
   158    74     2    15
   159    74     2    17
   160    74     2    19
   161    74     2    21
   162    74     2    23
   163    74     2    25
   164    74     2    27
   165    74     2    29
   166    74     2    31
   167    74     2    33
   168    74     2    35
   169    74     2    37
   170    74     2    39
   171    74     2    41
   172    74     2    43
   173    74     2    45
   174    74     2    47
   175    74     2    49
```

```
* VAPOR REYNOLDS NO/UNIT LENGTH (MOD)
    176    34    2    1
    177    34    2    3
    178    34    2    5
    179    34    2    7
    180    34    2    9
    181    34    2   11
    182    34    2   13
    183    34    2   15
    184    34    2   17
    185    34    2   19
    186    34    2   21
    187    34    2   23
    188    34    2   25
    189    34    2   27
    190    34    2   29
    191    34    2   31
    192    34    2   33
    193    34    2   35
    194    34    2   37
    195    34    2   39
    196    34    2   41
    197    34    2   43
    198    34    2   45
    199    34    2   47
    200    34    2   49
* VAPOR PRANDTL NUMBERS (MOD)
    201    36    2    1
    202    36    2    3
    203    36    2    5
    204    36    2    7
    205    36    2    9
    206    36    2   11
    207    36    2   13
    208    36    2   15
    209    36    2   17
    210    36    2   19
    211    36    2   21
    212    36    2   23
    213    36    2   25
    214    36    2   27
    215    36    2   29
    216    36    2   31
    217    36    2   33
    218    36    2   35
    219    36    2   37
    220    36    2   39
    221    36    2   41
    222    36    2   43
    223    36    2   45
    224    36    2   47
    225    36    2   49
```

```
* VAPOR SPECIFIC HEATS
  226   85    2    1
  227   85    2    3
  228   85    2    5
  229   85    2    7
  230   85    2    9
  231   85    2   11
  232   85    2   13
  233   85    2   15
  234   85    2   17
  235   85    2   19
  236   85    2   21
  237   85    2   23
  238   85    2   25
  239   85    2   27
  240   85    2   29
  241   85    2   31
  242   85    2   33
  243   85    2   35
  244   85    2   37
  245   85    2   39
  246   85    2   41
  247   85    2   43
  248   85    2   45
  249   85    2   47
  250   85    2   49
* LIQUID REYNOLDS NO/UNIT LENGTH (MOD)
  251   37    2    1
  252   37    2    3
  253   37    2    5
  254   37    2    7
  255   37    2    9
  256   37    2   11
  257   37    2   13
  258   37    2   15
  259   37    2   17
  260   37    2   19
  261   37    2   21
  262   37    2   23
  263   37    2   25
  264   37    2   27
  265   37    2   29
  266   37    2   31
  267   37    2   33
  268   37    2   35
  269   37    2   37
  270   37    2   39
  271   37    2   41
  272   37    2   43
  273   37    2   45
  274   37    2   47
  275   37    2   49
```

```
* LIQUID PRANDTL NUMBERS (MOD)
   276    39    2    1
   277    39    2    3
   278    39    2    5
   279    39    2    7
   280    39    2    9
   281    39    2   11
   282    39    2   13
   283    39    2   15
   284    39    2   17
   285    39    2   19
   286    39    2   21
   287    39    2   23
   288    39    2   25
   289    39    2   27
   290    39    2   29
   291    39    2   31
   292    39    2   33
   293    39    2   35
   294    39    2   37
   295    39    2   39
   296    39    2   41
   297    39    2   43
   298    39    2   45
   299    39    2   47
   300    39    2   49
* LIQUID SPECIFIC HEATS
   301    86    2    1
   302    86    2    3
   303    86    2    5
   304    86    2    7
   305    86    2    9
   306    86    2   11
   307    86    2   13
   308    96    2   15
   309    86    2   17
   310    86    2   19
   311    86    2   21
   312    86    2   23
   313    86    2   25
   314    86    2   27
   315    86    2   29
   316    86    2   31
   317    86    2   33
   318    86    2   35
   319    86    2   37
   320    86    2   39
   321    86    2   41
   322    86    2   43
   323    86    2   45
   324    86    2   47
   325    86    2   49
```

```
* AREA OF INTERFACE (STRATIFIED) (MOD)
   326    65    2    1
   327    65    2    3
   328    65    2    5
   329    65    2    7
   330    65    2    9
   331    65    2   11
   332    65    2   13
   333    65    2   15
   334    65    2   17
   335    65    2   19
   336    65    2   21
   337    65    2   23
   338    65    2   25
   339    65    2   27
   340    65    2   29
   341    65    2   31
   342    65    2   33
   343    65    2   35
   344    65    2   37
   345    65    2   39
   346    65    2   41
   347    65    2   43
   348    65    2   45
   349    65    2   47
   350    65    2   49
* VAPOR-INTERFACE H.T.TERM (~hA)
   351    95    2    1
   352    95    2    3
   353    95    2    5
   354    95    2    7
   355    95    2    9
   356    95    2   11
   357    95    2   13
   358    95    2   15
   359    95    2   17
   360    95    2   19
   361    95    2   21
   362    95    2   23
   363    95    2   25
   364    95    2   27
   365    95    2   29
   366    95    2   31
   367    95    2   33
   368    95    2   35
   369    95    2   37
   370    95    2   39
   371    95    2   41
   372    95    2   43
   373    95    2   45
   374    95    2   47
   375    95    2   49
```

```
* LIQUID-INTERFACE H.T. TERM (~hA)
   376   96    2    1
   377   96    2    3
   378   96    2    5
   379   96    2    7
   380   96    2    9
   381   96    2   11
   382   96    2   13
   383   96    2   15
   384   96    2   17
   385   96    2   19
   386   96    2   21
   387   96    2   23
   388   96    2   25
   389   96    2   27
   390   96    2   29
   391   96    2   31
   392   96    2   33
   393   96    2   35
   394   96    2   37
   395   96    2   39
   396   96    2   41
   397   96    2   43
   398   96    2   45
   399   96    2   47
   400   96    2   49
* VAPOR WALL FRICTION COEFFICIENT (MOD)
   401   99    2    1
   402   99    2    3
   403   99    2    5
   404   99    2    7
   405   99    2    9
   406   99    2   11
   407   99    2   13
   408   99    2   15
   409   99    2   17
   410   99    2   19
   411   99    2   21
   412   99    2   23
   413   99    2   25
   414   99    2   27
   415   99    2   29
   416   99    2   31
   417   99    2   33
   418   99    2   35
   419   99    2   37
   420   99    2   39
   421   99    2   41
   422   99    2   43
   423   99    2   45
   424   99    2   47
   425   99    2   49
```

```
* LIQUID WALL FRICTION COEFFICIENT (MOD)
  426   97   2   1
  427   97   2   3
  428   97   2   5
  429   97   2   7
  430   97   2   9
  431   97   2   11
  432   97   2   13
  433   97   2   15
  434   97   2   17
  435   97   2   19
  436   97   2   21
  437   97   2   23
  438   97   2   25
  439   97   2   27
  440   97   2   29
  441   97   2   31
  442   97   2   33
  443   97   2   35
  444   97   2   37
  445   97   2   39
  446   97   2   41
  447   97   2   43
  448   97   2   45
  449   97   2   47
  450   97   2   49
* INTERFACIAL FRICTION FACTOR
  451   98   2   1
  452   98   2   3
  453   98   2   5
  454   98   2   7
  455   98   2   9
  456   98   2   11
  457   98   2   13
  458   98   2   15
  459   98   2   17
  460   98   2   19
  461   98   2   21
  462   98   2   23
  463   98   2   25
  464   98   2   27
  465   98   2   29
  466   98   2   31
  467   98   2   33
  468   98   2   35
  469   98   2   37
  470   98   2   39
  471   98   2   41
  472   98   2   43
  473   98   2   45
  474   98   2   47
  475   98   2   49
```

```
* VAPOR ENTHALPY (MOD)
    476    67     2     1
    477    67     2     3
    478    67     2     5
    479    67     2     7
    480    67     2     9
    481    67     2    11
    482    67     2    13
    483    67     2    15
    484    67     2    17
    485    67     2    19
    486    67     2    21
    487    67     2    23
    488    67     2    25
    489    67     2    27
    490    67     2    29
    491    67     2    31
    492    67     2    33
    493    67     2    35
    494    67     2    37
    495    67     2    39
    496    67     2    41
    497    67     2    43
    498    67     2    45
    499    67     2    47
    500    67     2    49
*
*  COMPONENTS
*
FILL  1  1  SOURCE FOR STEAM AND WATER
  1   3  0
  1.  1000.  0.
  .025   4.8387E-04  0.75   0.13715  294.8
  0.101E+06  0.  0.  8.30495  411.3
*
**************
* FOR TEST 259 :
* .025   4.8387E-04  0.75   0.15975  297.4
* 0.101E+06  0.  0.  20.54291  415.5
**************
* FOR TEST 293 :
* .025   4.8387E-04  0.75   0.30039  298.1
* 0.101E+06  0.  0.  8.30495  410.2
* IF AIR INCLUDED : 0.101E+06  1.903E+3  0.  8.30495  410.2
**************
* FOR TEST 459 :
* .025   4.8387E-04  0.75   0.14936  325.3
* 0.101E+06  0.  0.  20.16893   415.5
* IF AIR INCLUDED : 0.101E+06  0.202E+04  0.  20.16893   415.5
**************
*
*
```

```
PIPE  2  2 EXPERIMENT FLOW CHANNEL
 50 0  1   2  0
 0  0  0  0
 .0785  .01  0.  0.  298.
 298.
F  .0250 E
F  4.8387E-04  E
F .0193548   E
F  0.  E
F  0.  E
F  0.23447  E
F  1  E
I  48  0.75     .80575 E
I  49  .13715   0.19089   E
I  49  8.30495  2.10177  E
I  48  294.8    331.7    E
F  411.3  E
I  48  1.01E5   1.010143E5  E
*  AIR PARTIAL PRESSURE CARD
F  0.  E
**************
*  FOR TEST 259 :
*  I  48  0.75     .90992   E
*  I  49  .15975   0.5083   E
*  I  49  20.54291 7.67923  E
*  I  48  297.4    349.0    E
*  F  415.5  E
*  I  48  1.01E5   1.010715E5  E
**************
*  FOR TEST 293 :
*  I  48  0.75     .69984   E
*  I  49  .30039   0.26404   E
*  I  49  8.30495  1.17626  E
*  I  48  298.1    319.5    E
*  F  410.2  E
*  I  48  1.01E5   1.010179E5  E
*  AIR PARTIAL PRESSURE CARD,
*  IF AIR INCLUDED : I  48  1.903E3   2.039E3  E
**************
*  FOR TEST 459 :
*  I  48  0.75     .90031  E
*  I  49  .14936   0.41015   E
*  I  49  20.16893  10.89717  E
*  I  48  325.3    357.8    E
*  F  415.5  E
*  I  48  1.01E5   1.010715E5  E
*  AIR PARTIAL PRESSURE CARD,
*  IF AIR INCLUDED : I  48  2.02E3   2.02142E3  E
**************
*
*
```

```
 BREAK  3  3  SINK
 2  0  2  0  1
 .025  4.8387E-04  0.80575  411.3  1.010143E+5
 0.  0.  1000.  1.E+5  0.
**************
* FOR TEST 259 :
* .025  4.8387E-04  0.90992  415.5  1.010715E+5
**************
* FOR TEST 293 :
* .025  4.8387E-04  0.69984  410.2  1.010179E+5
* IF AIR INCLUDED, THIRD BREAK CARD READS
* 2.039E3  0.  1000.  1.E+5  0.
**************
* FOR TEST 459 :*
* .025  4.8387E-04  0.90031  415.5  1.010715E+5
* IF AIR INCLUDED, THIRD BREAK CARD READS
* 2.02142E3  0.  1000.  1.E+5  0.
**************
*
*
* TIMESTEP CONTROL
*
 1.E-06  0.125  500.  1.
 10.  2.0  500.0
     -1.
*
```

DISTRIBUTION:

U. S. Government Printing Office
Receiving Branch (Attn: NRC Stock)
8610 Cherry Lane
Laurel, MD 20707
300 copies for R4

U. S. Nuclear Regulatory Commission (5)
Reactor Systems Research Branch
Division of Accident Evaluation
Office of Nuclear Regulatory Research
7915 Eastern Avenue
Silver Spring, MD 20910
Attn: F. Odar
L. M. Shotkin
D. Solberg
H. S. Tovmassian
N. Zuber

EG&G Idaho (6)
Idaho National Engineering Laboratory
P. O. Box 1625
Idaho Falls, ID 83415
Attn: T. R. Charlton
G. W. Johnsen
V. H. Ransom
S. Z. Rouhani
R. J. Wagner
G. E. Wilson

Los Alamos National Laboratory (3)
K553 Q-9
Los Alamos, NM 87545
Attn: Brent Boyack
T. D. Knight
Rick Jenks

U. S. Rohatgi, 130
Department of Nuclear Energy
Brookhaven National Laboratory
Associated Universities, Inc.
Upton, NY 11973

N. H. Shah
Babcock & Wilcox Co. (NPGD)
P. O. Box 1260
Lynchburg, VA 24505

Oddbjörn Sanderväg
Studsvik Energiteknik AB
S-611 82 Nyköping
SWEDEN

S. George Bankoff
Chemical Engineering Department
The Technological Institute
Northwestern University
Evanston, IL 60201

Jesse Fell (5)
Deputy Director, Water Reactor Programs
Atomic Energy Establishment
Winfrith
Dorchester, Dorset DT28DH
ENGLAND

6400 A. W. Snyder
6410 J. W. Hickman
6417 D. C. Carlson
6420 J. V. Walker
6421 T. R. Schmidt
6422 D. A. Powers
6423 P. S. Pickard
6425 W. J. Camp
6427 M. Berman
6440 D. A. Dahlgren
6442 W. A. von Riesemann
6444 L. D. Buxton (21)
6444 R. K. Byers
6444 R. K. Cole, Jr.
6444 D. Dobranich
6444 M. G. Elrick
6444 L. N. Kmetyk
6444 J. M. McGlaun
6444 J. L. Orman
6444 W. H. Schmidt
6444 R. M. Summers
6444 S. W. Webb
6449 K. D. Bergeron
3141 S. A. Landenberger (5)
3151 W. L. Garner
8024 P. W. Dean

NRC FORM 335 (2 84) NRCM 1102, 3201, 3202

U.S. NUCLEAR REGULATORY COMMISSION

BIBLIOGRAPHIC DATA SHEET

SEE INSTRUCTIONS ON THE REVERSE

1 REPORT NUMBER (Assigned by TIDC add Vol. No., if any)

NUREG/CR-4027
SAND84-2161

2 TITLE AND SUBTITLE

TRAC-PF1/MOD1 Independent Assessment: Condensation in Stratified Cocurrent Flow

3 LEAVE BLANK

4 DATE REPORT COMPLETED

MONTH: November — YEAR: 1985

5 AUTHOR(S)

Rupert K. Byers

6 DATE REPORT ISSUED

MONTH: February — YEAR: 1986

7 PERFORMING ORGANIZATION NAME AND MAILING ADDRESS (Include Zip Code)

Thermal/Hydraulic Analysis Division
Sandia National Laboratories
P. O. Box 5800
Albuquerque, NM 87185

8 PROJECT/TASK/WORK UNIT NUMBER

9 FIN OR GRANT NUMBER

A-1374

10 SPONSORING ORGANIZATION NAME AND MAILING ADDRESS (Include Zip Code)

Reactor Systems Research Branch
Division of Accident Evaluation
Office of Nuclear Regulatory Research
U. S. Nuclear Regulatory Commission
Washington, DC 20555

11a TYPE OF REPORT

Technical

b PERIOD COVERED (Inclusive dates)

12 SUPPLEMENTARY NOTES

13 ABSTRACT

The USNRC is funding efforts at several laboratories to assess the adequacy of various advanced, best-estimate systems codes for predicting the behavior of LWRs in accident and abnormal conditions. Sandia's participation in this project includes the use of TRAC-PF1/MOD1 to model stratified, horizontal cocurrent flow, for comparison with experimental data produced at Northwestern University. The experiments are very simple, and the results should display the effects of mass, momentum, and energy transfer at the interface, as well as those of wall friction.

Analyses were performed for four of the Northwestern experiments, which involved condensing steam/water flow in a rectangular channel. The study showed that the code's timestep control algorithm and criteria for steady-state convergence need attention, and that the interfacial heat transfer model generally overpredicts the rate of phase change for conditions of the experiments. In TRAC, horizontal stratified flow is assumed to occur in a channel of circular cross section; this precludes a simple and detailed quantitative comparison between calculated results and the reported experimental data. However, the qualitative effects of various changes in experimental conditions are well predicted in most cases. A very simple ad hoc modification to the interface treatment, based on boundary layer theory, was able to remove some of the larger discrepancies between the experimental and calculated results. Further improvements could probably result from analysis of the data in a different way from that presented in the experiment report, but this possibility was only briefly examined.

14 DOCUMENT ANALYSIS - a KEYWORDS/DESCRIPTORS

b IDENTIFIERS/OPEN-ENDED TERMS

15 AVAILABILITY STATEMENT

Unlimited

16 SECURITY CLASSIFICATION

(This page) Uncl

(This report) Uncl

17 NUMBER OF PAGES

18 PRICE

120555078877 1 1AN1R4
US NRC
ADM-DIV OF TIDC
POLICY & PUB MGT BR-PDR NUREG
W-501
WASHINGTON DC 20555

Org.	Bldg.	Name	Rec'd by	Org.	Bldg.	Name	Rec'd by

Sandia National Laboratories